

UNIVERSITÀ DEGLI STUDI DI PADOVA

DIPARTIMENTO DI INGEGNERIA INDUSTRIALE

STOCKHOLM UNIVERSITY

DEPARTMENT OF MATERIALS AND ENVIRONMENTAL CHEMISTRY

“LAUREA MAGISTRALE” IN MATERIALS ENGINEERING

Second-Level Degree Thesis in Materials Engineering

**BIONANOCOMPOSITE MEMBRANES BASED ON
CELLULOSE NANOFIBRILS: EFFECTS OF
GRAPHENE OXIDE AND CALCIUM IONS**

Supervisors: *Prof. Massimo Guglielmi*

Assoc. Prof. German Salazar-Alvarez, Dr. Bernd Wicklein

Student: *FEDERICO DAL MORO*

ACADEMIC YEAR: 2013 – 2014

Last revision: 28/02/2014 23.59

ABSTRACT

In the last years, the scientific community increased the effort to find new biomaterials that could substitute some of the petrochemical products largely used today. Also, in order to limit the deterioration of the environmental conditions it is fundamental to decrease the using of organic non sustainable substances and find new biocompatible solutions. A new frontier for a “greener” future is outlined by biodegradable polymers: polysaccharides (alginate, xanthan, carrageenan, cellulose, chitin, curdlan, gellan, pectin, pullulan, starch), proteins (collagen, gelatin, whey and soy proteins, zein) and aliphatic polyesters (poly(lactic acid), poly(hydroxybutyrate)). The majority of such biopolymers can find application in the food packaging market since they combine a total sustainability with relevant mechanical and barrier properties. However, one of the most fascinating biopolymer is cellulose, because with chemical and mechanical treatments is possible to obtain a new variety of nano-celluloses. In this regard cellulose nanofibers (CNF) represent an attractive building block for new “green” functional materials, showing the potential to a practical use in different applications.

The present thesis focuses on the design and characterization of bio-nanocomposite membranes based on CNF, evaluating the effects of graphene oxide (GO) and calcium ions on the rheological properties of aqueous dispersions and the mechanical properties of cast films. Moreover, the effects of GO and calcium ions on the water and ethanol vapor permeability of such CNF-GO membranes is also investigated.

The work was carried out during the internship at the Materials Chemistry Division of the Department of Materials and Environmental Chemistry, Stockholm University, from June 2013 to February 2014.

TABLE OF CONTENTS

INTRODUCTION.....	1
CHAPTER 1 – MATERIALS AND METHODS	4
1.1 MATERIALS	4
1.1.1 Nanofibrillated Cellulose (CNF)	4
1.1.2 Cross-linkers	6
1.1.3 Nanofiller	7
1.2 METHODS	8
1.2.1 Suspension preparation	8
1.2.2 Film preparation	10
1.2.3 Rheological Analysis	11
1.2.3.1 Dynamic shear viscosity	12
1.2.3.2 Complex viscosity	14
1.2.4 Dynamic Light Scattering	19
1.2.5 UV-VIS Spectroscopy	20
1.2.6 Raman Spectroscopy	21
1.2.7 Scanning electron microscope (SEM)	22
1.2.8 Mechanical tensile test	22
1.2.9 WVTR test	22
CHAPTER 2 – RHEOLOGICAL PROPERTIES OF CNF SUSPENSIONS	25
2.1 EXPERIMENTAL CONDITIONS	26
2.2 SHEAR THINNING BEHAVIOR.....	26
2.3 CNF SUSPENSIONS AS HIGH MOLECULAR WEIGHT POLYMER SUSPENSIONS	29
2.4 CROSS-LINKING OF CNF SUSPENSIONS	33
2.4.1 Power Law model for CNF-Ca ²⁺ Shear Viscosity	34
2.4.2 Viscoelastic properties of CNF-Ca ²⁺ suspensions	37
2.5 VISCOELASTIC BEHAVIOR OF CNF-GO-Ca ²⁺ SUSPENSIONS	41
2.6 DISCUSSIONS	42

CHAPTER 3 – MECHANICAL PROPERTIES OF CNF-GO NANOCOMPOSITE	45
3.1 TENSILE TEST RESULTS	45
3.1.1 <i>True Curve</i>	45
3.1.2 <i>Results</i>	47
3.2 COMPARISON BETWEEN RESULTS AND LITERATURE	48
3.3 THEORETICAL MODELS AND PREDICTIONS FOR CNF MEMBRANES	51
3.3.1 <i>CNF single fiber Young’s Modulus</i>	52
3.3.2 <i>CNF membrane Young’s Modulus</i>	56
3.4 THEORETICAL MODELS AND PREDICTIONS FOR CNF NANO-COMPOSITE MEMBRANES	63
3.4.1 <i>Young’s modulus prediction for CNF nanocomposite membranes</i>	64
3.4.2 <i>Young’s modulus prediction for CNF-GO membranes</i>	66
3.5 DISCUSSIONS	69
CHAPTER 4 - BARRIER PROPERTIES	73
4.1 EXPERIMENTAL CONDITIONS	73
4.2 WVTR OF CNF NANO-COMPOSITE MEMBRANES	73
4.2.1 <i>Parameters of influence on the WVTR of CNF membranes</i>	73
4.2.2 <i>WVTR Results</i>	75
4.2.3 <i>Membrane hydrophobicity</i>	77
4.2.4 <i>Comparison between results and literature</i>	80
4.3 ETHANOL-VTR OF CNF NANOCOMPOSITE MEMBRANES	83
4.4 DISCUSSIONS	84
CONCLUSIONS	87
ANNEX A	91
A-1) EFFECT OF MIXING ON CNF-GO UV-VIS SPECTRA	91
A-2) DYNAMIC LIGHT SCATTERING FOR ROD SHAPED PARTICLES	92

ANNEX B.....	95
B-1) ENGINEERING CURVE	95
B-2) CONTINUUM MECHANICS IN COMPOSITE MATERIALS	95
B-3) NANO-COMPOSITE MATERIALS: A BRIEF INTRODUCTION	99
B-4) POPULAR MICROMECHANICAL MODELS FOR YOUNG’S MODULUS PREDICTION	99
AKNOWLEDGMENTS.....	105
REFERENCES.....	108

INTRODUCTION

In Sweden 66% of the whole land area is covered by forest and together with mines, wood is one of the most abundant resources that this country exploits, resulting in a huge benefit for its economy.

However, the rapid rising of IT sector, concurrently with the quick developing of countries as India, China and Brazil led the Swedish paper industry look for new solutions in order to maintain its competitiveness. The birth of new technologies as smartphones and tablets is rendering superfluous other information system as for example the traditional and daily “newspaper”. In the meanwhile, many other competitors from Asia and Latin America are reducing the business of the paper Swedish industry in the remaining part of the market.

Therefore, Sweden is focusing its attention and efforts on researching new ways to take advantage of its enormous forests. In the last years a considerable amount of investments are concentrated on developing new high-value materials coming from exploiting of woods.

This is the reason for which the Wallenberg Wood Center has born, together with many research projects in the main Swedish universities: Stockholm University, Chalmers University and KTH Royal Institute of Technology.

One material in particular seems to be a good investment for the current researching activity: nanocelluloses obtained from mechanical and chemical treatments of cellulosic materials. According to SciFinder the number of publications released yearly about nanocellulose materials is increasing tremendously ⁽¹⁷⁾.

Especially cellulose nanofibers (CNF) show impressive properties ⁽²⁾ and they can be used as reinforcement in nanocomposites or to make transparent bio-membranes, finding applications in the packaging, medical transport and electronic fields ⁽¹⁾. Their “sustainable image” is due, for instance, to the possibility to incinerate the material in the end of its lifetime with a negligible load of CO₂ in the atmosphere if compared to the quantity of CO₂ taking up by the plant during its life ⁽⁹¹⁾.

Recently, higher is the effort to increase the strength and gas/water impermeability of CNF membranes, through the design of new bio-nanocomposite hybrids containing nanocellulose fibers and inorganic fillers ^(76, 49, 45, 92). A part of the current study (Chapters 3 and 4) wants to evaluate the effects of graphene oxide and possible crosslinkers on the properties of the final dried membrane, but also the initial suspensions are characterized (Chapter 2) in order to better understand the behavior of the CNF fibers into an aqueous medium.

All the experimental results discussed in the following sections are accompanied by prediction models and compared with other data available in the literature, in order to give also qualitative interpretations about the features of such materials. Importantly it is also presented an attempt for anew modelling approach of the elastic modulus of a neat CNF membrane considering it as a “fabric” made by nanofibrillated cellulose fibers: this could help to understand the factors that influence the mechanical behavior of the film. The modification of such fabric-model is then considered when a nano-filler as graphene oxide is added.

Furthermore, the rheological analysis of CNF suspension gives information about the viscoelasticity and about behavior of the fibers subjected to flow fields. Significantly, the viscoelastic estimations normally used for polymer solutions seem to well describe the properties of low concentrated CNF suspension and CNF-Calcium gels when they are tested through rheological oscillating measurements

CHAPTER 1

MATERIALS AND METHODS

This chapter summarizes the materials and techniques used during the research activity. In this way, it is possible to understand the discussions and interpretations coming from the experiments and theoretical modelling that will be treated in next chapters.

1.1 Materials

Essentially three different materials have been used. This classification is based on the role assumed by each component for a specific purpose:

1. Nature-based material: the “nanofibrillated cellulose” (CNF) has been chosen as the main bio-material on which concentrate the research effort. Sometimes in the scientific literature the name “microfibrillated cellulose” (MFC) is used as synonym to CNF. From now just the word “cellulose nanofibrils” (CNF) will be used, in order to avoid any misunderstandings;
2. Cross-linker: the effect of calcium ions and Boric Acid have been studied for a possible crosslinking between nanocellulose fibrils;
3. Nanofiller: Graphene Oxide (GO) flakes have been used for making CNF/GO hybrids. The effect of partially reduced GO (r-GO) sheets has also been investigated.

Additionally, it has been tested also the effect of a fluorinated layer on the permeability of CNF membranes. The fluorination has been realized through the physical vapor deposition (PVD) of (Tridecafluoro-1,1,2,2-Tetrahydrooctyl) Trichlorosilane.

1.1.1 Nanofibrillated Cellulose (CNF)

Cellulose is the most abundant natural polymer and it has accompanied the human civilization across the millennia through its using as energy source, for clothing, building material and for the transmission of human culture. However, the role of this material is intended to change: not just anymore for a primary use in the common life, but also for making materials with high added value.

In the last years, the science has worked out novel forms of cellulose, from different sources and variously named: nanocrystals, whiskers, nanofibrils, nanofibers, crystallites (**Fig. 1.1**). In

particular, the cellulosic materials that show a nanometric dimension are referred to as “nanocelluloses”.

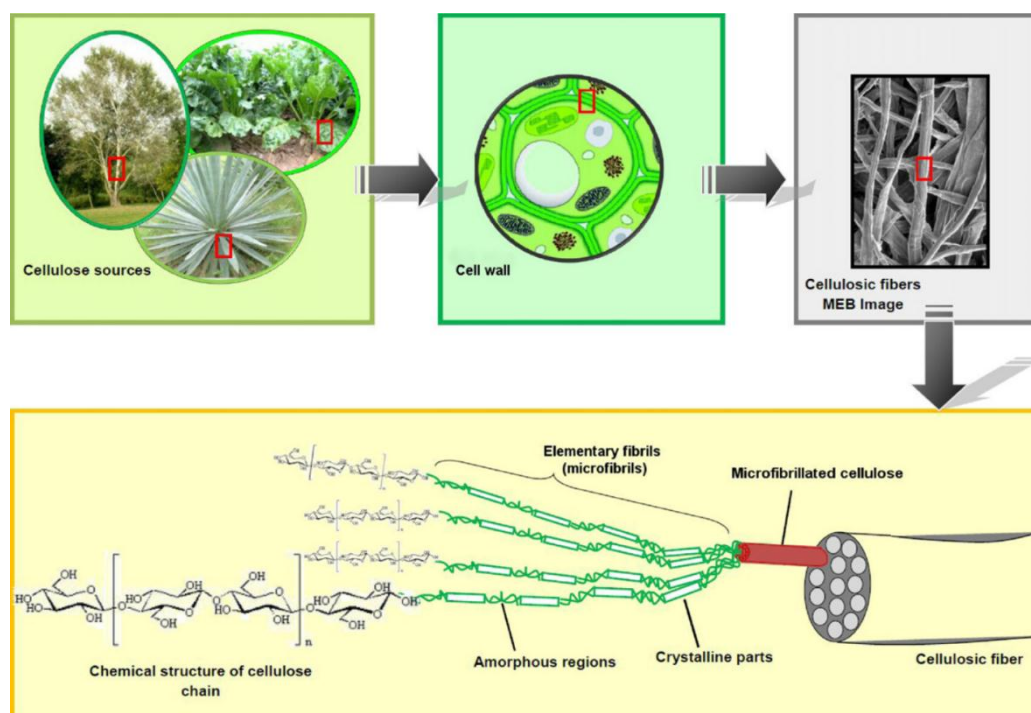


Fig. 1.1: From the cellulose sources to the cellulose molecules: details of the cellulosic fiber structure with emphasis on the cellulose microfibrils. Figure taken from (3)

Nanocelluloses may be classified in three main subcategories, depending mainly on the cellulosic source and on the processing conditions, as shown in **Table 1.1** (4).

Type of nanocellulose	Synonyms	Typical sources	Formation and average size
Nanofibrillated Cellulose (CNF)	MFC, nanofibrils, microfibrils, NFC	Wood, sugar beet, potato tuber, hemp, flax	Delamination of wood pulp by mechanical pressure before and/or after chemical or enzymatic treatment. Diameter: 5-60 nm Length: several micrometers
Nanocrystalline cellulose (CNC)	Cellulose nanocrystals, crystallites, whiskers, rod like cellulose microcrystals	Wood, cotton, hemp, flax, wheat straw, mulberry bark, ramie, Avicel, tunicin, cellulose from algae and bacteria	Acid hydrolysis of cellulose from many sources. Diameter: 5-70 nm Length: 100-250 nm (from plant celluloses); 100 nm to several micrometers (from celluloses of tunicate, algae, bacteria)
Bacterial cellulose network (BCN)	Bacterial cellulose, microbial cellulose, biocellulose	Low-molecular-weight sugars and alcohols	Bacterial synthesis Diameter: 20-100 nm; different types of nanofiber networks

Table 1.1: The family of nanocellulose materials. Table taken from (4).

The type of nanocellulose used in this study is, as previously mentioned, the Nanofibrillated Cellulose (CNF), which is normally produced from wood by the high-pressure homogenization of pulp suspensions. To promote the delamination of the fiber walls, charged groups such as carboxymethylated groups, are introduced into the pulp. In this way, through carboxymethylation, the fibers are negative surface charged and the electrostatic repulsion makes the delamination process more efficient (less energy consumption in the homogenization passes). Through many delamination passes in the homogenization equipment, that applied high shear stresses to the pulp, it is possible to obtain CNF with gellike characteristics. Another positive aspect of a carboxymethylated CNF is the drastic decrease in fiber-fiber interaction and therefore, the inferior propensity to flocculate in a water suspension.

Carboxymethylated transparent CNF-water suspensions were provided by Innventia Group with a concentration of $2,3\text{mg/ml}$.

A single fiber is a sequence of crystalline and semi-crystalline regions, made by cellulose chains where the repeat unit is comprised of two anhydroglucose rings linked together through an oxygen (Fig. 1.2) ⁽⁵⁾.

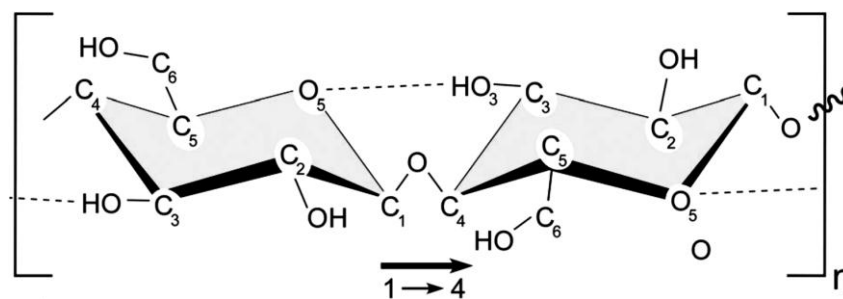


Fig 1.2: Schematics of a single cellulose chain repeat unit. Figure taken from ⁽⁵⁾.

The cellulose chains can order themselves in different crystalline polymorphs: crystalline cellulose I, II, III and IV. Cellulose I has two polymorphs, a triclinic structure ($I\alpha$) and a monoclinic structure ($I\beta$), which coexist in various proportions depending on the cellulose source. The polymorph predominant in the woods cellulose is the $I\beta$ and therefore is the crystalline form present in the nanofibrils used in this study.

1.1.2 Cross-linkers

Previous studies showed that negatively charged polysaccharides, as alginate, are able to gel in the presence of Ca^{2+} ⁽⁶⁾. Moreover, also boric acid has been proved to have a role in the

cross-linking of polysaccharide guaran (7). The Ca^{2+} has been added in the form of CaCl_2 and in all the graphs and pictures of next chapters the expression “% Calcium Ions” is referred to the wt% of CaCl_2 in respect to the CNF mass contained in the suspension.

The effects of these two substances were investigated as possible cross-linkers between carboxymethylated CNF fibers.

1.1.3 Nanofiller

Nanofillers are normally used to make composite materials for two reasons:

1. a small amount of nanofiller can considerably improve the global mechanical properties;
2. the great surface area brought by nanoparticles can turn out in huge benefits also for the impermeability of the composite, decreasing the diffusivity of molecules such as Oxygen, Water or Organic Compounds (as Ethanol) through the material (8,9).

In this study it has been used Graphene Oxide (GO), in form of nanosheets produced from natural graphite and obtained as exfoliated powder from JCNano Inc., Nanjing, China. Also the effects of partially reduced GO have been tested on the membrane barrier properties. In the following, the nomenclature “r-GO_{1min}”, “r-GO_{5min}”, “r-GO_{10min}” corresponds to different (crescent) degrees of GO reduction. Therefore “r-GO_{10min}” means that this graphene oxide is more reduced than “r-GO_{5min}” and so on. The nomenclature “% GO” will be referred as the wt% of the CNF mass. Higher is the level of reduction worse is the quality of the suspensions, with the presence of evident agglomerates. Graphite oxide is a layered material consisting of hydrophilic oxygenated graphene sheets bearing ketone, epoxy, hydroxyl and carboxyl functional groups on their basal planes and edges (Fig. 1.3) (10).

Reduced GO sheets are produced via the reduction of GO through different techniques.

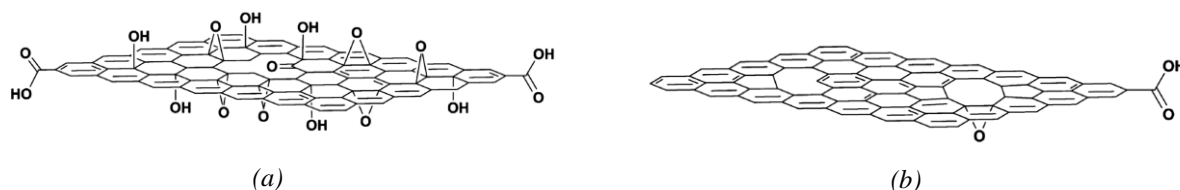


Fig 1.3: Graphene oxide (a) and reduced graphene oxide (b) single layer. Figure taken from (11).

A single flake has many carbon atoms densely packed in a regular sp^2 – bonded atomic scale hexagonal pattern. Graphene is a one-atom thick layer of graphite, which provides excellent

mechanical and electronic properties. However the quality of these properties decreases with the ratio of oxidation and exfoliation process, necessary to produce GO flakes, as more defects are introduced in the structure. Moreover, these abundant defects, that can degrade for instance the electrical conductivity and mechanical stiffness, still exist after reduction (necessary to produce Reduced-GO and Graphene) and particular techniques are required to repair the edge defects and holes (¹²).

Graphene, Highly Reduced Graphene Oxide and especially Graphene Oxide can be dispersed in aqueous and organic media. This characteristic is crucial for making a good and environmentally friendly composite material, since both CNF and graphene-based nanosheets can be well dispersed in water.

In this sense it is essential to make a “good” suspension, where the word “good” means minimize the presence of clusters, agglomerates and in-homogeneities. Being able to control the properties of the suspension leads to a low variability of the characteristics of the final dried composite membrane. Therefore, it is important not only to characterize the film but also the starting suspension, using the appropriate investigation techniques.

1.2 Methods

In this section will be described how suspensions and dried hybrids have been prepared, putting particular attention on the operative details. Moreover, also the techniques used for the different characterizations will be illustrated.

1.2.1 Suspension preparation

As it has been mentioned above, the goal is to obtain a good suspension, in which all the components are well dispersed, preventing any kind of phenomena that can negatively affect the properties of the final solid composite. Then, in agreement with this purpose is desirable to work with diluted suspensions in order to avoid the formation of agglomerates (nanomaterials could tend to form clusters). Furthermore it is fundamental to promote the uniform distribution of all the components in the total volume through an adequate mixing of the dispersions.

Different mixing techniques were tested, and each of them is characterize by a definite amount of energy put into the suspension (or by different intensities of shear stress applied):

- ❖ Vortex mixer: is a simple device used often in bioscience laboratories to mix small vials of liquid. This mixer induces a vortex inside the liquid, through a high frequency oscillation motion of the support that grabs the sample (**Fig. 1.4**).



Fig 1.4: Vortex mixer (left) and the induced vortex (right) Picture taken from <http://www.pocdsscientific.com.au>.

- ❖ Rolling mixer: the vial is put inside a cylindrical tube that rolls around its main axis, providing a gentle mixing ($\sim 70 - 80rpm$).
- ❖ Shaking mixer: similar to the vortex mixer but in this case no vortex is induced in the liquid.
- ❖ “Turrax” mixer: uses the rotor-stator principle (**Fig. 1.5**).

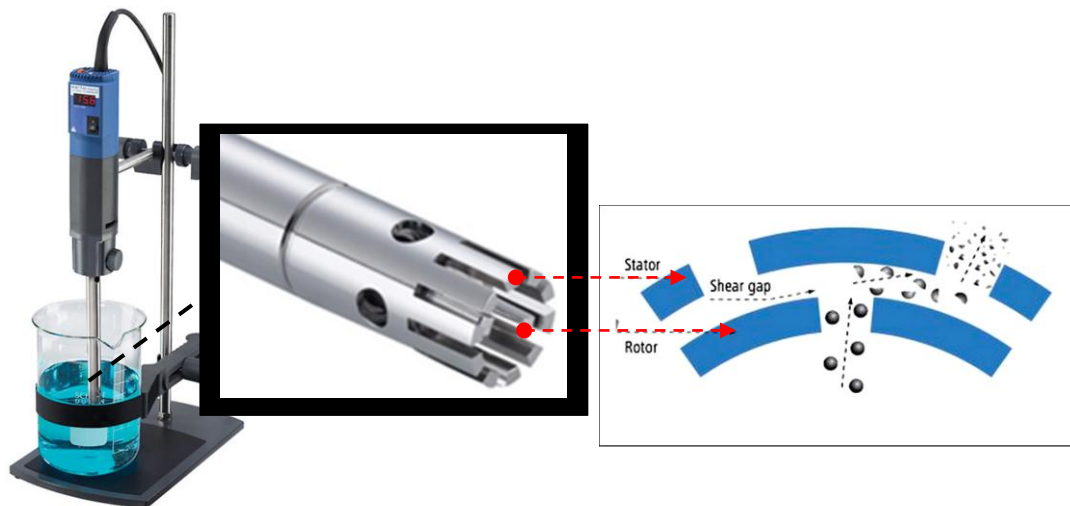


Fig 1.5: “Turrax” mixer (left), head (center) and stator-rotor principle (right). Picture taken from <http://www.coleparmer.com>

The system consists of a rotor within a stationary stator. Due to the high circumferential speed, the medium to be processed is drawn axially into the dispersion

head and then forced radially through the slots in the rotor-stator arrangement. The high speed and the minimal gap between rotor and stator produces extremely strong shear forces and collisions that disperse the material suspended in a media. The maximum speed is about $\sim 13500rpm$.

After the mixing, all the suspensions were degased with a “water pump” in order to limit the presence of gas bubbles inside the suspension. The vacuum was applied until no more bubbles have been seen in the samples. This procedure, first mixing and then vacuum, was applied to all the suspensions before any kind of investigation and before making the films.

The techniques that have been used to characterize the suspensions are:

- ❖ Rheological analysis;
- ❖ Dynamic Light Scattering;
- ❖ UV-VIS spectroscopy.

1.2.2 Film Preparation

To prepare the films the suspensions were poured into Petri dishes and left to dry in a chamber at $30^{\circ}C$ and 50% of relative humidity (where Relative humidity is defined as the ratio of the partial pressure of water vapor in an air-water mixture, to the saturated vapor pressure of water at a given temperature).

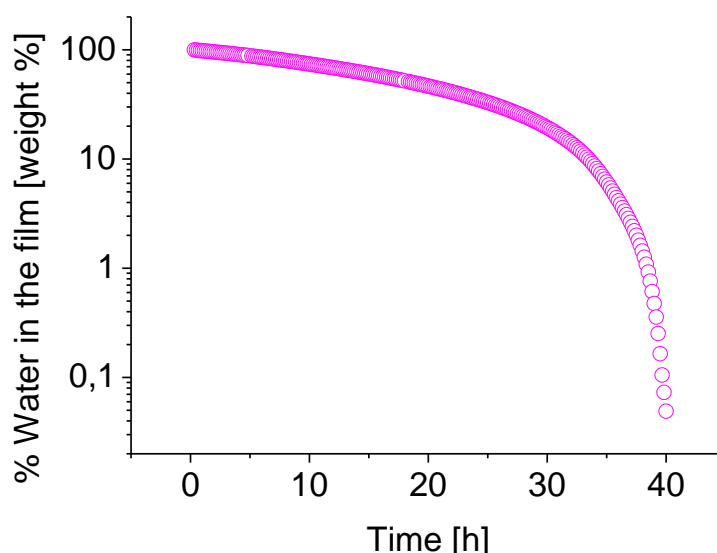


Fig 1.6: Drying time for a film with grammage $12g/m^2$.

One important parameter that characterize a dried film is the “grammage”, defines as:

$$g = \frac{m}{A} \quad (1.1)$$

Where m is the mass (in *grams*) and A is the area (in *square meters*) of the film.

To reach a certain film grammage it is necessary to calculate how much suspension is needed. For example, the volume of CNF suspension (with a concentration of $C_{NFC} = 2,3 \text{ mg/ml}$) necessary to obtain a 12 g/m^2 circular film of radius $r = 8,5 \text{ cm}$ is $V_{NFC} = 29,6 \text{ ml}$. This value can be easily calculated through:

$$V_{NFC} = \frac{g \cdot A}{C_{NFC}} \quad (1.2)$$

Normally, to obtain a dried 12 g/m^2 film are necessary 40 hours in the conditions of humidity and temperature previously mentioned (**Fig. 1.6**).

The films are approximately $13 \mu\text{m}$ thick and transparent; the addition of GO gives a light brown color to the membranes (**Fig. 1.7**).



Fig 1.7: CNF membranes with increasing content (left towards right) in GO.

The tests and methods used to characterize the films have been:

- ❖ Mechanical tensile test;
- ❖ WVTR test (ASTM e96-80);
- ❖ Raman spectroscopy;
- ❖ Scanning electron microscope (SEM).

1.2.3 Rheological Analysis

The rheological analysis is a common technique used to investigate the properties of a viscoelastic liquid. Rheology can be defined as the study of the “flow” and deformation of materials: the term flow means that elements of the liquid are deforming, and adjacent points in the liquid are moving relative to one another.

1.2.3.1 Dynamic Shear Viscosity

There are two kind of flows: shear and extensional flows (**Fig. 1.8**).

In shear flows liquid elements flow over or past each other, while in extensional flow, adjacent elements flow towards or away from each another.

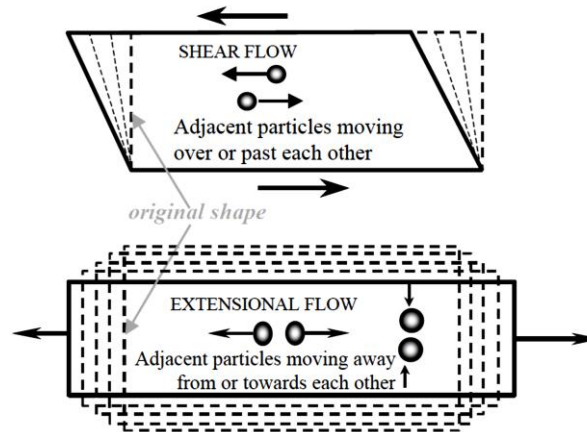


Fig 1.8: Shear flow (up) and extensional flow (down. Picture taken from (13)).

One of the most important variables that can be measured with a rheometer is “viscosity”. The viscosity can be defined as the resistance that a fluid opposes to the deformation applied to it, so it is a measure of the resistance of a liquid to flow.

In this study the shear viscosity is analyzed (not the extensional one), that is the viscosity that results from a shear deformation.

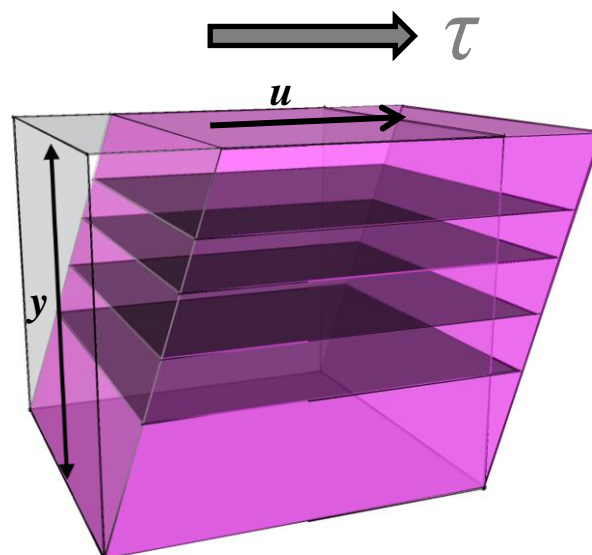


Fig 1.9: Shear flow: when a shear stress try to deform the system the friction (viscosity) between different layers of fluid causes a velocity gradient.

The dynamic (shear) viscosity can be defined through the idealized situation known as a Couette flow (laminar flow), where a layer of fluid is trapped between two horizontal plates,

one fixed and one moving horizontally at constant speed u (**Fig. 1.9**). Each layer of fluid will move faster than the one just below it, and friction between them will give rise to a force resisting their relative motion. The velocity u of the upper layer results as consequence of an applied force F . The magnitude of F is proportional to the speed u and area A of each plate, and inversely proportional to their separation y :

$$F = \eta A \frac{u}{y} \quad (1.3)$$

The proportionality factor η in the formula is the dynamic viscosity of the fluid, measured in $[Pa \cdot s]$. Instead of using the above (1.3) it is better to use:

$$\tau = \eta \frac{\partial u}{\partial y} \quad (1.4)$$

Where $\tau = F/A$ is the shear stress and $\partial u/\partial y$ is the local shear velocity, called also shear rate $\dot{\gamma}$, defined as:

$$\dot{\gamma} = \frac{\partial u}{\partial y} \quad (1.5)$$

Therefore (1.4) becomes:

$$\tau = \eta \dot{\gamma} \quad (1.6)$$

Therefore τ is measured in $[Pa]$ and $\dot{\gamma}$ in $[1/s]$. This formula assumes that the flow is moving along parallel lines and the y axis (see **Fig. 1.9**), perpendicular to the flow, points in the direction of maximum shear velocity.

In Eq. (1.6) the viscosity can be constant or not, during the application of a shear stress: if $\eta = const$ the fluid is called “Newtonian”, if not it is called “non-Newtonian”.

Of course the non-Newtonian behavior is more common and usually is the case for structured liquids such as polymer solutions and suspensions where the viscosity decreases with increasing shear rate, such liquids undergo “shear thinning”. Occasionally, situations arise where the opposite is true, and the viscosity increases with increasing shear rate: these are called “shear-thickening” liquids.

The viscometer used in this study to determine the non-newtonian behaviour is the Coaxial Cylinder Rheometer (“Anton Paar” rheometer).

The liquid is placed inside the gap existing between two concentric cylinders of radii r_e (external radius) and r_i (internal radius). The inner cylinder is rotated with a set speed: this determines the shear rate inside the annulus (gap between the cylinders). The liquid tends to drag the exterior cylinder round and the force it exerts on that cylinder (torque) is measured and then converted to a shear stress (cross section presented in **Fig. 1.10**).

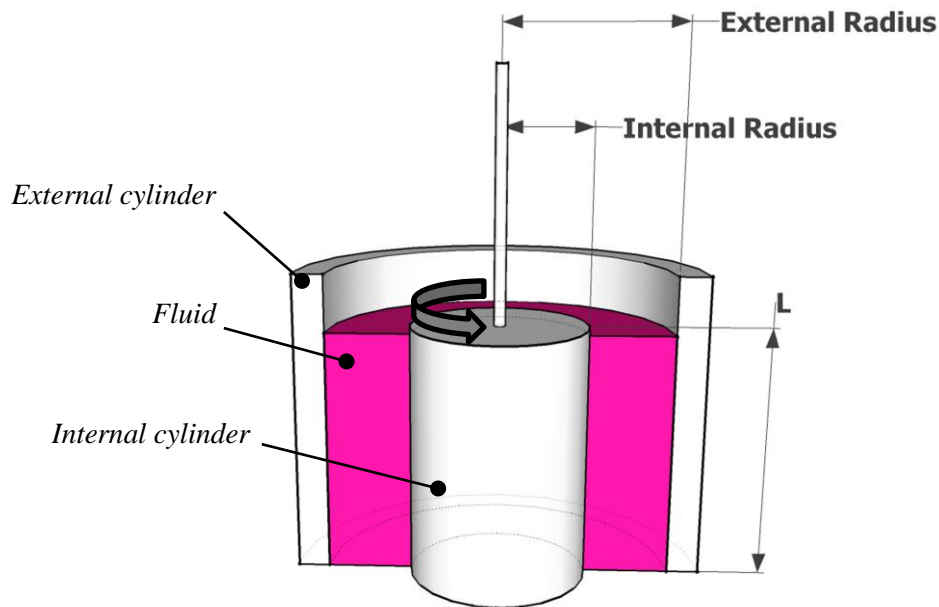


Fig 1.10: Concentric Cylinder Rheometer

If $\delta = r_e/r_i$ is the ratio between the external and internal radius and M is the measured torque, the shear stress is:

$$\tau = \frac{1 + \delta^2}{2000 \cdot \delta^2} \cdot \frac{M}{2\pi L \cdot r_i^2 \cdot C_L} \quad (1.7)$$

Where C_L is an empirical value equal to 1.1 for Newtonian liquids and up to 1.2 for shear thinning liquids.

1.2.3.2 Complex Viscosity

With a rheometer it is possible to investigate many properties of a liquid or suspension and in particular the viscoelastic variables. In general, viscoelasticity is a superposition of properties characteristic for liquids (viscous dissipative losses) and solids (storage of elastic energy) that lead to a delayed development of stresses and deformations in time (¹⁴).

In all the fluids exists a natural resting state of the microstructure, which represents the state of minimum energy. When such liquids are deformed, the thermodynamic forces try to restore the initial configuration, in the same way that a deformed spring tries to reach its original length. The elastic component arises every time the system stored energy: this might be potential (as a stretched polymer segment) or entropic energy (as polymer random coil deformed from its spherical rest state). The elastic force manifests itself at small deformations as various elastic moduli (such as the storage modulus) and all the liquids show an elastic response at a short enough time or high enough frequency. The viscous component is not the consequence of a conservative force but comes from dissipative forces. For example any kind of entity in movement inside a liquid continue phase or the sliding of polymeric chains over one another contribute to dissipates energy. Many studies are focused on the linear viscoelasticity: linear viscoelastic materials are those for which there is a linear relationship between stress and strain (at any given time). Linear viscoelasticity is a reasonable approximation under relatively low stress. The linear viscoelastic behavior is described by differential equations, where the coefficients are constant and they represent material parameters as the viscosity or the elastic modulus, and they cannot change as the stress changes. The equation that describes the linear viscoelastic behavior, for solids and liquids, is:

$$\left(1 + \alpha_1 \frac{\delta}{\delta t} + \alpha_2 \frac{\delta^2}{\delta t^2} + \dots + \alpha_n \frac{\delta^n}{\delta t^n}\right) \tau = \left(\beta_0 + \beta_1 \frac{\delta}{\delta t} + \beta_2 \frac{\delta^2}{\delta t^2} + \dots + \beta_n \frac{\delta^n}{\delta t^n}\right) \gamma \quad (1.8)$$

The first approach to understand the viscoelastic behavior of a fluid is to model it through a sequence of springs and dashpots, where the first ones represent the elastic response and the second ones the viscous response. The elastic element attests that the shear stress is directly proportional to the shear strain:

$$\tau = G\gamma \quad (1.9)$$

Where G is the elastic constant of proportionality (shear elastic modulus). Time does not come into this behavior, so that if it is applied a stress τ to the unstrained model, the resultant strain γ appears instantly (if the stress is removed, the strain falls immediately to zero). The linear viscous response can be modeled using a dashpot, physically represented with a prolonged moving through a very viscous Newtonian liquid:

$$\tau = \eta\dot{\gamma} \quad (1.10)$$

Only the rate of deformation matters, and for an applied stress τ , the dashpot immediately starts to deform and goes on deforming at a constant deformation rate $\dot{\gamma}$ without any change with time until the stress is removed, and then the deformation stops immediately. From the combination of different parallels and series connections it is possible to obtain different viscoelastic models (**Fig. 1.11**). The simplest way to represent a viscoelastic liquid is the Maxwell combination: a spring and a dashpot connected in series:

$$\gamma = \tau \left(\frac{1}{G} + \frac{t}{\eta} \right) \quad (1.11)$$

Where t is the time. The Eq. (1.11), at very short times, is characterized by an immediate elastic response, $\gamma = \tau/G$, and at very long times, when $t \gg \eta/G$, by simple viscous behavior, $\gamma = \tau \cdot t/\eta$. Here η/G is called the relaxation time t_k .

Another model is the Kelvin-Voigt model that can be obtained from Eq. (1.8) if $\beta_i = \alpha_i = 0$:

$$\tau = G\gamma + \eta\dot{\gamma} \quad (1.12)$$

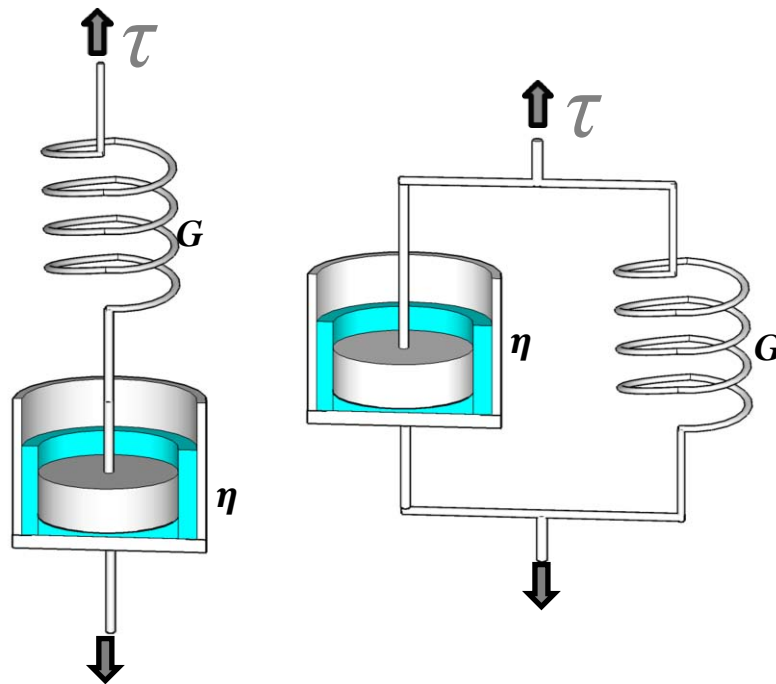


Fig 1.11: Maxwell model (left) and Kelvin-Voigt model (right).

If a constant tension $\bar{\tau}$ is applied at the instant $t = 0$, to find the total strain it is necessary to solve the above differential equation (1.12) in the variable γ :

$$\gamma = \left(\frac{\bar{\tau}}{G}\right) \left[1 - \exp\left(\frac{-t}{t_k}\right)\right] \quad (1.13)$$

The difference between the Hooke's model, Eq. (1.9), and Kelvin-Voigt's model is that the final deformation in the first case is reached instantly, in the second case there is a delay. There are also more complex models, as for example the Burger's model, made by connecting the Kelvin-Voigt's model in series with the Maxwell's one. The Maxwell and Kelvin-Voigt models may be expanded to give either multiple Maxwell models, which are usually combined in parallel, or else multiple Kelvin-Voigt models, which are usually combined in series. To detect the linear viscoelastic behavior of a fluid the "oscillatory testing" is a valid technique. For this purpose a Cone and Plate Rheometer ("Anton Paar" rheometer) has been used (**Fig. 1.12**).

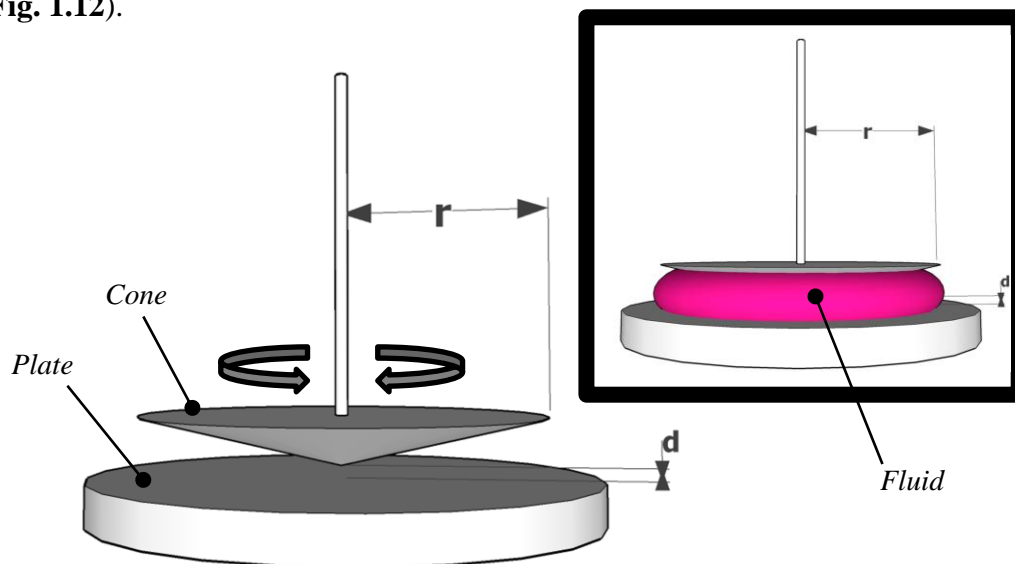


Fig 1.12: Cone and Plate Rheometer's geometry (left) and the correct amount of sample (right).

The mechanism of function for the Cone and Plate rheometer is similar to that one that governs the Concentric Cylinder Rheometer: the cone of radius r (expressed in $[m]$) rotates and the plate measures the torque M (expressed in $[N \cdot m]$), from which the shear stress is calculated:

$$\tau = \frac{1}{1000} \cdot \frac{3M}{2\pi r^3} \quad (1.14)$$

Cone and plate are separated by a gap, d . However, in the oscillating test the cone oscillates over the plate: in this way an oscillating stress or strain is applied as an input to the liquid and the resulting oscillatory strain or stress is monitored as output.

If the oscillatory test is performed by applying a sine wave shaped input of either stress or strain, through electronic methods is possible to separate the resulting sinusoidal strain or stress output into a certain amount of solid-like response and a corresponding amount of liquid like response. For an elastic solid the signal is in phase with the input, but for a viscous liquid is $\pi/2$ out of phase. For a material that has no pure solid or pure liquid like behavior, therefore for a viscoelastic fluid, the response is δ out of phase, where $0 < \delta < \pi/2$ (**Fig. 1.13**).

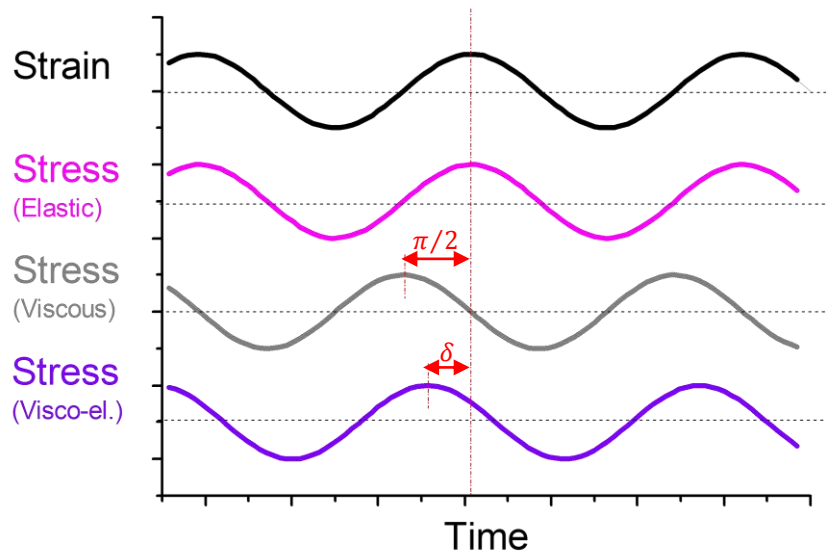


Fig 1.13: Schematic stress response to oscillatory strain deformation for an elastic solid, a viscous fluid and a viscoelastic material.

Normally the viscoelastic parameters are analyzed as function of the angular frequency. Then, at short times correspond high frequencies, and long times are related to low frequencies. For real materials elastic response dominates for high frequencies (short time), while the viscous response dominates for low frequencies (long time). The solid-like component at any particular frequency is characterized by the storage modulus, G' , and the liquid-like response is described by the complementary loss modulus, G'' . The unit of both these moduli is $[Pa]$. The values of both these parameters vary with applied angular frequency, $\omega = 2\pi f$, where f is the frequency in hertz $[Hz]$ and n is the speed $[turns/min]$ of the cone in the Cone and Plate Rheometer:

$$f = \frac{n}{60} \quad (1.15)$$

From G' and G'' is possible to obtain other parameters as:

$$\diamond \text{ Dynamic viscosity: } \eta' = G''/\omega \quad (1.16)$$

$$\text{❖ Loss tangent:} \quad \tan \delta = G''/G' \quad (1.17)$$

$$\text{❖ Complex modulus:} \quad G^* = \sqrt{G'^2 + G''^2} \quad (1.18)$$

$$\text{❖ Complex viscosity:} \quad |\eta^*| = \left[(\eta') + \left(\frac{G''}{\omega^2} \right) \right] \quad (1.19)$$

1.2.4 Dynamic Light Scattering

The Dynamic Light Scattering (sometimes referred to as Photon Correlation Spectroscopy or Quasi-Elastic Light Scattering) is a technique for measuring the size of particles typically in the sub micron region. Shining a monochromatic light beam, such as a laser, into a solution with spherical particles in Brownian motion causes a Doppler Shift when the light hits the moving particle, changing the wavelength of the incoming light. This change is related to the size of the particle. Therefore it is possible the determination of the sphere size distribution and describe the particle's motion in the medium.

The theory behind this technique is based on two assumptions:

1. The particles are in Brownian motion ("random walk"). In this situation the probability density function associated to the position of the particle going under a Brownian movement is:

$$P(r, t|0,0) = (4\pi Dt)^{-\frac{3}{2}} \exp\left(-\frac{r^2}{4Dt}\right) \quad (1.20)$$

Where D is the diffusion constant.

2. The second assumption is that the suspension there are spherical shaped particles with a diameter small compared to the molecular dimensions. The Stoke-Einstein equation gives the diffusion constant:

$$D = k_B T / 6\pi\eta a \quad (1.21)$$

Where a is the radius of the beads, k_B is the Boltzmann constant, T the temperature in Kelvin degrees and η is the viscosity of the solvent.

The light scattering analysis gives information about the particle's position and then it is possible to determine the radius of the beads with the formulas (1.20) and (1.21).

1.2.5 UV-VIS Spectroscopy

This method takes advantage of the capability of many molecules to absorb ultraviolet or visible light. The UV-VIS spectroscopy is based on the excitation of valence electrons. When radiation interacts with matter, a number of processes can occur, including reflection, scattering, absorbance, fluorescence/phosphorescence (absorption and reemission), and photochemical reaction (absorbance and bond breaking). When light passes through or is reflected from a sample, the amount of light absorbed is the difference between the incident radiation (I_0) and the transmitted radiation (I). The amount of light absorbed is expressed as either transmittance or absorbance. The transmittance is expressed as:

$$T = \frac{I}{I_0} \cdot 100 \quad (1.22)$$

And the absorbance is defined as:

$$A = -\log_{10} \frac{T}{100} \quad (1.23)$$

UV-visible spectra generally show only a few broad absorbance bands; therefore this technique provides a limited amount of qualitative information. Most absorption by organic compounds results from the presence of π bonds. A molecular group containing π bonds is called chromophore, and in the following **Table 1.2** are listed the wavelengths of some chromophore's absorbance peaks:

Cromophore	Formula	λ_{max} (nm)
Ketone	RR'C=O	271
Aldehyde	RHC=O	293
Carboxyl	RCOOH	204
Amide	RCONH ₂	208
Ethylene	RCH=CHR	193
Acetylene	RC=CR	173
Nitrile	RC=N	<160
Nitro	RNO ₂	271

Table 1.2: Wavelengths of some chromophore's absorbance peaks.

The presence of an absorbance band at a particular wavelength often is a good indicator of the presence of a chromophore. However the position of the absorbance maximum is also function of the molecular environment of the chromophore, the solvent, the pH and the temperature.

1.2.6 Raman Spectroscopy

This is a spectroscopic technique based on inelastic scattering of monochromatic light, usually from a laser. The Raman spectroscopy is a method of determining modes of molecular motions, especially vibrations. The laser light interacts with molecular vibrations, resulting in the energy of the laser photons being shifted up or down. The shift in energy gives information about the vibrational modes in the system. The difference between the IR and the Raman spectroscopy is that in the first one is analyzed the absorbed radiation, while in second case is the Raman scattered radiation to be investigated (**Fig. 1.14**).

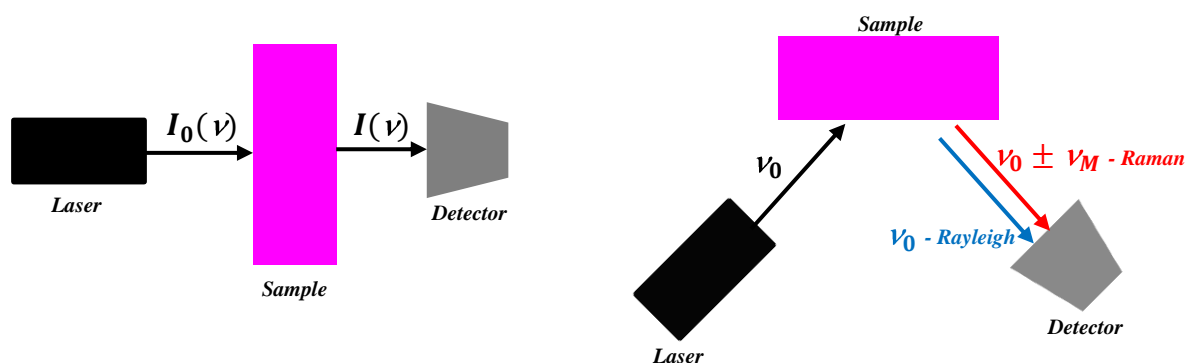


Fig. 1.14: IR Spectroscopy - Absorption (left) and Raman Spectroscopy - Scattering (right).

The Raman effect comprises a very small fraction, about one in 10^7 of the incident photons, so its detection is difficult. The Rayleigh scattering is an elastic interaction (no kinetic transfer of energy between molecule and photon, so the frequency of the scattered photon is more or less equal to the one of the incident photon). The Raman scattering is, instead, an inelastic interaction with a transfer of energy, so the scattered photon has a different frequency.

The Raman spectrum is a plot of the intensity of Raman scattered radiation as a function of its frequency difference from the incident radiation (expressed in wavenumbers): this difference is called the “Raman shift”.

Classically, the observed intensity of Raman scattering is defined as:

$$I_R = \mu(\nu_0 \pm \nu_j)^4 \alpha_j^2 Q_j^2 \quad (1.24)$$

Where μ is the reduced mass, ν_0 is the laser light frequency, ν_j is the frequency of the j^{th} mode (where the term mode means the kind of molecular vibration), Q_j the displacement and α_j is the polarizability of that mode. Raman spectroscopy is commonly used in chemistry, since vibrational information is specific to the chemical bonds and symmetry of molecules. Therefore, it provides a fingerprint by which the molecule can be identified.

1.2.7 Scanning Electron Microscopy (SEM)

This kind of microscope uses a collimated electron beam that scans the surface of the sample producing better images with high resolution (till 1nm).

The electron beam can be produced by different sources and it is focused by one or two condenser lenses to a spot about 0.4nm to 5nm in diameter. The beam is then deflected in the x and y axes in order to scan in a grid fashion over a rectangular area the sample surface.

1.2.8 Mechanical tensile test

The tensile test of thin film concerns to apply an increasing deformation to the sample, measuring the main mechanical properties and behavior until the break. The measured properties are:

- ❖ Stress at break (resistance): the last stress registered before the breaking of the sample.
- ❖ Elastic modulus (stiffness): it's the proportional constant between stress and deformation in the elastic range.
- ❖ Tensile energy absorption (toughness): total energy absorbed per unit surface of the specimen up to the point of rupture;
- ❖ Strain at break (deformability): measures the elongation percentage that sample reach before the breaking.

The tensile test has been conducted at Innventia, thanks to collaboration with the Material Chemistry Division of Stockholm University.

1.2.9 WVTR test

This method tests the water vapor permeability of a membrane. For this purpose it has been used a special trap for water vapor, with a particular design (section presented in **Fig. 1.15**). Inside the cup has been put a small quantity of dried silica gel (20 grams) in order to establish a gradient of water concentration with the external environment (at 23°C and 50% of Relative Humidity) and attract the water molecules. The Water Vapor Transmission Rate (WVTR) is defined as steady water vapor flow in unit time through unit area of a body, normal to specific parallel surfaces, under specific conditions of temperature and humidity at each surface:

$$WVTR = \frac{m}{t \cdot A} \quad (1.25)$$

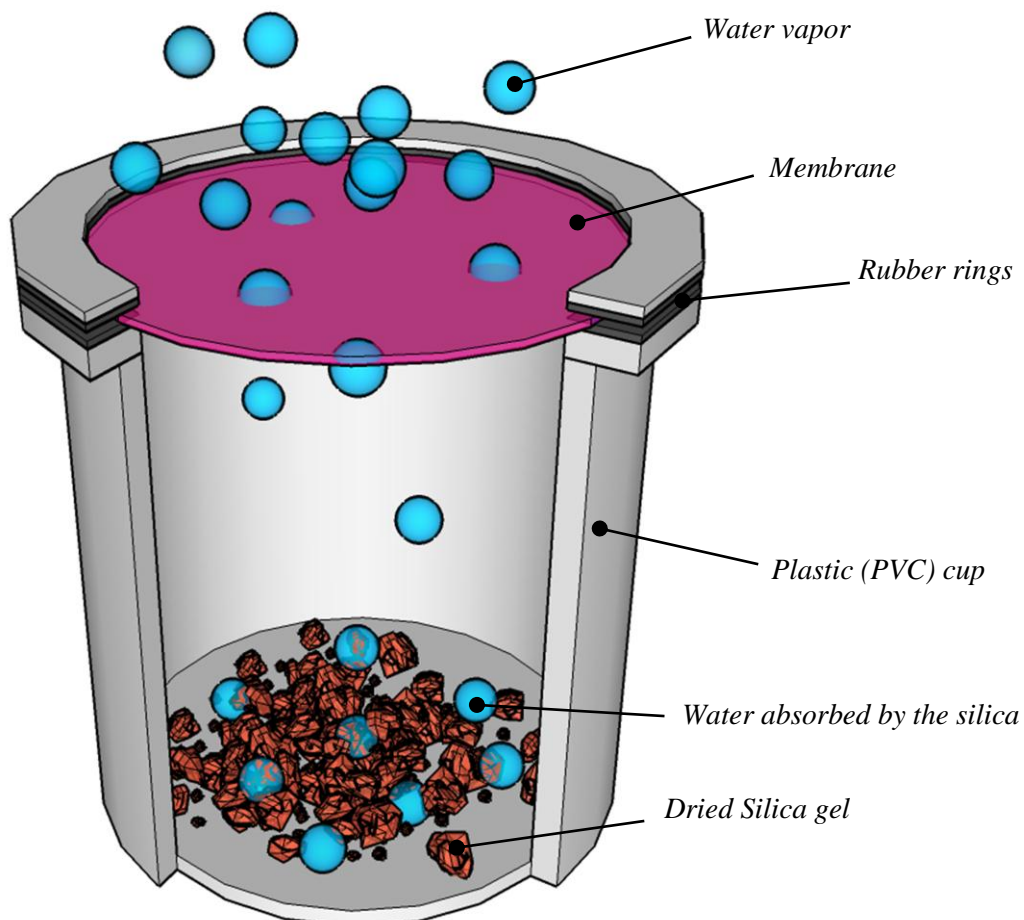


Fig. 1.15: Water trap.

Where m is the mass of water absorbed by the dried silica in the time t (expressed in days) and A is the tested area. Therefore, what is measured in weight change is the water absorbed by the silica gel, i.e. the water passed through the membrane at the established time and tested area. The WVTR is measured in $[g/(d \cdot m^2)]$.

CHAPTER 2

RHEOLOGICAL PROPERTIES OF CNF SUSPENSIONS

The study of CNF suspensions is a complementary and not negligible part in the characterization of CNF material, since some of the final membrane properties are related to the drying process and to the state of the initial suspension. For instance, the presence of clusters and agglomerates in aqueous CNF-system can still be present in the dried film: in that case the advantage of a nano-filler is lost and the mechanical and barrier properties will be consequently influenced. Furthermore, it is vital to recognize the nature of these fiber suspensions, if they behave as a colloid made by rigid-rod shaped particles (¹⁵) or more as a dilute polymer suspension, in which the single fibers are like semi-flexible polymeric chains (¹⁶). Since the preparation of such films is a process involving different dynamics, as the mixing, the application of vacuum and the final water evaporation, it is essential to understand how CNF behave in the medium when different flow fields are applied. Generally fiber suspensions can be considered structured fluids that show features (shear thinning (⁴²), viscoelasticity (⁴³) and Weissenberg effect (⁴¹)) similar to those of polymer melts and solutions. In particular, as it will be possible to see in Chapter 3, the nano-fibrillated fibers have a high aspect ratio (~ 100) and they are not completely rigid as stick, but they have an entangled configuration, similar to a “spaghetti” system. Therefore, it seems reasonable consider this kind of fiber as a semi-flexible macromolecule in solution. As previously mentioned in §1.1.1 the CNF receives a carboxymethylation pre-treatment: the presence of carboxylate groups on the surface lead to electrostatic repulsion between the fibrils. The carboxylate content with negative surface charge, which causes this electrostatic repulsion, is typically 0.5 mmol/g (¹⁷). Anyway, the suspensions provided for this study have been previously treated and modified by Innventia Group, so the aim of this work is not to analyze the stability of such suspensions, but just characterize their rheological behavior, evaluating the effect of graphene oxide and/or calcium ions. In particular, eventual cations present (added) in solution should modify the reciprocal electrical interaction between the fibers (¹⁸).

Normally the analysis of rheological parameters is applied for industrial purposes, to solve practical problems (design a plastic part, analyze a Non-Newtonian flow through a pipe, etc) or in science for the characterization of new materials (¹⁹). In this study rheology is used to examine the behavior of CNF suspension and the effects of Graphene Oxide and Calcium Ions on the viscoelastic and shear thinning properties. All rheological properties depend on the structure of the suspension, which is determined by dispersion medium properties, flow field applied, fiber characteristics and interactions (⁴⁰).

2.1 Experimental conditions

The viscosity depends on many factors, as temperature, concentration and pressure. The effect of the temperature on a Newtonian fluid (Newtonian means that shear viscosity is constant over the shear rate) follows the Arrhenius law:

$$\eta = A \cdot \exp\left(\frac{E}{RT}\right) \quad (2.1)$$

Where A is a constant, R is the universal gas constant, T the temperature in Kelvin and E is the activation energy (that measures the height of a potential energy barrier associated with the force needed to produce elemental quantum steps in the movement of molecules). Eq. (2.1) attests that the shear viscosity decreases with the temperature. The rheological properties have a strong dependence from the CNF fibers concentration (²⁰) and in particular the shear viscosity increases when the CNF concentration increases. The effect of pressure on viscosity is such that as the pressure increases, the viscosity increases; however the extent is quite small and can be neglected. For the shear viscosity analysis the Coaxial Cylinder rheometer (**Fig. 1.10**) requires 20ml of fluid, while for the oscillating test the optimal quantity (**Fig. 1.12**) is 160 μ l. In this study for all the rheological measurements the temperature is maintained constant at 293K (equal to 23°C, the room temperature).

2.2 Shear Thinning Behavior

First of all the shear thinning behavior has been analyzed, in order to determine if such suspensions can be considered as Newtonian or Non-Newtonian fluids. After that, oscillating tests have been used to determine the viscoelastic properties. CNF suspensions show a shear thinning behavior; this means that the viscosity decreases as the shear rate increases (**Fig. 2.1**). For low shear rate the suspension appears with a zero-shear viscosity η_0 , while for high shear rates the viscosity approach to a lower value, η_∞ . Shear thinning of fibers (with an

aspect ratio ≥ 100) suspensions has been already demonstrated for nylon, glass and vinylon fibers in glycerin⁽⁴²⁾ and it depends by many parameters as: fiber aspect ratio, flexibility (*flexibility* $\propto 1/EI$, where E is the fiber's Young's modulus and I is the area moment of inertia defined as $I = \pi r^4/4$; r is the radius of the fiber, imaging it as a cylinder), adhesive contacts between fibers (that depend by fiber's surface morphology and chemical composition) and concentration. The decrease in viscosity of **Fig. 2.1** could be explained as the disentanglement and the progressive alignment of the fibers along the directional fluid field generated by the increasing shear rate. Therefore, a more ordered structure opposes an inferior shear rate and the suspension results to have an inferior viscosity. Also, CNF suspensions can demonstrate a time-dependent rheological behavior (thixotropy)⁽²¹⁾. Thixotropy can be defined as "decrease [in time] of ... viscosity under constant shear stress or shear rate, followed by a gradual recovery when the stress or shear rate is removed"⁽²²⁾.

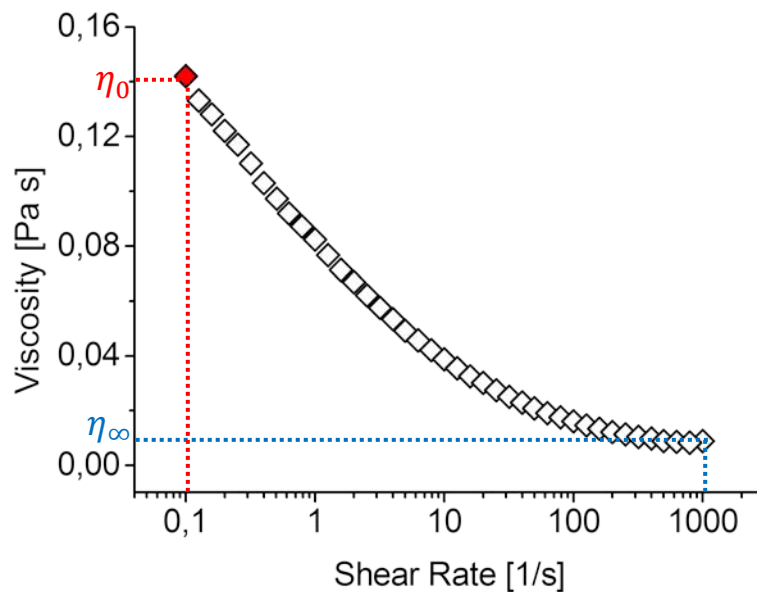


Fig. 2.1: Viscosity vs Shear rate for a pure CNF suspension (*conc.* = 2,3mg/ml).

One of the most common ways of measuring thixotropy is to perform a loop test: this means to increase the shear rate (or sometimes shear stress) from zero to a maximum value, and then to return at the same rate to zero⁽²³⁾. The evaluation of the area produce by such hysteresis loop is a rough measure of thixotropy, for a quick and qualitative procedure. However, the least laborious evaluation to determine the thixotropic degree involves measuring the distance between the up and down flow curves at mid-point of the applied shear rate range⁽²⁴⁾. For highly thixotropic fluids the up and down curves are far away to each other, enclosing a large area⁽²⁵⁾.

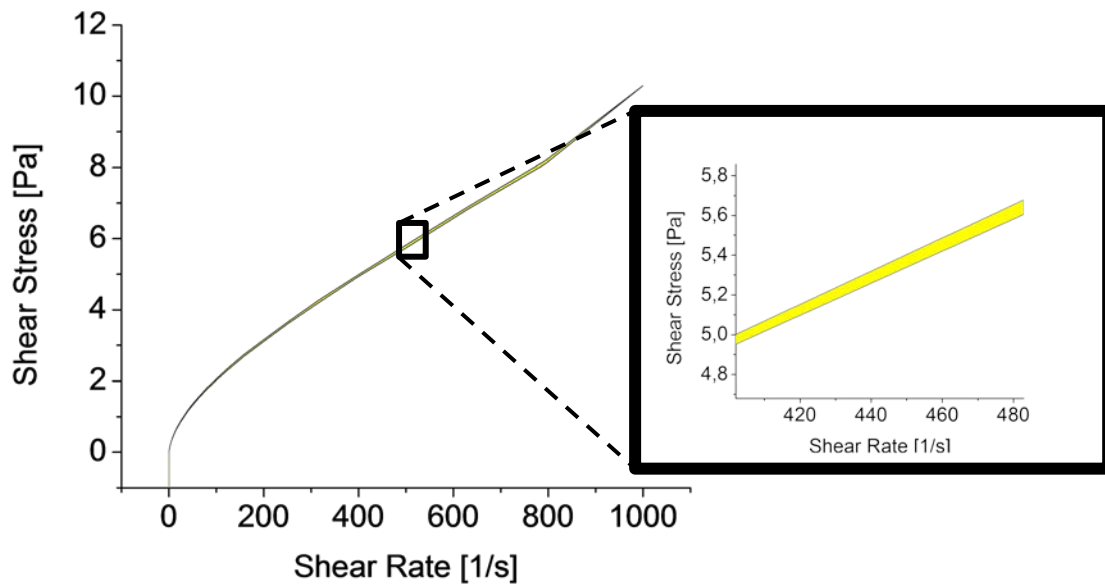


Fig. 2.2: Breakdown area for a 2,3mg/ml NFC suspension.

In **Fig. 2.2** is possible to see the hysteresis cycle produced by a shear rate loop test performed on a 2.3mg/ml CNF suspension. The “breakdown area” enclosed in the cycle is really small (the up and down curves almost overlay each other) and this means a not pronounced thixotropic behavior.

The shear thinning behavior is evident also for CNF suspensions containing Graphene Oxide. The quality of such bi-component depends by many factors, but the mixing is an essential procedure to assure a good dispersion of all the phases inside the media, preventing the formation of agglomerates.

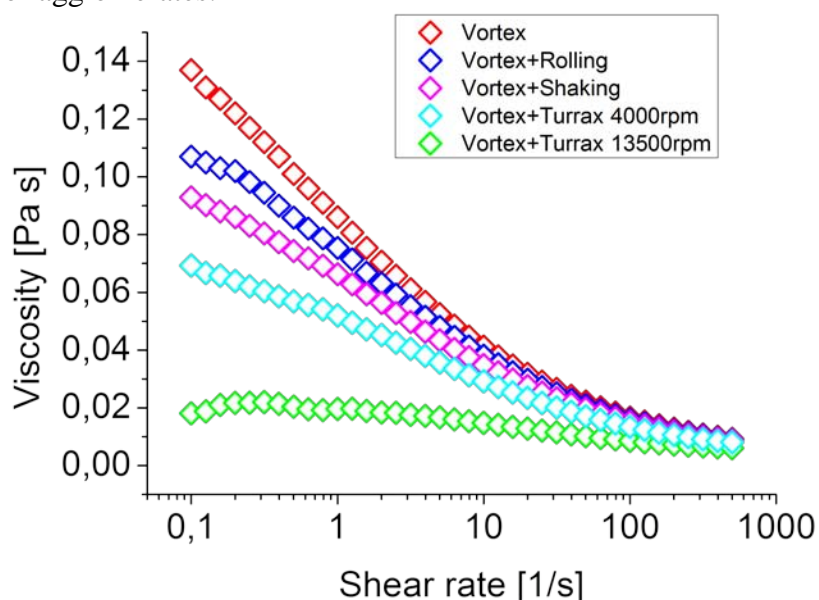


Fig. 2.3: Shear Viscosity for NFC-2,5%GO mixed with different techniques.

Therefore, different mixing techniques (§1.2.1) have been tested, investigating in particular their rheological properties. **Fig. 2.3** shows that the simple vortex mixing has the highest

shear viscosity, while Turrax at 13500rpm (maximum speed) for one hour shows the lowest one. So, more is the energy put inside the system, or in other words, the higher the applied shear/strain, the smaller is the viscosity. The “mixing strength” can be classified for different techniques as: *Vortex* < *Rolling* < *Shaking* < *Turrax 4000rpm* < *Turrax 13500rpm*. This is reflected on rheology: $\eta_{vortex} > \eta_{rolling} > \eta_{shaking} > \eta_{tur.4000} > \eta_{tur.13500}$. Furthermore, for high energy mixing there is a reduced shear thinning effect: a vigorous mixing produce a more Newtonian fluid (viscosity independent from shear rates). This behavior could not depend by thixotropy: the time between the suspension preparation and the rheometer analysis was about 15-20 minutes. Therefore, the microstructure had enough time to recover its initial configuration. The reducing in viscosity could be related with a better dispersion of GO inside the “fiber network” of the suspension. In fact, Graphene Oxide flakes are negatively charged (²⁶), and an efficient mixing can better disperse them between the negatively charged CNF fibers: the electrostatic repulsion decreases the reciprocal adhesive interactions (decreasing of shear thinning behavior and viscosity). It is well known that the “flocculation” phenomena is related to wider ranges of shear rates over which shear thinning is present: a prolonged Newtonian behavior over a wide range of shear rates proof the good homogeneity of the suspension (⁴⁰). The better dispersion can be related also with the breaking of the weak GO flakes. For instance, higher is the rotational speed of the Turrax, higher is the kinetic energy of the fluid through the rotor-stator arrangement and the GO flakes will impact with much more violence (higher intensity and number of impacts) on the metallic structures of the mixer. Therefore, high speeds of mixing means high kinetic energy of the GO flakes, and therefore high probability to break them after collisions with the surrounding. Smaller GO flakes can “diffuse” better between CNF fibers and the suspensions show an inferior resistance to flow.

UV-Vis spectroscopic analysis has been conducted for CNF-GO suspensions mixed for different times with “turrax” at maximum power (**ANNEX A-1**).

2.3 CNF suspension as high molecular weight polymer suspensions

The evaluation of parameters as the Storage and Loss Moduli is fundamental for the determination of the viscoelastic properties.

From the oscillating test results (§1.2.3.2, **Fig. 1.12**) interesting interpretations can be done, about the behavior and the characteristic microstructure of CNF suspensions.

As mentioned in the beginning of this chapter, CNF suspensions are sometimes treated as a colloid made by rigid or semi-rigid rod shaped particle, otherwise as a polymeric suspension. In the literature appear many different expressions to describe the CNF fibers: polymer whiskers (²⁹), CNF particles (³⁰), semiflexible rod-like macromolecular chain (¹⁶)...etc. This can generate confusion during the interpretation of rheological data, because in rheology exist many different models (for polymer solutions, gels, colloids, melts, particle suspensions...etc), and many of them are valid just for certain condition of CNF concentration or aspect ratio. In fact, the dynamic storage modulus increases in proportion to the $9/4^{\text{th}}$ power of the fiber concentration (¹⁵): this power is coincident to that one for polymer gels. However for diluted CNF suspensions, the approximation to a rod-like particle suspension is more suitable, since the excluded volume of one fiber is calculated consider it as a rigid long cylinder of diameter d and length l (³¹). Defining V_a as the actual volume of fiber and V_e as the effective volume swept out by a rotating fiber (and equals to a sphere with a diameter of one fiber length):

$$V_a = (d/2)^2 \pi l \quad (2.2)$$

$$V_e = \frac{4}{3} (l/2)^3 \pi \quad (2.3)$$

Moreover the critical fraction, φ_0 , at which fibers are no longer able to undergo free rotation, is:

$$\varphi_0 = \frac{V_a}{V_e} = \frac{(d/2)^2 \pi l}{\frac{4}{3} (l/2)^3 \pi} = \frac{3}{2} \left(\frac{d}{l} \right)^2 = \frac{3}{(2p^2)} \quad (2.4)$$

Where $p = l/d$ is the aspect ratio of the fiber.

So, when the CNF fraction is higher than φ_0 , the effect of the fiber steric interaction becomes important. Since the value of φ_0 is really small, also few fibers present in the media are still able to perceive their reciprocal presence. For a $2,3 \text{ mg/ml}$ CNF suspension, considering an aspect ratio $p \sim 100$: $\varphi_0 = 3/(2p^2) = 0,015 \text{ vol}\%$. Therefore, for this value of φ_0 , the critical mass concentration (called also overlap concentration) is: $C_0 = \varphi_0/\rho = 0,00935 \text{ wt}\%$, where the fiber density, ρ , has been taken equal to 1600 kg/m^3 (§Chapter 3).

However, this critical concentration is based just on geometrical considerations, since that in the above discussion are not mentioned the short- and long- range interactions as the van der

Waal and electrostatic existing between carboxymethylated CNF fibers. As previously mentioned, the CNF fibers are negative charged: this is performed in order to prevent the agglomeration, because without any kind of pre-treatment, as the carboxymethylation, Cellulose nanofibrils are able to form gel clusters, in particular at low fibril concentrations (³²). In that case the cross-linking between fibers is physical (hydrogen bonds, van der Waals interactions, hydrophobic-hydrophobic interactions) (³³).

Performing a simple oscillating test on a 2,3mg/ml CNF suspension and plotting the storage modulus, G' , over the angular frequency, ω , it is possible to see a tendency like that one presented in **Fig. 2.6**. In classical viscous fluids, the elastic and loss modulus have a characteristic frequency dependency, that is, $G' \propto \omega^2$ and $G'' \propto \omega^1$, whereas an ideal gel behaves elastically and $G' \propto \omega^0$ (the storage modulus is independent from the frequency ω).

The interesting aspect is that for intermediate angular frequency ($0,1\text{Hz} \leq \omega \leq 15\text{Hz}$) the storage modulus follows a power-law in which the exponent is $2/3$, i.e., $G' \propto \omega^{2/3}$. This relation of proportionality doesn't change for lower CNF concentration than 2,3mg/ml, i.e., 1,15mg/ml, 0,46mg/ml and 0,23mg/ml.

What is surprising is that $G' \propto \omega^{2/3}$ is the typical behavior for dilute high molecular weight polymers in theta solvents (³⁴). A theta solvent is a solvent in which polymeric chains assume exactly their random walk coil dimensions. Thermodynamically, the excess chemical potential of mixing between a polymer and a theta solvent is zero.

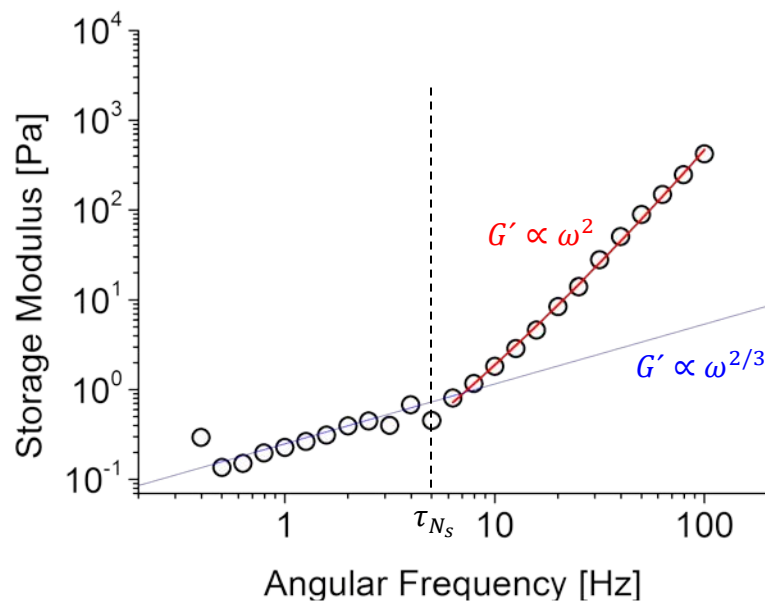


Fig. 2.6: G' vs ω for a 2,3mg/ml NFC suspension.

This prediction considers polymers as series of bead and springs chains: the springs mimic the elastic forces and beads produce hydrodynamic drag (**Fig. 2.7**). The simplest beads and spring model is the elastic dumbbell, which has a single spring connecting two beads. When one bead moves an hydrodynamic force arises on the other beads. The model that combines the beads-spring assumption with the effect of hydrodynamic interactions exerted by polymeric coils in a theta solvent is given by the Zimm Theory (³⁵). For intermediate angular frequencies it relates the loss and storage moduli as:

$$G'' - \eta_s \omega = \sqrt{3} G' \propto \omega^{2/3} \quad (2.5)$$

Where η_s is the viscosity of the solvent and $\sqrt{3}$ is a proportionality constant confirmed experimentally for polymer solution. For CNF suspension in this study this proportionality constant is lower than 1. However, for high frequencies the CNF suspension behaves like a viscous fluid ($G' \propto \omega^2$). Above the intermediate-frequency regime, which spans from the inverse of the longest Zimm time, $1/\tau_1$, to the inverse shortest time, $1/\tau_{N_s}$, there is the high frequency regime ($\omega > \tau_{N_s}$). For $\omega = \tau_{N_s}$ the Zimm theory predicts a crossover from $G'' - \eta_s \omega \sim \omega^{2/3}$ to $G'' - \eta_s \omega = 0$. Therefore, for high frequencies the dynamic viscosity $\eta' = G''/\omega$, that is a measure of viscous dissipation, is predicted to be equal to η_s , without any kind of contribution from the polymer.

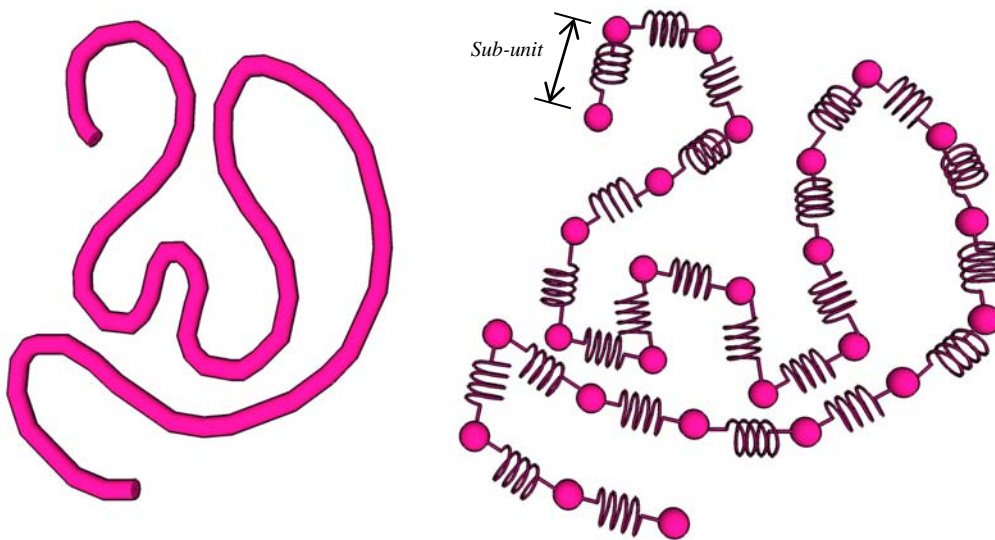


Fig. 2.7: A polymeric coil (left) and the spring-beads model (right).

At high frequency the deformation is too fast for the individual spring of the elastic dumbbell to relax, and the polymer does not dissipate energy. Experimentally, for polymeric solutions,

G''/ω approach a constant η'_{∞} at high ω , and this η'_{∞} is usually greater than the solvent viscosity (³⁴). For the 2,3mg/ml CNF suspension is $\sim 0,2 \text{ Pa} \cdot \text{s}$ (**Fig. 2.8**).

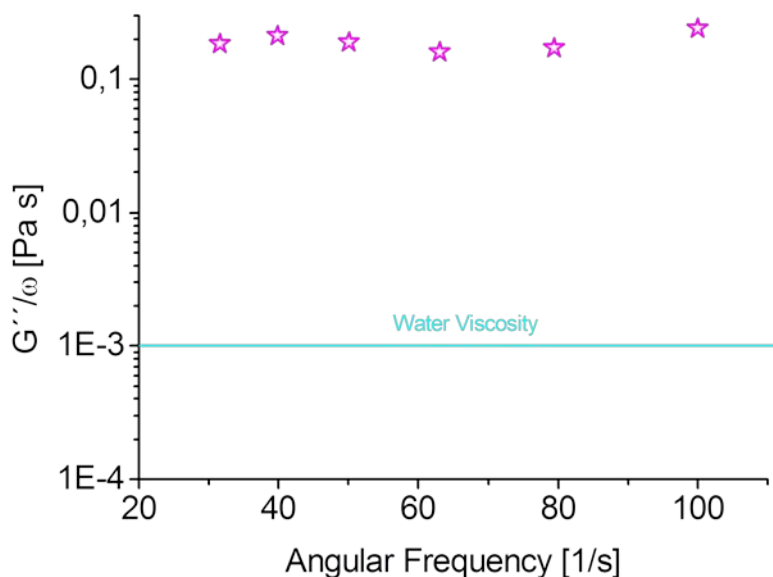


Fig. 2.8: G''/ω (for $\omega > \tau_{Ns}$) measured in 2,3mg/ml NFC suspension

If the effect of hydrodynamic interactions is neglected, the model follows the Rouse prediction: in that case, $G' \propto \omega^{1/2}$ for intermediate frequencies (³⁶). This is not the case because hydrodynamic interactions in CNF semi-diluted suspensions cannot be ignored, and the tendency of G' vs ω follows the Zimm prediction. However for a right determination of dynamic moduli through the theory normally applied to polymers, it is necessary to add another variable to the system: the existence of “entanglements” between fibers (but this is not the purpose of this study, that wants to give just a qualitative interpretation).

2.4 Cross-linking of CNF suspensions

It has been showed in many studies that carboxylic groups can bind divalent cations such as Ca^{2+} (³⁹). Moreover, CNF suspension start to gel at low pH (pH<3) (¹⁸), and some reviews, also report the possibility to cross-link polysaccharides with boric acid (⁷). Examining the shear viscosity, for a constant shear rate (shear rate=0,2 Hz), as function of the linker percentage it is possible to see some tendencies. For instance, the Boric Acid seems to weakly crosslink the nanocellulose fibers: for the 0,5% of boric acid the viscosity increases only of 7% with respect to the pristine CNF. For higher concentrations of boric acid, no effects are seen. The situation is completely different considering the Calcium Ions (**Fig. 2.9**). Adding 5% of calcium increases the CNF viscosity by more than two orders of magnitude. This

means that the fluid friction is higher and a higher shear stress is required to strain the suspension. However for $0\% < \%Ca < 1.5\%$, there is an evident decreasing in viscosity.

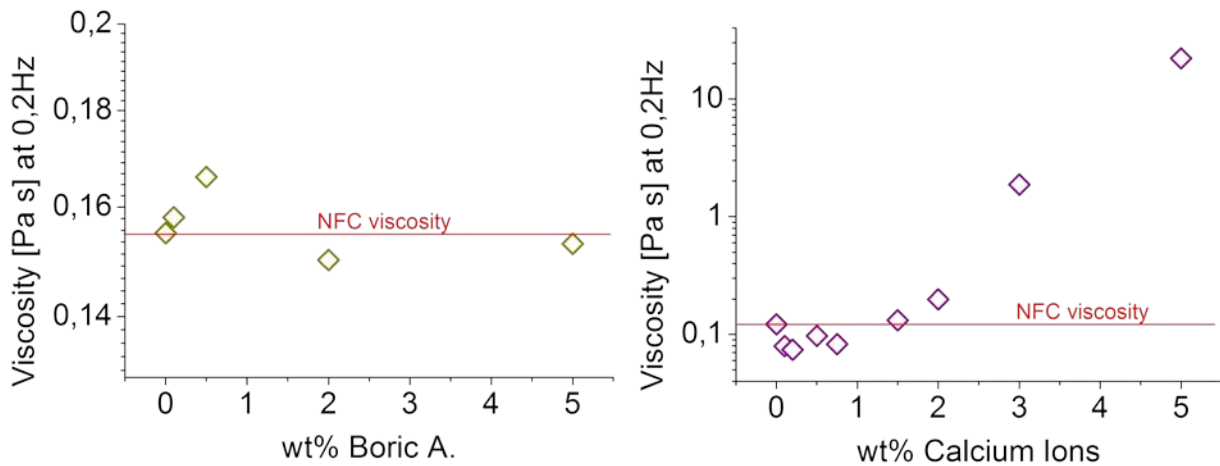


Fig. 2.9: Viscosity (for shear rate=0,2Hz) for NFC-Boric Acid (left) and for NFC-Calcium (right) suspensions. $T=5^{\circ}\text{C}$ for NFC-Boric A. and $T=25^{\circ}\text{C}$ for NFC-Calcium.

2.4.1 Power Law model for CNF- Ca^{2+} Shear Viscosity

Shear thinning means that the viscosity decreases with the shear rate: this is because the fiber configuration is forced to align itself along the flow direction caused by the rotational motion of the cylinder. At low shear rate, the suspension manifests a high friction because the fibers are randomly disposed in the space and their reciprocal interactions make difficult to align the system along the flow direction; with an increase of shear rate the majority of the fibers are aligned with the flux and the system offer a less resistance (viscosity) to be sheared. For really high shear rate the viscosities of all the suspensions approach the same value η_{∞} : this in agreement with the fact that for high shear rates the structured liquid is so well deformed along the flux direction that the effect of CNF fibers presence is minimum.

The simplest way to model the shear viscosity is through the power law model:

$$\eta = k\dot{\gamma}^{n-1} \quad (2.6)$$

Where k is called the consistency index and n the power law index. The consistency index is the viscosity (or stress) at a shear rate of 1s^{-1} . The power law index is dimensionless and ranges from 1 for Newtonian liquid towards 0 for very non Newtonian liquids: this is, in essence, a measure of non-Newtonianness. The relation (2.6) can be used when $\eta_0 \gg \eta_{\infty}$, or when η_{∞} is small. Moreover, according the power law model the relation between the shear stress and shear rate can be written as:

$$\tau = k\dot{\gamma}^n \quad (2.7)$$

Where τ is the shear stress and $\dot{\gamma}$ the shear rate.

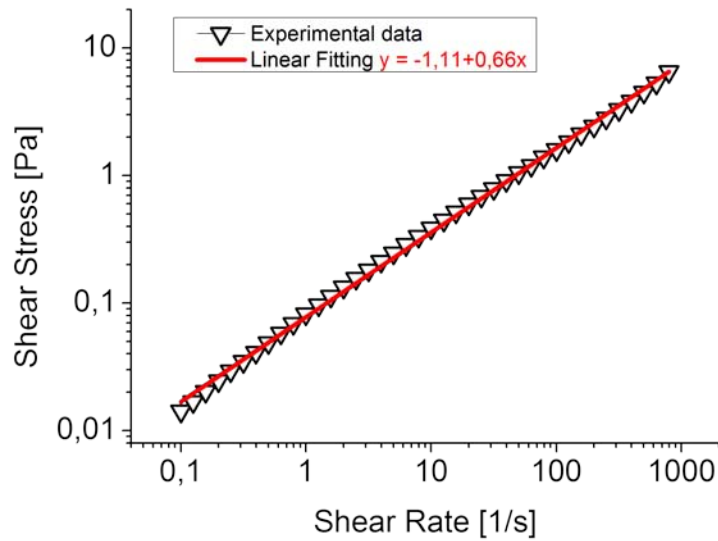


Fig. 2.10: Experimental data for a pure 2,3mg/ml NFC suspension and power law fitting.

To find n and k , that are parameters that characterize the material in the experimental condition chosen, it is useful to work with the logarithmic scale of Eq. (2.7):

$$\log \tau = n \log(\dot{\gamma}) + \log k \quad (2.8)$$

The Eq. (2.8) represents a straight line, where n is the slope and $\log k$ the intercept (**Fig. 2.10**). From the previous linear fitting it is possible to obtain: $n = 0,66343$ and $\log k = -1,11047$, so $k = 0,07754$. Through these index the shear viscosity can be modeled (**Fig. 2.11**).

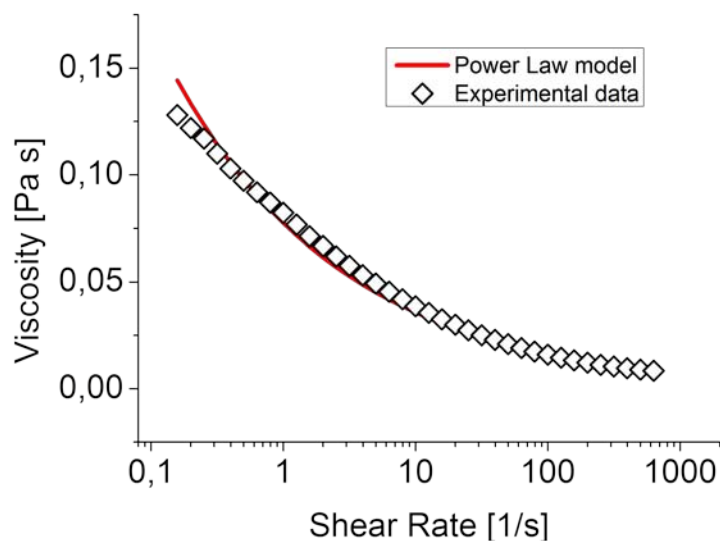


Fig. 2.11: Power law model applied for a pure 2,3mg/ml suspension.

Repeating this procedure for all the concentrations of Calcium, the values of n and k for each sample are (**Table 2.1**):

% Calcium	k	n
0	0,07754	0,66343
0,1	0,05574	0,70944
0,2	0,05412	0,72068
0,5	0,06307	0,67719
0,75	0,05744	0,68429
1,5	0,07732	0,61678
2	0,10123	0,55743

Table 2.1: Power law and consistency index for samples with different percentage of Calcium.

With these a relation between n , k and calcium concentration can be found (**Fig. 2.12**).

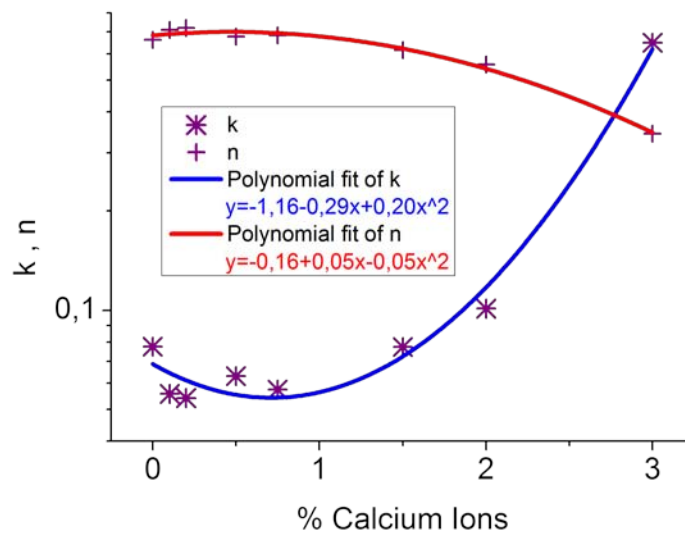


Fig. 2.12: Polynomial fitting of n and k as function of Calcium percentage.

$$\log(k) = -1,16335 - 0,28833\%Ca + 0,20243 (\%Ca)^2 \quad (2.9)$$

$$\log(n) = -0,16556 + 0,0451\%Ca - 0,0478 (\%Ca)^2 \quad (2.10)$$

From Eq. (2.9) and (2.10) it is possible to obtain approximated relations between n , k and the calcium concentration. Combining Eq. (2.9) and (2.10) with (2.6), the approximated formula that relates together the shear viscosity, the shear rate and the percentage of Calcium is:

$$\eta = (10^{-1,16335 - 0,28833\%Ca + 0,20243 (\%Ca)^2}) \cdot \dot{\gamma}^{(10^{-0,16556 + 0,0451\%Ca - 0,0478 (\%Ca)^2}) - 1} \quad (2.11)$$

Looking the **Fig. 2.13** the (2.11) seems to approximate quite good the experimental data. However, for high concentration of calcium the (2.11) starts to diverge: this is because the

suspension start to be a strong gel and the model for shear thinning fluids cannot be applied anymore.

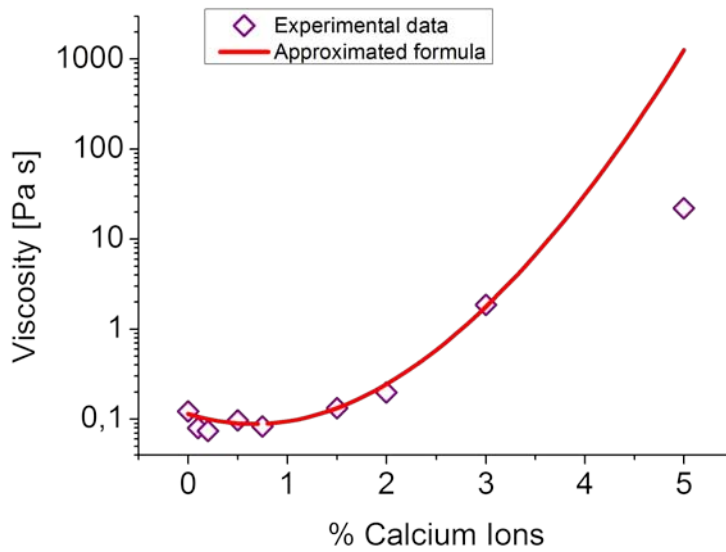


Fig. 2.13: Experimental data and approximated formula (Eq. (2.13)).

2.4.2 Viscoelastic properties of CNF- Ca^{2+} suspensions

As mentioned in §2.3, the exponent j of the relation $G' \propto \omega^j$, for intermediate frequencies, can be a proof for the viscous or elastic nature of the suspension. When calcium ions are added to a CNF suspension the power dependence of G' vs ω starts to change (**Fig. 2.14**).

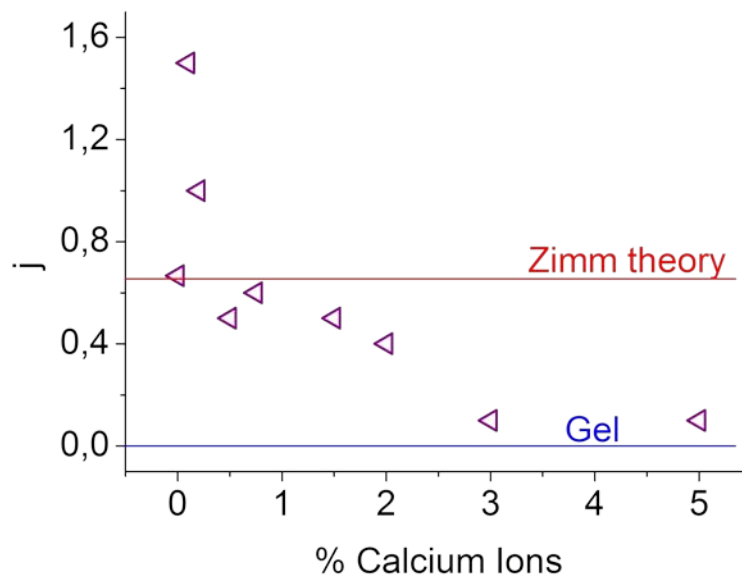


Fig. 2.14: Exponent j (of the relation $G' \propto \omega^j$) for different calcium concentrations

Therefore considering $G' \propto \omega^j$ (for $1/\tau_1 < \omega < 1/\tau_{N_s}$), the tendency of j as function of the calcium content shows a decay for high calcium concentration: j goes forward zero, i.e., $G' \propto \omega^0$. In particular $j = 0$ for $\%Ca \geq 3\%$. This independency from the frequency proofs

the gel-like behavior of the suspension, and the existing of strong interactions between calcium ions and the CNF fibers. The gelation can be defined as “... the conversion of a liquid to a disordered solid by formation of a network of chemical or physical bonds between the molecules or particles composing the liquid”⁽³⁴⁾ and it can be chemical (with the formation of covalent bonds, typically permanent at high temperatures) or physical (in this case is a result of weak intermolecular association, as clusters produced by Van der Waal forces, electrostatic attractions or hydrogen bonding). For chemically cross-linked polymeric macromolecules is valid the Kramers-Kroening relation^(34,37):

$$G'(\omega) = \frac{G''(\omega)}{\tan\left(n \cdot \frac{\pi}{2}\right)} \quad (2.14)$$

Calculating the G' (at intermediate frequencies: $0,1\text{Hz} \leq \omega \leq 15\text{Hz}$) with the above equation, for CNF-Calcium suspensions the best fitting gives $n \sim 0,63$ for 3%Ca and $n \sim 0,70$ for 5% and 20%Ca (**Fig. 2.15**). Normally, for polymer gels, n varies over the wide range 0.19-0.92 for chemically cross-linked systems.

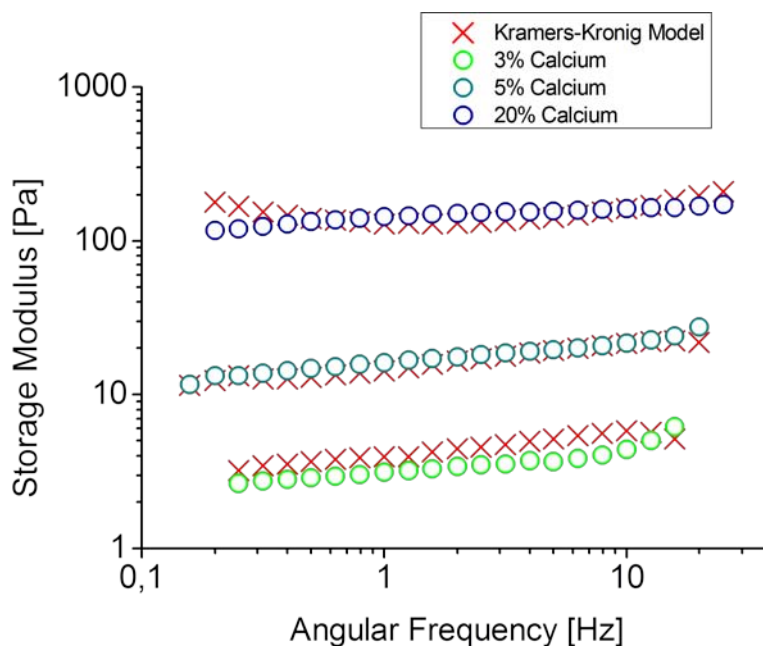


Fig. 2.15: Kramers-Kronig Model applied to Ca^{2+} -NFC suspension for high Calcium concentration

Therefore, if a CNF-calcium suspension can be modelled with an equation normally used in chemical cross-linked system (where the crosslinking is due to the formation of strong covalent bonds), it means that the interactions between the CNF fibers and the divalent calcium ions are not weak at all and lead to a formation of a strong network.

The relation between the strength of this network and the storage modulus is given by (38):

$$G'(\omega) = \Gamma(1 - n) \cos\left(\frac{n\pi}{2}\right) S \omega^n \quad (2.15)$$

Where n is the same coefficient as in Eq. (2.14), $\Gamma()$ is the gamma function and S is the strength of the gel. Finding the value of S , a comparison of different gels strength is possible. Then, the gel strength can be obtained using:

$$S = \frac{G'(\omega)}{\Gamma(1 - n) \cos\left(\frac{n\pi}{2}\right) \omega^n} \quad (2.16)$$

For $\omega = 0,501\text{Hz}$ the gel strength for the calcium concentration reported on **Fig. 2.15** are:

% Calcium	n	$\Gamma(1 - n)$	$G'(\omega = 0,501)$	$S [\text{Pa}]$
3	0,63	2,40	3	4
5	0,70	2,99	15	18
20	0,70	2,99	131	156

Table 2.2: Gel strength for 2.3mg/ml NFC suspensions with different calcium concentrations .

Table 2.2 shows that $S \propto G'$ and therefore the gel strength increases with the calcium concentration. For high angular frequencies G''/ω approach the same value, for all %Calcium (**Fig. 2.16**): at high ω the viscoelastic properties depend on the solvent.

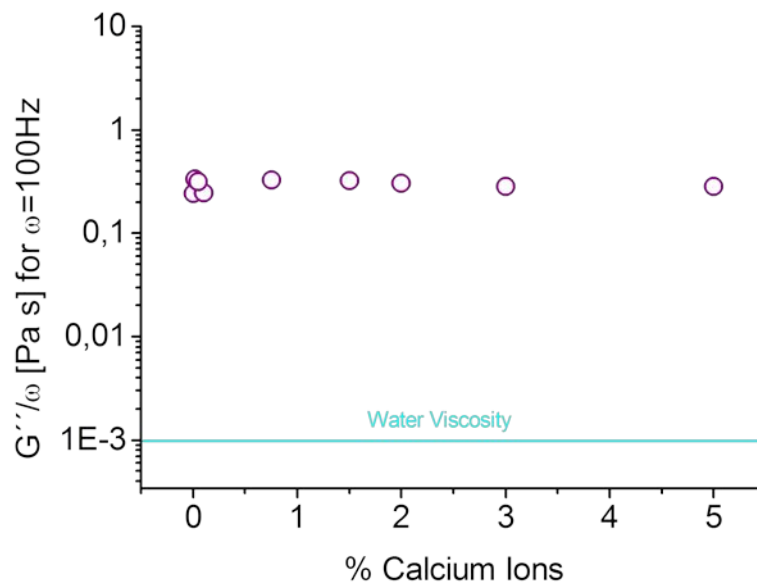


Fig. 2.16: G''/ω for different Calcium concentrations.

Analyzing more in detail the rheological properties of CNF- Ca^{2+} suspensions, there are two different and opposite tendencies for low and high calcium concentration ranges. The Storage

Modulus shows the same tendency of the shear viscosity: an initial decrease for $0\% < \%Ca \leq 1.5\%$ and then increases for higher percentage of calcium (**Fig. 2.17**).

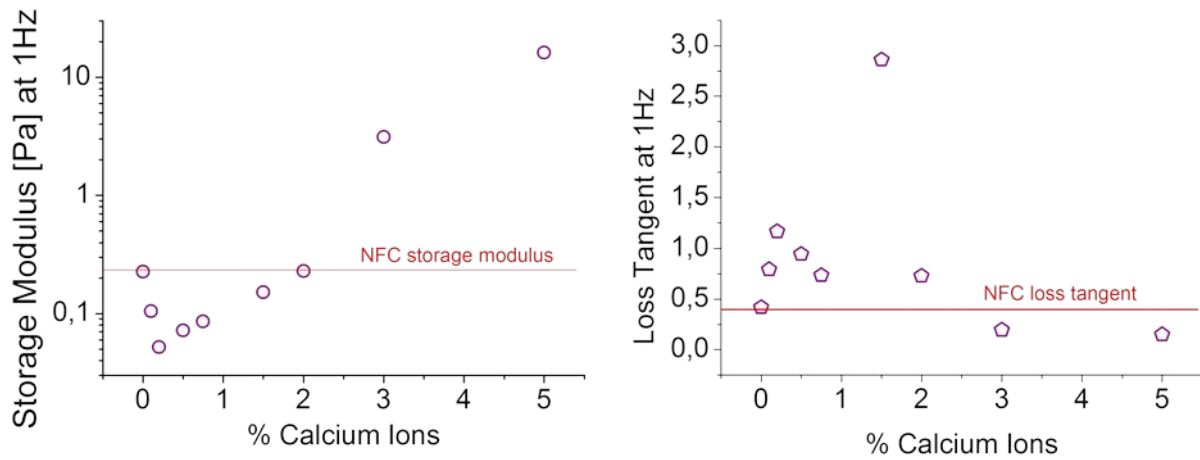


Fig. 2.17: Storage modulus and loss tangent for different calcium concentrations.

This means that for $0\% < \%Ca \leq 1.5\%$ the suspension is more liquid-like than a suspension that contains just CNF. The liquid-like behavior is more evident plotting the loss tangent parameter defined by the (1.16) in §1.2.3.1. For higher percentage of Calcium the behavior is more solid-like and this indicates a higher possibility for the system to store elastic energy. For a completely solid like behavior (just elastic response), $\tan\delta = 0$ while for a completely liquid like behaviour (just viscous response), $\tan\delta = \infty$. Therefore if the loss tangent increases the fluid becomes more liquid-like, if it decreases the fluid becomes more solid-like. The decreasing of viscosity and elastic properties for low calcium concentrations can be explained with the partial agglomeration of some fibers ⁽⁴⁰⁾. For a fibers suspension the viscosity is determined by the possibility of them to rotate in spherical zone of space of radius equal, with a good approximation, to half fiber ⁽⁴⁴⁾ (to be more precise instead of the fiber length it would be better to take the average end-to-end distance for the fiber since it is quite flexible). A small amount of Ca^{2+} can bind surface functional groups within a single fiber or from different fibers, resulting in a smaller effective rotational diameter and a higher available space for free fiber rotation. This can be the explanation for the more liquid-like behavior of the suspension registered for low calcium concentration. Since a single fiber can move in a space defined by the (2.3), without calcium ions the necessary space for the free rotation, for instance, of four fibers is equal to $4V_e$. With a small amount of divalent ions as Calcium, these four fibers can electrostatically interact and they form a fiber agglomerate that can rotate in a volume V inferior to $4V_e$ (**Fig. 2.18**).

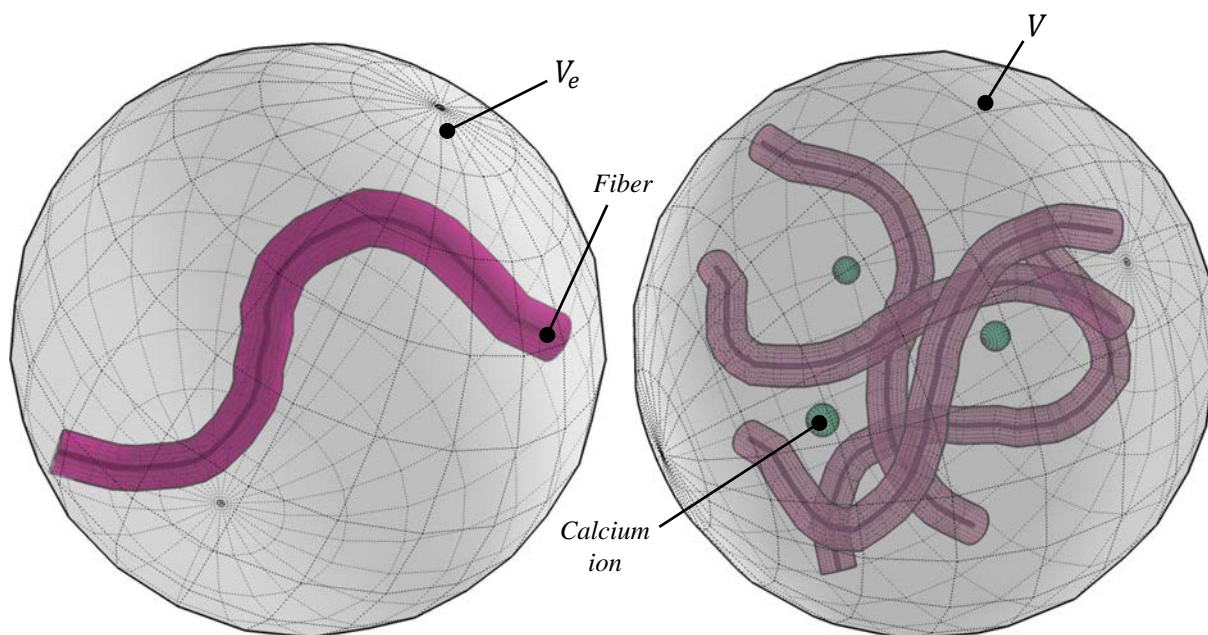


Fig. 2.18: Excluded volume for a single fiber (left) and for an agglomerate (right).

However, for an increasing concentration of calcium in the system, more coiled fibers start to interact with each other, forming a network made by electrostatic interactions: this is why the viscosity and the storage modulus increases for high percentage of Ca^{2+} .

2.5 Viscoelastic behavior of CNF-GO- Ca^{2+} suspensions

In §2.2 it has been already introduced the effect of a vigorous mixing of CNF-GO suspensions. In this section it will be investigated how the viscoelastic properties of CNF and calcium ions suspensions can be influenced by the presence of graphene oxide.

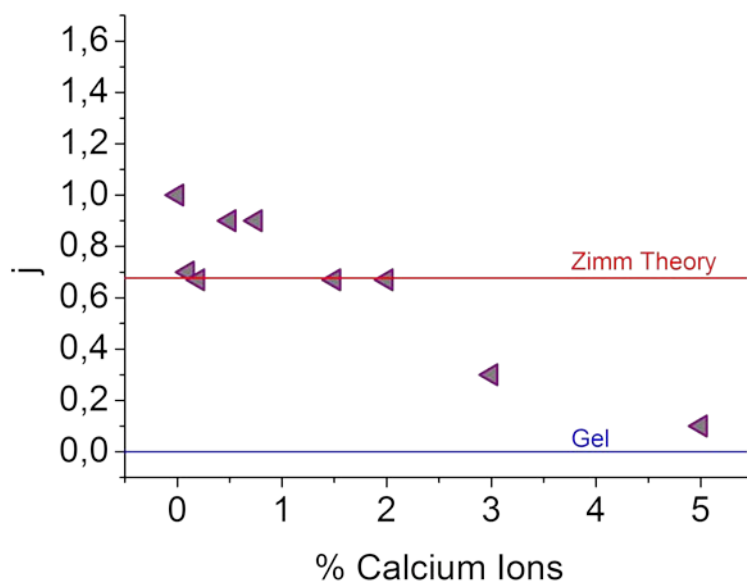


Fig. 2.19: Exponent j (of the relation $G' \propto \omega^j$) for suspensions with 5%GO and different calcium concentrations.

The relation $G' \propto \omega^j$ can be examined again in order to see if suspensions with different calcium concentrations maintain the same frequency dependence when 5% GO is added). In this case the weight percentage of GO is referred to the CNF mass, and the calcium weight percentage is related to the sum between the CNF and GO mass.

Comparing **Fig. 2.14** with **Fig. 2.19** it is possible to see that the 5% GO:

1. reduces the tendency of agglomeration for low calcium concentrations, and the Zimm proportionality relation ($G' \propto \omega^{2/3}$) is maintained for a wider range of %Ca²⁺;
2. retards the gel formation due by the calcium ions, since in **Fig. 2.19** j for 3% Ca²⁺ is higher than the one for 5% Ca²⁺.

Furthermore, GO influences all the viscoelastic properties of CNF-calcium suspensions: in particular it gives a more liquid-like behavior of such suspensions, reducing the storage modulus and increasing the loss tangent (**Fig. 2.20**).

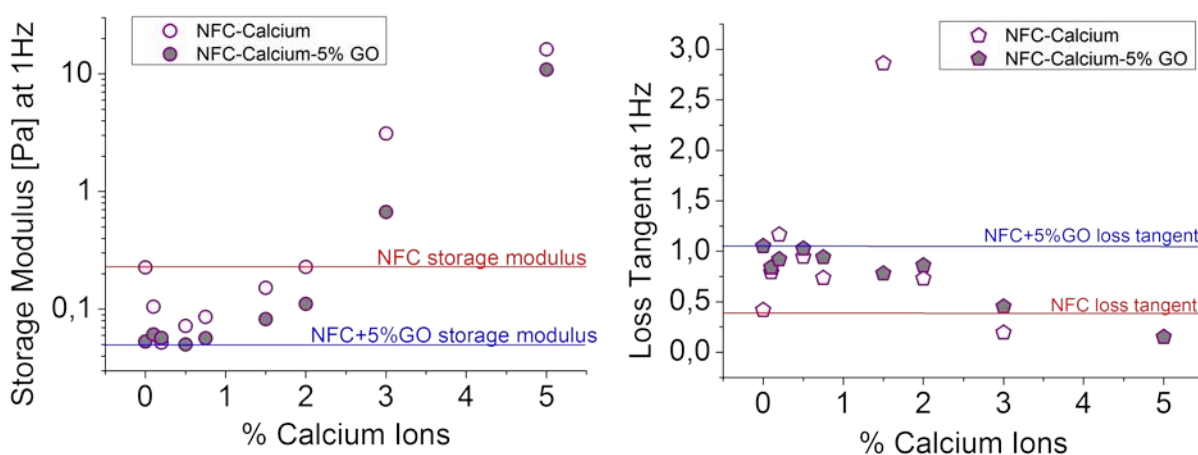


Fig. 2.20: Storage modulus and loss tangent (for angular frequency=1Hz and $T=25^{\circ}\text{C}$) for NFC-Ca²⁺-GO suspensions, as function of Ca²⁺ percentage.

2.6 Discussions

The rheology of these suspensions is not so easy to analyze, since many factors have to be taken in account. First of all, the fibers are a bit rigid (quite high elastic modulus due to the presence of crystalline regions), but flexible enough to be considered in a first approximation as big macromolecules. Under an oscillating test the reciprocal hydrodynamic interaction lead the fibers to behave as polymeric chains in their “random walk” configuration. Therefore during an oscillating fluid field applied to the suspension, for intermediate frequencies, a CNF assume a configuration in which the average end-to-end distance is not equal to its length, l , but it is $i \cdot \sqrt{N}$, where N is the number of sub-units in **Fig. 2.7** and i the

length of one subunit. This means that the fiber in particular flow conditions can assume a more coiled configuration and they are not completely rigid. Such little flexibility is well shown in next chapter (**Fig. 3.3**) and it should be possible to calculate the average end-to-end distance assuming that one sub-unit is long as a cellulose nanocrystal. The rigidity of the fibers is always related to their elastic modulus (⁴⁰): higher is the elastic modulus lower is the flexibility. However for the elastic modulus of a CNF fiber is necessary to consider its amount of crystalline and amorphous phase (Chapter 3, section §3.3.1). The crystalline domains are not flexible at all and they show high Young's modulus. Thus, if the CNF fibers are flexible it means that the amorphous fraction is not negligible and it plays a fundamental role in the mechanics.

Moreover, divalent ions, as calcium cations can crosslink CNF fibers forming a stable gel. Moreover, from the previous viscoelastic analysis it seems that calcium ions can interact also with GO flakes: GO flakes present carbonyl groups, more likely as carboxylic acids along the sheet edge (¹¹). In the literature is reported the possibility to link the edge-bound carboxylic acid groups of adjacent sheets with divalent cations (Mg^{2+} or Ca^{2+}) (⁷³). So, calcium ions have theoretically the possibility to interact with both CNF and GO flakes and this is seen in the rheology as a delayed gelling made by Ca^{2+} when GO is also present in the suspension. Moreover in situ treatment with 1wt% of divalent cations of fabricated graphene oxide paper lead to an improving of Young's modulus by 10-40% and tensile strength by 10-80% (⁷³). So, the calcium can have an active role on the properties of NCF-GO composite membranes, since as GO flakes have low mechanical properties (Chapter 3, §3.4.1).

Another instrument of investigation that has been used in order to support the rheological data is the dynamic light scattering. However the DLS bases its analysis on the assumption that the particles in suspension are spherical, and therefore to have quantitative interpretations is necessary to build a new model for rod-shaped particles, characterized by three (two translational and one rotational) diffusivity coefficients. Further information connected to the problem of using this technique are reported in **ANNEX A-2**.

CHAPTER 3

MECHANICAL PROPERTIES OF CNF-GO NANOCOMPOSITE

In the following are presented, first of all, the results achieved for the mechanical properties measurements of CNF-GO membranes and then some theoretical models for the Elastic Modulus. The Elastic Modulus is one of the most important properties evaluated in mechanical analysis and its modeling can help to interpret the mechanisms that govern the mechanic of such bionanocomposite membranes.

3.1 Tensile Test Results

Circular membranes with 8.5cm radius have been prepared for tensile testing. The thickness of the films can influence some of the mechanical properties as the stress at break or the tensile absorption energy. If there are the same statistical defects distribution and percentage of porosity inside the material for any kind of grammage (that is proportional to the thickness), the Young's modulus has to remain constant. For the mechanical measurements, a grammage of $20\text{g}/\text{m}^2$ has been chosen, for two reasons: a thick film is easier to handle and this is the specific that a packaging application requires. In fact, the CNF films can find some applications in the packaging market, and here the mechanical properties assume a central importance. The membranes have been divided into six stripes and the mechanical properties of each of them were investigated by tensile test. From a single tensile test it is possible to get two curves of the stress as function of the strain applied: the Engineering Curve and the True Curve. For this measurement just the true curve has been evaluated.

3.1.1 True Curve

This curve is obtained plotting the true stress against the true strain. The true stress is defined as:

$$\sigma = \frac{F}{A} \tag{3.1}$$

Where A is the instantly cross section area and F is the applied force. The true strain is:

$$\varepsilon = \ln \frac{L_f}{L_0} \quad (3.2)$$

Where L_f and L_0 are respectively the initial and final length of the specimen.

The function $\sigma(\varepsilon)$ is a crescent curve and no maximum is shown before the rupture (**Fig. 3.1**). For values of applied stress inferior to the Yeld Stress the material has an elastic response and this means that $\sigma(\varepsilon)$ follows the Hook's Law:

$$\sigma = E \cdot \varepsilon \quad (3.3)$$

Where E is the constant Young's modulus.

After the Yeld Stress (point 1 in the picture below) a general material shows a plastic non recoverable deformation until the rupture.

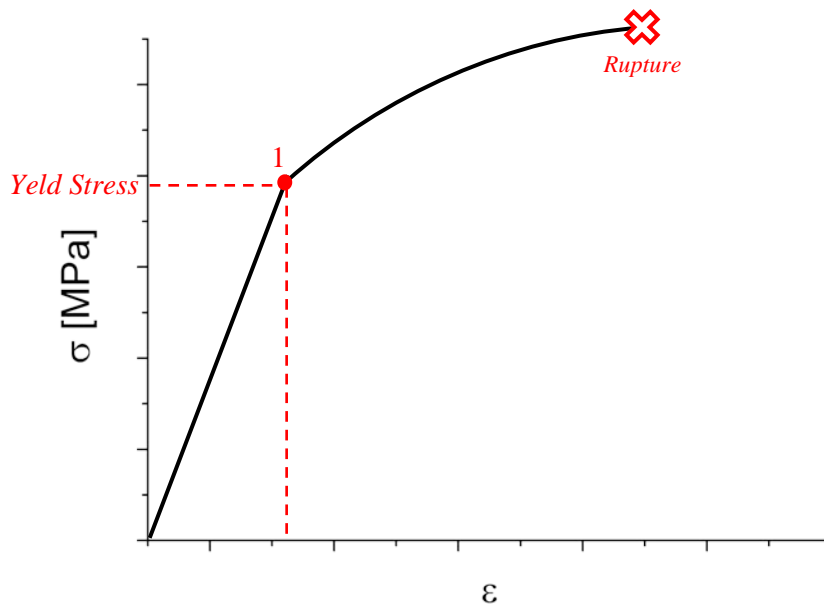


Fig. 3.1: Typical True Curve for a general material.

However in the true curve is not possible to see for which value of strain begins the instable and not uniform reduction of the cross section. This can be seen in the engineering curve and this moment corresponds to the maximum point reached by the function (**ANNEX B-1**).

Of course these considerations are valid for an uniaxial tensile test (tensile test performed just in one direction): therefore what is measured are the mechanical properties of the material along the axis in which the load is applied.

3.1.2 Results

The membranes had different contents (percentage in weight referred to CNF mass) of GO.

The results, from true curves, are summarized in the following **Table 3.1**.

%GO*	Grammage [g/m ²]	Thickness [μm]	Density [kg/m ³]	Stress at Break [MPa]	Elastic Modulus [GPa]	Tensile Energy Absorption [kJ/m ²]	Strain at Break [%]
0%	19,10	13,3 ± 1,6	1446	215,9 ± 30,6	13,1 ± 0,9	0,09 ± 0,01	4,0 ± 0,5
1%	19,30	13,0 ± 1,2	1481	228,3 ± 8,6	14,9 ± 0,8	0,08 ± 0,01	3,8 ± 0,5
2,5%	19,55	11,9 ± 0,5	1642	243,2 ± 5,0	16,0 ± 0,8	0,08 ± 0,01	3,9 ± 0,1
5%	20,25	12,5 ± 1,0	1601	210,3 ± 21,0	14,2 ± 0,6	0,07 ± 0,01	3,5 ± 0,5
10%	20,70	12,6 ± 0,6	1646	234,8 ± 15,9	16,0 ± 1,8	0,07 ± 0,01	3,3 ± 0,4

Table 3.1: Mechanical properties for different GO contents.

The above data show a tendency with the GO content (**Fig. 3.2**).

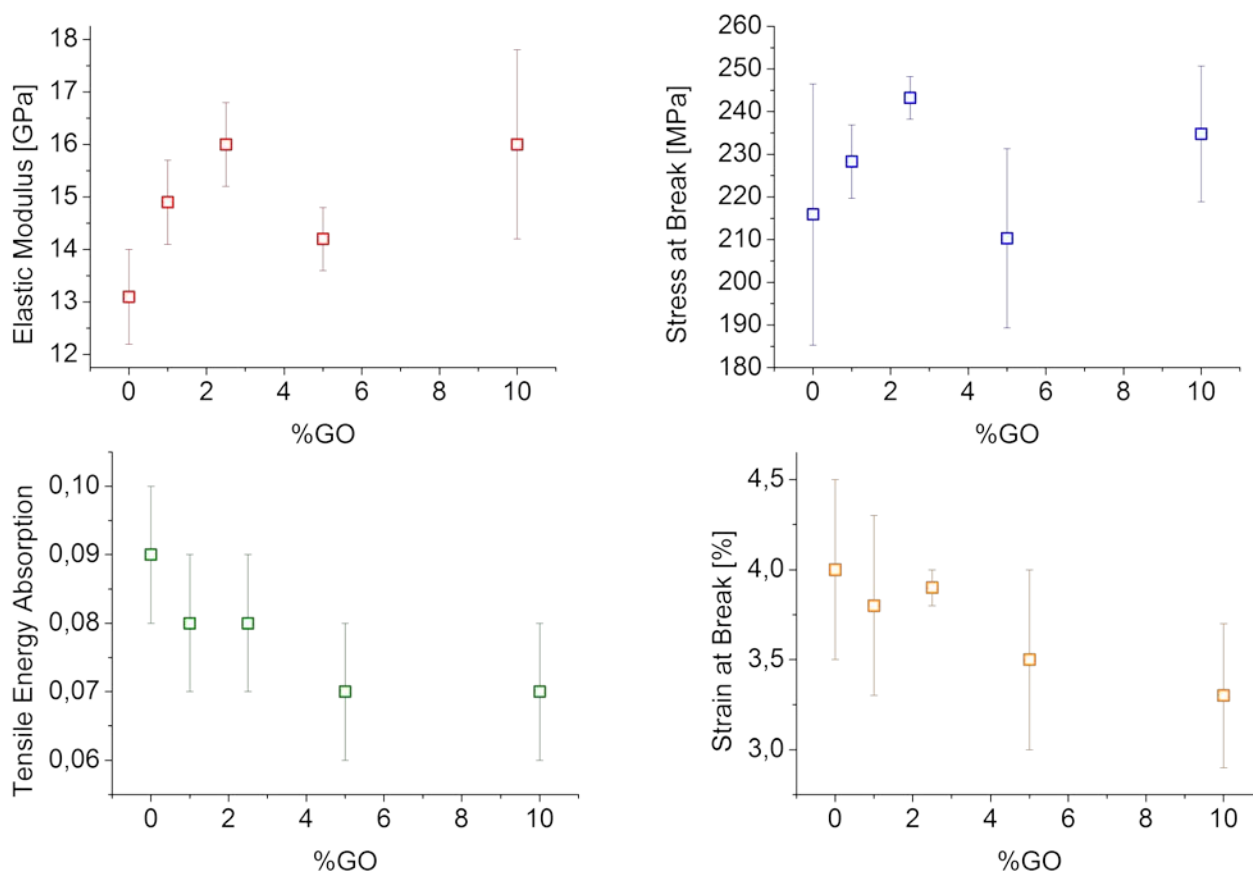


Fig 3.2: Mechanical properties tendency for different GO contents.

For a content of 2,5wt% GO the Young's Modulus shows an increase of ~23% (from $13,1 \pm 0,9$ GPa for pristine CNF up to $16,0 \pm 0,8$ GPa). For the same percentage of GO the Stress at

Break shows an increasing of ~12,5% but with a loss in deformability (decreasing in Strain at Break) suggesting that GO makes more stiffens the nanocomposite. The reason for the small improving of the mechanical properties is due by the relatively low mechanical properties of Graphene Oxide: although these nanoflakes can assure a good interface with carboxymethylated CNF, they are full of defects (since the oxidation of graphite makes different functional groups on the sheet's surface) and this affects negatively the mechanics. The difference of using GO or Graphene will be presented in the predictions of section §3.4.1.

3.2 Comparison between results and literature

The previous results can be compared with the ones for other biomaterials, in order to verify the mechanical properties quality of the CNF-GO membranes. First of all the comparison can be done with other CNF composite materials, in which the CNF can be considered as the “matrix”. Tensile properties of composite films of commercially used base paper, non-modified CNF film and trimethylammonium-modified nanofibrillated cellulose (TMA-CNF) with different types of layered silicates (50 wt%) are reported in **Table 3.2** (⁴⁵).

Film sample	Thickness [μm]	Elastic modulus [GPa]	Tensile strength [MPa]	Strain at break [%]
Commercially used base paper	130 ± 5	1,8 ± 0,9	30 ± 2	5,3 ± 0,6
Non-modified CNF	47 ± 2	6,4 ± 0,2	140 ± 6	4,9 ± 0,6
Non-modified CNF/Mica R120	52 ± 1	7,3 ± 0,1	90 ± 3	2,2 ± 0,2
TMA-CNF	63 ± 12	4,9 ± 0,1	87 ± 4	2,6 ± 0,3
TMA-CNF/montmoril. EXM1246	53 ± 8	7,4 ± 0,6	116 ± 5	3,0 ± 0,6
TMA-CNF/Kaolin Barrisurf HX	68 ± 14	6,6 ± 0,5	85 ± 12	2,4 ± 0,7
TMA-CNF/Talc	76 ± 15	4,7 ± 0,2	67 ± 13	2,9 ± 0,9
TMA-CNF/Vermiculite grade 4	67 ± 3	5,9 ± 0,5	90 ± 3	4,1 ± 0,7
TMA-CNF/Mica PW30	64 ± 8	6,4 ± 1,0	56 ± 6	1,1 ± 0,2
TMA-CNF/Mica R180	82 ± 12	6,6 ± 1,0	81 ± 20	2,1 ± 0,6
TMA-CNF/Micavor 20	119 ± 20	3,8 ± 0,4	57 ± 3	2,6 ± 0,2
TMA-CNF/Mica MU-M 2/1	55 ± 5	4,6 ± 0,3	62 ± 6	2,2 ± 0,3
TMA-CNF/Mica SYA 31R	46 ± 5	9,8 ± 0,7	100 ± 8	1,8 ± 0,2
TMA-CNF/Mica Sublime 325	51 ± 7	7,5 ± 0,3	68 ± 2	1,4 ± 0,1
TMA-CNF/Rona Flair Silk Mica	50 ± 2	9,6 ± 0,3	111 ± 3	2,3 ± 0,1

TMA-CNF/Mica SX400	78 ± 2	$3,4 \pm 0,1$	50 ± 3	$2,7 \pm 0,4$
TMA-CNF/Mica R120	51 ± 1	$9,5 \pm 0,2$	104 ± 5	$1,9 \pm 0,3$

Table 3.2: Mechanical properties for different composite films (Table taken from (45)).

The CNF-GO membranes analyzed in this study show better properties than the materials presented in the previous table: in particular the improvement is ten times higher in respect to the commercial paper and 3-4 times in respect to the other TMA-CNF composites. The cellulosic membrane obtained from carboxymethylated CNF has greater elastic modulus and stress at break than the trimethylammonium-modified nanofibrillated cellulose.

However, other studies for CNF composites with inorganic filler show similar results to those obtained for CNF-GO. In particular the mechanical properties for hybrid films based on CNF with different weight percent of vermiculite (49) are reported in **Table 3.3**.

Film sample	Thickness [μm]	Elastic modulus [GPa]	Tensile strength [MPa]	Ultimate strain [%]
CNF	$12,3 \pm 0,5$	$14,2 \pm 0,6$	256 ± 15	$6,6 \pm 0,5$
CNF+5% VER	$12,9 \pm 0,5$	$16,0 \pm 0,6$	257 ± 19	$5,1 \pm 0,6$
CNF+10% VER	$12,6 \pm 0,5$	$16,4 \pm 0,7$	245 ± 22	$4,8 \pm 1,0$
CNF+20% VER	$13,3 \pm 0,5$	$17,3 \pm 0,4$	244 ± 24	$4,8 \pm 0,7$

Table 3.3: Mechanical properties for CNF-Vermiculite composites (Table taken from (49)).

For the composites in the above table, the values of the elastic modulus and strength are quite similar to those ones of **Table 3.1**; however to reach the same properties of CNF-10% VER membrane is necessary just an adding of 2,5% GO to the pristine CNF. Therefore, also if CNF-GO nanocomposites have approximately the same mechanical properties of CNF-VER hybrids, they require a less quantity of filler (at least four times lower).

However, in the literature are present also studies reporting the possibility to make CNF composite membranes with really high mechanical properties. For instance transparent nanocellulose films with the 16 vol% of titania nanoparticles show a very high Young's modulus up to 44GPa (76). Furthermore, recently it has been developed a new membrane based on nanofibrillar cellulose and synthetic saponite (SPN) nanoplatelets of low aspect ratios: the composite with 5.6% volume fraction of SPN exhibits a Young's modulus of 14GPa , tensile strength of 420MPa , and strain-to-failure of 10% (78). These CNF-SPN membranes show a really high toughness (high stress at break and high ultimate strain).

Other ways to make bionanocomposites is to use CNF fibers as reinforcement in different kind of matrix. A bio-polymer studied quite a lot is chitosan: a linear polysaccharide derived from chitin by N-deacetylation (^{46,47}). Chitosan (CS) has different applications: for waste treatment, packaging, food processing and in medicine. A recent work (⁴⁸), shows the possibility to prepare by solution casting transparent chitosan nanocomposite films reinforced with CNF. The thickness of the such films is between 0,10 and 0,15mm and the mechanical properties for different wt% of CNF are reported in **Table 3.4**.

Film sample	E-modulus [GPa]	Ultimate strength [MPa]	Elongation at break [%]
CS	1,7 ± 0,3	46,5 ± 14,9	36,5 ± 7,1
CS+1%CNF	2,1 ± 0,5	41,8 ± 15,2	24,0 ± 6,7
CS+2%CNF	2,2 ± 0,6	42,6 ± 16,1	22,1 ± 6,1
CS+4%CNF	2,0 ± 0,6	45,2 ± 17,4	20,3 ± 7,2
CS+8%CNF	2,1 ± 0,9	49,9 ± 15,8	18,2 ± 6,8
CS+16%CNF	2,3 ± 0,5	51,9 ± 15,4	12,2 ± 7,2
CS+32%CNF	3,4 ± 0,7	58,3 ± 16,2	7,6 ± 3,5

Table 3.4: Mechanical properties for CS films reinforced with CNF fibers (Table taken from (⁴⁸)).

Chitosan-CNF films show inferior ultimate strength and elastic modulus than CNF-GO membranes, but they have a higher deformability. The deformability of CS-CNF composites decreases with increasing the %wt of CNF reinforcement.

Another bio-based polymer often studied is the Xyloglucan (XG)(⁷⁵): tensile test results for modified NG films (prepared at 23°C and 50%RH) are reported in the following table.

Film sample	E-modulus [GPa]	Tensile strength [MPa]	Elongation at break [%]
XG	4,6 ± 0,2	78 ± 8,6	5,7 ± 3,6
mXG34%	4,7 ± 0,4	76,9 ± 4,3	5,9 ± 1,7
mXG41%	5,4 ± 0,2	88,0 ± 0,7	2,8 ± 0,4
mXG43%	5,1 ± 0,2	55,9 ± 0,0	1,7 ± 0,4

Table 3.5: Tensile properties of XG and galactose removed XGs (different percentage) (Table taken from (⁷⁵)).

It is possible to increase the stiffness of native XG with the adding of inorganic nanoplates, as montmorillonite (MTM): the elastic modulus for XG/MTM nanocomposite is 13.7GPa and

tensile strength is $\sim 100\text{MPa}$, that can further improved with XG oxidation (oxidXG/MTM shows a Young's Modulus of 30GPa and 147.5MPa of tensile strength) (⁷⁷).

CNF fibers can be also used as reinforcement in a polymeric matrix, as can be the polyvinyl alcohol since it is a biodegradable, water-soluble polymer. In this case it is possible to obtain foams with quite low mechanical properties (for PVOH-10%CNF: stress at break $\sim 20\text{MPa}$ and elastic modulus $\sim 50\text{MPa}$ (⁴⁸)) if compared with CNF-GO films.

Other biomaterials membranes can be used for packaging applications. Some works, for instance, present the possibility to make poly lactic acid (PLA)-chitosan (CS)-epoxidised natural rubber (ENR) composites through casting solution. However, also these biomembranes are less stiff and resistant than the CNF ones (**Table 3.6**).

Film sample	E-modulus [GPa]	Tensile strength [MPa]	Elongation at break [%]
PLA	0,0039	19,00	–
PLA+5%CS	4,1	30,95	6,86
PLA+10%CS	4,5	28,71	5,22
PLA+15%CS	3,8	27,50	4,98
PLA/ENR	4,7	10,00	–
PLA/ENR+5%CS	5,0	16,20	12,16
PLA/ENR+10%CS	5,6	14,78	8,40
PLA/ENR+15%CS	5,2	12,28	6,10

Table 3.6: Mechanical properties for PLA-ENR-CS composites (Table taken from (⁵¹)).

3.3 Theoretical models and predictions for CNF membranes

The experimental data can be interpreted by different composites mechanical models. These models are used in order to predict the different mechanical properties, in particular the strength at break and young's modulus. Moreover, many solid materials present a viscoelastic behavior: for an applied stress, the total deformation is the sum of the elastic and plastic ones. The majority of the models consider their predictions just for the range of stresses in which the material has an elastic behavior (described by the elastic modulus). The continuum mechanics (**ANNEX B-2**) is applied to a general solid body in order to evaluate the “stiffness matrix” that characterize the material: with some approximations deriving from symmetry is possible to evaluate the elastic properties just in three directions. In this work, some models

are applied just for the estimation of the Young's modulus CNF fiber, CNF membrane and CNF-GO composite membrane, avoiding the studying of the Poisson's coefficients (that is also needed to evaluate completely the stiffness matrix).

3.3.1 CNF single fiber Young's Modulus

For understanding the elastic properties of a CNF membrane, it is necessary to know in detail the main characteristics of a single CNF fiber. The fibers used in this study have a length approximately equal to $2\mu\text{m}$ and a diameter two orders of magnitude smaller: 25nm .

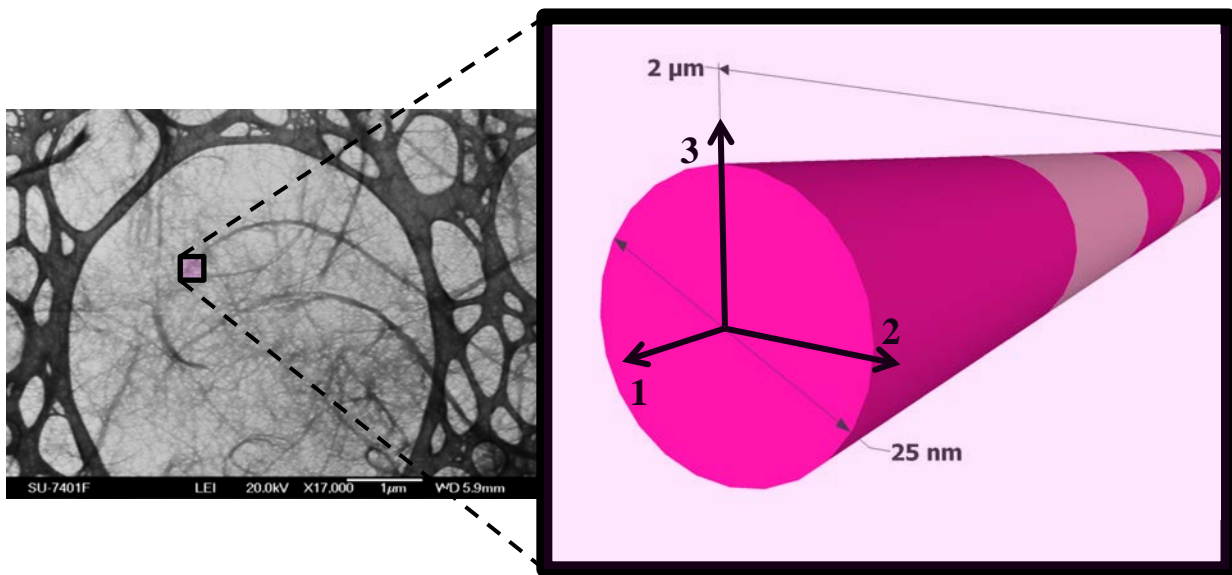


Fig. 3.3: SEM image (left) and ideal fiber geometry (right).

All the CNF fibers contain a crystalline phase, in which the cellulose chain is packed and organized in a particular. As mentioned in §1.1.1, in this study the CNF fibers present Crystalline Cellulose I β regions, which have in general the following properties (⁵):

- ❖ $\delta_c = 1600 \text{ Kg/m}^3$ (Density);
- ❖ $\sigma_f = 7,5 - 7,7 \text{ GPa}$ (Tensile Strength at break);
- ❖ $E_A = 110 - 220 \text{ GPa}$ (Elastic modulus in axial direction 1);
- ❖ $E_T = 10 - 50 \text{ GPa}$ (Elastic modulus in transversal directions, 2 and 3)

Looking to the image above (**Fig. 3.3**) the axial direction is the “direction 1” and along the directions 2 and 3 the fiber is considered to have the same Transversal Elastic modulus (reasonable approximation). The previous values of Young's modulus cover a wide range of numbers: this is because different sources (plant, wood, tunicate, algae) produce crystals with different mechanical properties. In order to estimate the Young's modulus of one CNF fiber is fundamental to know a reasonable value for the crystalline phase elastic modulus. In the

literature can be found different of the Axial and Transversal Elastic Modulus for the Crystalline Cellulose I β (⁵²) (**Table 3.7**) obtained from different sources and using different techniques/models (by different researching groups):

MATERIAL	E_A (GPa)	E_T (GPa)	Experimental technique/model force field
EXPERIMENT			
Cellulose fibrils	120 – 138	-	XRD
Cellulose fibrils	220 \pm 50	15 \pm 1	IXS
CNC-plant	105	-	Raman
CNC-wood	-	18-50	AFM ident.-FEA
CNC-Tunicate	143	-	Raman
CNC-Tunicate	151 \pm 29	-	AFM-3pt bend
CNC-Tunicate	-	2-25	AFM indentation
CNC-wood	-	24,8 \pm 7,0	AFM ident.-FEA
CNC-cotton	-	17,7 \pm 5,0	AFM ident.-FEA
MODELING			
Single chain	168	11-50	Dreiding
Single chain	145	-	COMPASS
1x1x1 unit cell	149	18-47	COMPASS
1x1x1 unit cell	148	-	CHARMM
1x1x1 unit cell	111	-	COMPASS
3x3x2 unit cell	136	-	GROMOS
4x4x10 unit cell	125	-	COMPASS
4x4x8 unit cell	156	-	GROMOS

Table 3.7: CNF Young's Modulus obtained with different methods (Table taken from (⁵²)).

The single fiber is a sequence of crystalline (CNC) and “amorphous” (or semi-crystalline) regions, with rather different properties. Moreover it is also necessary to know how much is the crystalline phase, if it predominant or not in the CNF fiber. Mechanically, the fiber can be imaged as a composite material made by two phases: one crystalline and one completely amorphous (⁵³). In this way is possible to obtain bounds for the modulus by assuming that the crystals are either in a parallel or in a series arrangement (⁵⁴) (**Fig. 3.4**). If a tensile test is performed on the CNF fiber, according to the series hypothesis the applied load is the same

for both phases (uniform stress), while for the parallel assumption is the resulting deformation to be the same for both phases (uniform strain). For the parallel arrangement E is given by the Voigt model as:

$$E = E_c V_c + E_a (1 - V_c) \quad (3.2)$$

for a series arrangement E is given by the Reuss model as:

$$\frac{1}{E} = \frac{V_c}{E_c} + \frac{(1 - V_c)}{E_a} \quad (3.3)$$

where E_c is the Young's modulus of the crystalline phase, E_a the Young's modulus of the amorphous phase, V_c the volume fraction of crystals in the fiber and E the elastic modulus of the CNF fiber. For the crystal elastic modulus 150GPa is a reasonable value, which is consistent with the recent theoretical prediction (see table above). For the amorphous phase it can be taken a value of 5GPa (^{53,55}), since this is close to the modulus for a glassy polymer. Other works take a value for the amorphous Young's modulus also lower than the previous one (⁵). From X-Ray analysis, we know that the volume fraction of crystalline phase in the fiber is approximately the 50%.

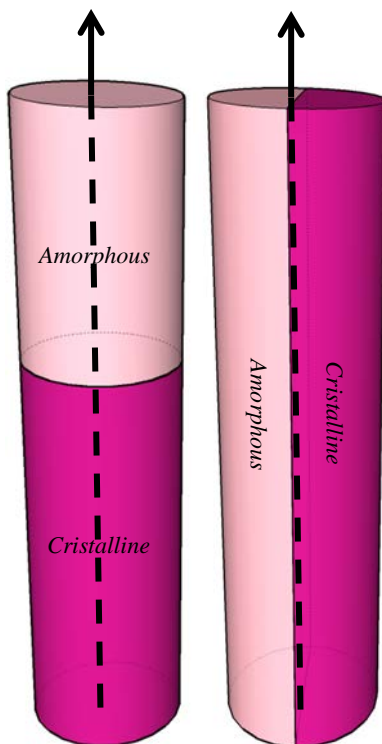


Fig. 3.4: Series (left) and parallel (right) arrangements between amorphous and crystalline regions in one CNF fiber.

Therefore for the Voigt model:

$$E = 150 \cdot 0,5 + 5(1 - 0,5) = 73\text{GPa} \quad (3.4)$$

And for the Reuss model:

$$\frac{1}{E} = \frac{0,5}{150} + \frac{0,5}{5} \rightarrow E = 10\text{GPa} \quad (3.5)$$

So, for a CNF fiber the elastic modulus in the axial direction should be between 10 and 73GPa .

For the Crystalline Cellulose 1β the elastic modulus in the transversal direction is between 10 and 50GPa (⁵⁶). A practical value for the transversal elastic modulus could be 25GPa for wood CNC (⁵⁷).

So, assuming a series connection between the crystalline and amorphous phases along the fiber axis, it means that in transversal direction they are

connected in parallel, so the transversal modulus is predicted by the Voigt relation.

The transversal elastic modulus for the amorphous region is still $5GPa$, due to the isotropic behavior of glass materials.

$$E = 25 \cdot 0,5 + 5(1 - 0,5) = 15GPa \quad (3.6)$$

In the case of the two phases connected in parallel along the fiber axis, in the transversal direction the Reuss model is valid:

$$\frac{1}{E} = \frac{0,5}{25} + \frac{0,5}{5} \rightarrow E = 8GPa \quad (3.7)$$

Therefore, the CNF fiber's transversal elastic modulus spans between 8 and $15GPa$.

Different works show that is more probable a series arrangement in the axial direction, since the experimental data are closer to the Reuss lower bound (⁵³). However, sometimes the uniform stress condition seems to be contradictory and furthermore, considering a perfect series connection the fiber results to be isotropic ($10GPa$ in the axially and $15GPa$ transversally), but this is not possible since the fibers orientation affects a lot the final membranes properties (⁵⁸). Thus, it is better to stay between the Voigt and Reuss bounds, since it is not completely clear how the crystalline and amorphous zones are organized in the space inside the fiber. Since the CNC with is estimated to be between 2 and $20nm$, and the diameter of the CNF fiber is $25nm$, it should be possible for some crystalline domains to arrange also in a parallel configuration. A good approximation is to maintain the estimation in the center between Voigt and Reuss limits. Therefore in this study the axial and transversal moduli are respectively considered to be equal to: $E_A = (73 + 10)/2 = 42GPa$ and $E_T = (15 + 8)/2 = 12GPa$. These elastic properties are good enough to consider the CNF fibers for a hypothetical reinforcement for composite materials. The approximated Young's modulus for some common materials is reported in the following table:

Material	E-modulus [GPa]
Rubber	0,01 – 0,1
HDPE	0,8
PET	2 – 2,7
Nylon	2 – 4
Hemp fiber	35

Flax fiber	58
Glass	50 – 90
Aramid	70,5 – 112,4
Steel	200
Titanium	110,3
Aluminium	69
Carbon fiber	300

Table 3.8: Elastic properties for some common material (Table taken from [wikipedia](#)).

3.3.2 CNF membrane Young's Modulus

Despite the single CNF fiber having good elastic properties (even in presence of amorphous regions), the final dried membrane loses this potential. Performing the tensile test on a carboxymethylated-CNF membrane, $13,3\mu\text{m}$ thick, obtained from drying a $2,3\text{mg/ml}$ suspension at 23°C and 50% of relative humidity, the resulting properties are:

- ❖ $\delta_{\text{membrane}} = 1446 \text{ Kg/m}^3$
- ❖ $\sigma_f = 216,85 \pm 30,62 \text{ MPa}$
- ❖ $E = 13,10 \pm 0,85 \text{ GPa}$

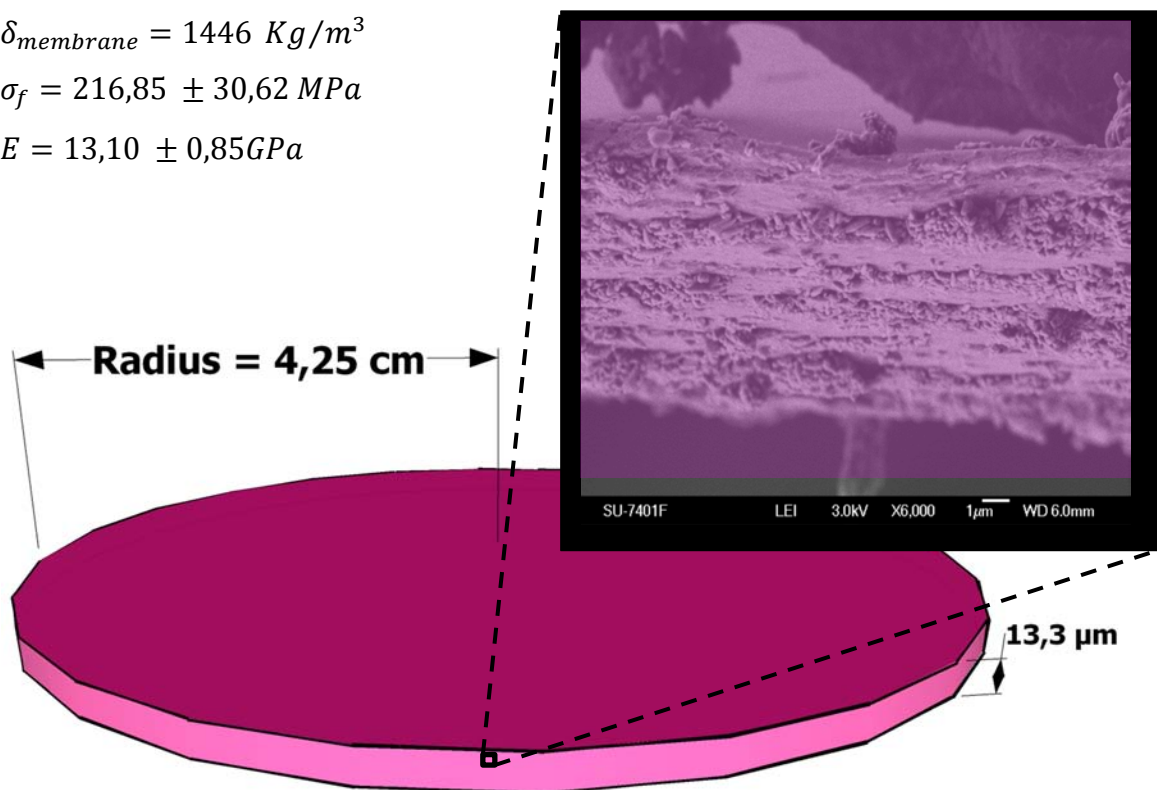


Fig. 3.5: CNF membrane (in pink) and its SEM cross-section.

The values of σ_f and E are the tensile stress at breaking and the Young modulus respectively. The elastic modulus of the membrane is near to the value estimated for the fiber Young's

modulus in the transversal direction ($\sim 12\text{GPa}$), losing completely the axial benefit ($\sim 42\text{GPa}$). The mechanical properties of a membrane depend on many aspects but the principals are:

1. Fiber orientation: in the membrane the fibers are randomly oriented in the membrane plane. This means that different fibers respond in different ways when a stress is applied. The progressive orientation of the fibers along a certain direction leads to higher stiffness and resistance of the membrane in that direction. Experimentally it has been found that for an high orientation degree the membrane Young's modulus is 33GPa and the strength is 400MPa (⁵⁸);
2. Presence of porosity: as the porosity increases, the mechanical properties dramatically decrease. The porosity reduces the film section and it constitutes a relevant weak point for the material (eventual cracks can easily start to propagate from porous). Normally other phases can be present, as the water trapped inside the film during the drying, and this also reduces the material density and resistance. In many cases cellulose materials contain a percentage of porosity between 10 and 20%. The porosity is determined during the drying state and it depends also by the gas content of the initial suspension;
3. Fiber mechanical properties: the mechanical properties of the dried film depend obviously by those ones of the single fibers. Thus, it is crucial to understand how the fiber is structured and how much is the fraction of amorphous phase, since it is the weak point of the material. Moreover it is important also to have a clear idea about the mechanical properties of the amorphous domains, since in the literature they are considered as a rubber or glassy phase;
4. Interaction between fibers: this interaction can be seen as the coefficient of friction between fibers (that depends by the surface geometry/morphology and surface composition/functionalization of fibers). The rupture of the membrane can be the consequence of two concomitant factors: the rupture of the fibers and the rupture of the interface between fibers (sliding of the fibers over each other). The first mechanism depends by the fiber properties but the second one depends by the fiber interactions;
5. Quality of initial suspension: the suspension must be homogeneous in order to avoid the presence of agglomerates and a non-constant thickness of the final membrane.

So, to answer the question of why such a good fiber can produce a membrane with so different mechanical properties, it is fundamental to understand how the membrane cross section looks like:

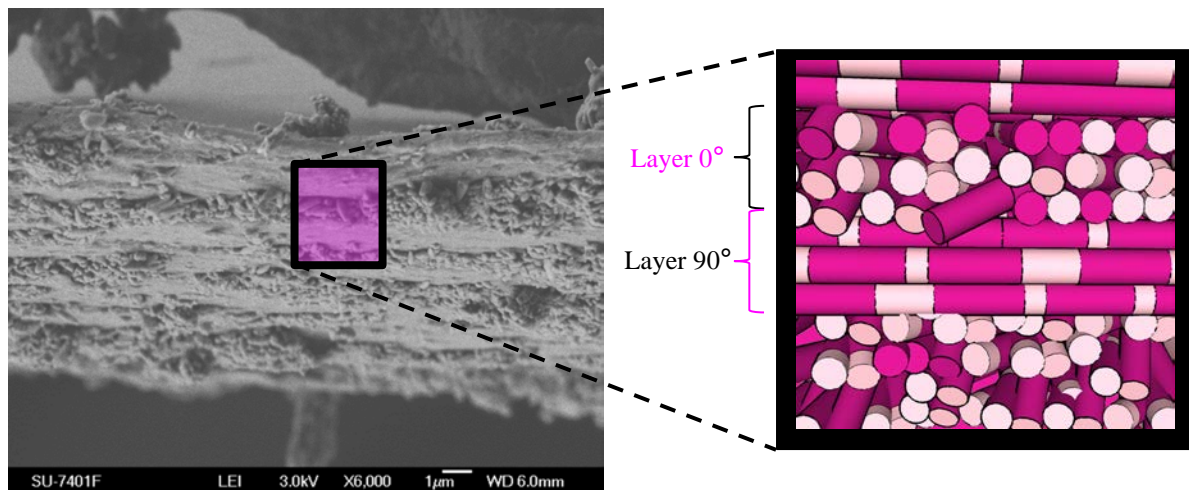


Fig. 3.6: CNF membrane cross section (left) and cross-ply model (right).

From SEM image, it seems reasonable to assume that the fibers are organized in a cross-ply configuration, where different layers of parallel fibers are rotated by 90 degrees from each other (**Fig. 3.6**).

In composite materials the cross-ply configuration is designed in order to have a more isotropic material: long fibers are organized, inside a polymeric matrix, at right angles in order to increase the mechanical properties of the transversal direction.

However, in this case the theory of composite materials can not help: all the equations used in this field of study expect the presence of a phase, the matrix, that link together the fibers.

In some approaches the CNF membrane is considered as a composite material with a glassy matrix that links cellulose nanostructures (⁵): this model is consistent with the experimental data ($E = 13,10 \pm 0,85 GPa$) assuming the 10% of cellulose nano-structures with an elastic modulus of $150 GPa$, inside a glassy matrix with a Young's modulus equal to $2,5 GPa$.

However, the CNF membrane can be seen also as a fabric of CNF fibers, which have the elastic moduli estimated in §3.3.1.

The CNF-fabric should have a structure similar to a cross-ply composite material made by different fiber layers, oriented at 0 and 90 degrees. The cross section of **Fig 3.7** shows that in every layer the fibers are organized in different parallel “bouquet”.

Therefore the modeling of such system can consider:

1. the CNF membrane made by layers oriented at 90 degrees in respect to each other, similar to a cross-ply composite material;

2. each layer made by many parallel bunches of twisted and entangles fibers;

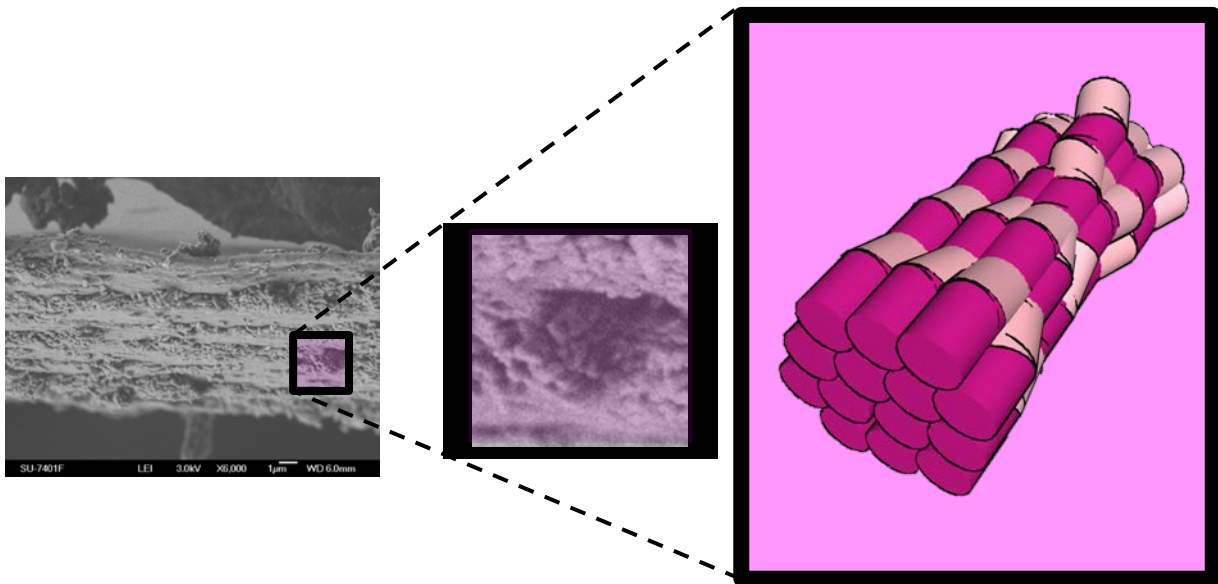


Fig. 3.7: “Bouquet” of fibers that sprigs up from the cross section.

The issue of the last assumption is to understand how the “twisting” of the fibers can influence the elastic modulus of the fabric. In order to overcome this problem it should be possible through the theory of textile industry to understand how the young modulus changes when there are tangled fibers: a solution can be to model one fiber layer as an ensemble of CNF spun yarns parallel to each other. The mechanical properties of a layer made by parallel fibers should not be the same to those of a layer made by many parallel yarns.

Therefore the first idea has been to model the elastic behavior of one of this layer using the mechanic theory coming from studies about the elastic properties of plain weave fabrics (⁵⁹).

Normally fabric mechanics is described in mathematical form based on geometry. Therefore, different models are available, coming from different geometrical hypothesis: in this work is adopted the spun yarn Young’s Modulus equation developed by Hearle in 1969 (⁶⁰). This model assumes that:

1. the fiber yarn is circular and it contains many fibers of limited length and homogeneously packed;
2. the fibers are considered to follow a helical path, with a constant number of turns per unit length along the yarn;
3. the fibers have identical properties and they are perfectly elastic;
4. the strains involved are assumed to be small;

5. the transverse stresses between the fibers at any point are assumed to be the same in all directions perpendicular to the fiber axis.

The Hearle's equation attests that the Young's modulus of the yarn along his axis is:

$$E_{yA} = E_A \times \frac{1 - \frac{2}{3L_f} \left\{ \frac{a\gamma W_y^{1/2} (1 + 4\pi v_f \varphi^{-1} \tau^2 10^{-5})^{1/2}}{4\tau\mu [1 - (1 + 4\pi v_f \varphi^{-1} \tau^2 10^{-5})^{-1/2}]} \right\}^{1/2}}{(1 + 4\pi v_f \varphi^{-1} \tau^2 10^{-5})} \quad (3.8)$$

Where:

- ❖ E_{yA} is the yarn Young's modulus along its main axis. The "y" means yarn and "A" is for axial;
- ❖ E_A is the axial elastic modulus of the fiber. In the previous analysis of the CNF Young's modulus the estimation predicts: $E_A = 42 \text{ GPa}$;
- ❖ L_f is the fiber length and for the CNF is equals to $2\mu\text{m}$. In the above formula it must be expressed in millimeter;
- ❖ a is the fiber radius and for CNF is equals to $12,5\text{nm}$, since the fiber diameter is estimated to be 25nm . In the above formula it must be expressed in millimeter;
- ❖ γ is the migration ratio. Fiber migration can be defined as the variation in fiber position within the yarn. For a spun yarn $\gamma = 4$, and for a first approximation we can assume the same value also for the CNF fiber;
- ❖ W_y is yarn count and it as a measure of the linear density. Normally it is expressed in "tex": one "tex" is the weight in grams of one kilometer of fiber length. For CNF:

$$W_y = \text{density} \cdot \text{Area} \quad (3.9)$$

For a $\text{density} = 1500 \text{ Kg/m}^3$ and for a section $\text{Area} = \pi a^2$, $W_y = 7,4 \cdot 10^{-7} \text{ tex}$;

- ❖ v_f is the specific volume of the fiber. The specific volume is $0,65\text{cm}^3/\text{g}$ for a cotton fiber. For the CNF fiber $v_f = 1/\text{density} = 0,67\text{cm}^3/\text{g}$;
- ❖ φ is the packing fraction. A reasonable value for CNF fibers is $\varphi = 0,9$, and this means that the fibers are well packed in the yarn;
- ❖ τ is twist factor. This parameter measures how much twisted is the yarn and can be calculated by counting the number of twists in an inch of yarn. Migration and twist are two necessary components to generate strength and cohesion in spun yarns. Twist increases the frictional forces between fibers preventing their reciprocal sliding, while

fiber migration ensures that some parts of the all fibers are locked in the structure. The twist factor is expressed in $\text{tex}^{1/2}\text{turn/cm}$:

$$\tau = \text{number of turns per cm length} \cdot \sqrt{W_y} \quad (3.10)$$

❖ μ is coefficient of friction of the fiber. For the cellulose this value is: $\mu = 0,96$.

The parameter that affects a lot the (3.8) is the twist factor. The dependence of the yarn Young's modulus from the number of turns is showed in the next **Fig. 3.8**.

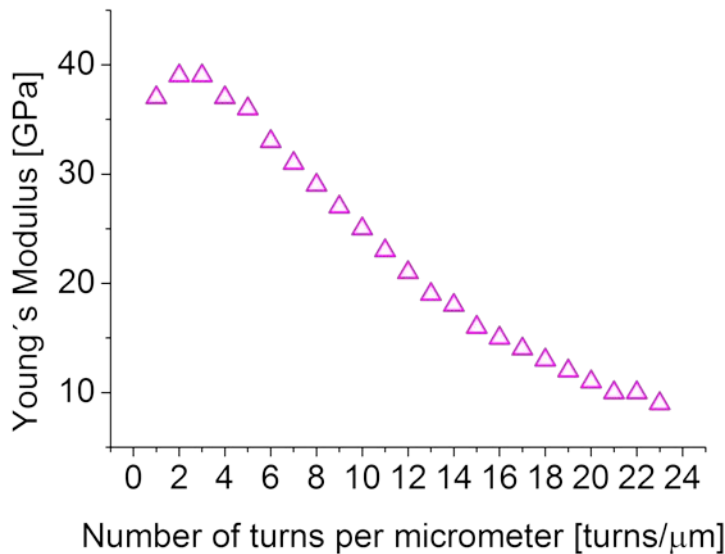


Fig. 3.8: The yarn axial Young's modulus decreases as the twist increases.

Qualitatively **Fig 3.8** means that the more snarled are the fibers, more is the reduction of the roving Young's modulus. This effect of twisting on the elastic properties is well known in the textile field: "...the twist could only increase the inter-fiber friction and decrease the elastic modulus of the roving..."⁽⁶¹⁾.

A reasonable value for the twisting factor can be $8 \text{ turns}/\mu\text{m}$: this means 1 turn every 125nm. Using the last value: $E_{yA} = 29\text{GPa}$.

Moreover for two subsequent layers the yarns are oriented at 90 degrees in respect to each other: therefore, the yarns with the axis parallel to the tensile stress will exhibit the axial Young's modulus, but the yarns at 90 degrees will give the Transversal Young's modulus (**Fig. 3.9**). So the problem is to estimate the transversal elastic modulus of the yarn.

The transversal Young's modulus of the single CNF fiber could be equals to is $E_T = 12\text{GPa}$. Using the last value in Eq. (3.8), instead of E_A , it should be possible to have a first approximation of the yarn's transversal elastic modulus: $E_{yT} = 8\text{GPa}$.

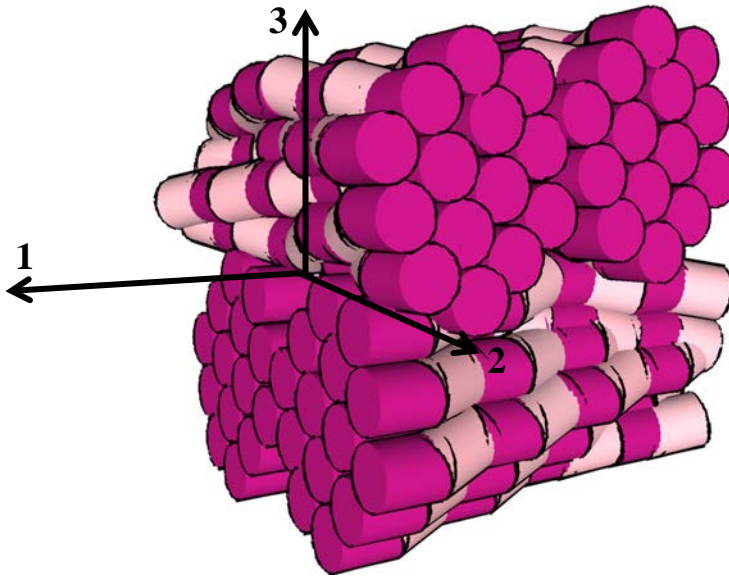


Fig. 3.9: Yarns organized in different layers

The elastic properties of element in **Fig. 3.9** can be estimated with a “rule of mixtures” normally used to approximate the elastic modulus of cross-ply laminate ⁽⁶²⁾:

$$E_{laminar} = \frac{mE^0 + nE^{90}}{m + n} \quad (3.11)$$

Where E^0 , E^{90} , m , and n are respectively the Young’s modulus of 0- and 90- layer and the number of layers. Considering the same numbers of 0 and 90 degrees layers the Eq. (3.11) becomes:

$$E_{laminar} = \frac{E^0 + E^{90}}{2} \quad (3.12)$$

Using E_{yA} and E_{yT} instead of E^0 and E^{90} the elastic modulus for the element in **Fig. 3.9** results to be $\sim 19GPa$. A CNF membrane is made by the connection of many of such elements. To evaluate how the porosity influences the Young’s modulus could be useful the theory about porous particulate materials. The simplest model is to consider the elastic modulus of the material inversely proportional to the porosity ⁽⁷⁹⁾:

$$E = E_c(1 - \varphi) \quad (3.13)$$

Where E and E_c are the elastic moduli of the porous material (with a porosity φ) and of the bulk respectively. Therefore, the Young’s modulus of the membrane is further reduced by the

presence of porosity, and considering the 20% of porosity and bulk elastic modulus of 19GPa the above Eq. (3.13) gives a value of $\sim 15\text{GPa}$, that is quite near to the value measured for a nanocellulose membrane ($\sim 13\text{GPa}$).

3.4 Theoretical models and predictions for CNF Nano-composite membranes

A way to improve the mechanical properties of the CNF membrane is to use a filler, in such a way to make a composite material (ANNEX B-3). Normally, the filler should have better mechanical characteristics, in order to be considered as reinforcement and must be compatible with the matrix. In order to increase the mechanical properties of the CNF films it has been used graphene oxide as nanofiller and the results have been already presented in the beginning of this chapter. However, GO doesn't change in a considerably manner the initial film's properties. To understand the reasons of the poor benefit led by GO on the CNF mechanical behavior, it is a good idea to use some predicting models for composite materials.

The "fabric" model for the CNF membrane presented previously has many parameters and approximation and the adding of another phase would complicate too much the system. Therefore, the CNF+GO membrane has to be modeled according another points of view: one solution could be to consider the CNF as the "matrix" of a composite material (without thinking about fibers, crystalline or amorphous domains) and GO as a nano-reinforcement. This matrix will have the same mechanical properties measured for the neat CNF membrane, so, for instance, the Young's modulus will be: $E = 13,10 \pm 0,85\text{GPa}$.

In this section, the attention will be focused again on the elastic behavior, but in this case for the CNF-GO composites.

The models for the prediction of the mechanical properties of composite materials are a good instrument not only for making interpretations about the final experimental results, but they can be used also for design new materials, since they can help to understand which are the main factor that influence the mechanics.

In general, to design a new composite is necessary to know which will be its applications during the life time: in particular, one important aspect is to define the state of stress that the material will have to tolerate. Since, composite materials are normally anisotropic, they must be designed in such a way to show the best mechanical properties where they will be more stressed. For example, for a polymeric material reinforced with long parallel fibers, the higher strength and elastic modulus are in the same direction of the fiber axis and therefore the load

should be applied in that direction. Usually a membrane during its life is many times stressed by a planar state of stress: thus the filler could have a “plate” geometry, since the resistance along the thickness is not so much relevant (however, also the shear stress and strains are important). Moreover the filler should be well dispersed (importance of rheology) and the flakes must be parallel to membrane plane.

3.4.1 Young's modulus prediction for CNF nanocomposite membranes

In the literature are present many different models to describe the elastic behavior of composite materials; some of them care just about the Young's moduli of matrix and reinforcement, but others focus their attention also in the filler aspect ratio ⁽⁶³⁾ (ANNEX B-4).

In this study the “Hui and Shia” model will be used, since it predicts of composite with aligned reinforcements with emphases on fiber-like and flake-like reinforcements ⁽⁶⁴⁾:

$$E_A = E_m \left[1 - \frac{\phi}{\xi} \right]^{-1} \quad (3.13)$$

$$E_T = E_m \left[1 - \frac{\phi}{4} \left(\frac{1}{\xi} + \frac{3}{\xi + \Lambda} \right) \right]^{-1} \quad (3.14)$$

Where E_A and E_T are respectively the composite axial and transversal elastic moduli. Moreover:

$$\xi = \phi + \frac{E_m}{E_f - E_m} + 3(1 - \phi) \left[\frac{(1 - g)\alpha^2 - g/2}{\alpha^2 - 1} \right] \quad (3.15)$$

$$\Lambda = (1 - \phi) \left[\frac{3(\alpha^2 + 0.25)g - 2\alpha^2}{\alpha^2 - 1} \right] \quad (3.16)$$

$$g = \begin{cases} \frac{\alpha}{(\alpha^2 - 1)^{3/2}} \left[\alpha\sqrt{\alpha^2 - 1} - \cosh^{-1}\alpha \right] & \alpha \geq 1 \\ \frac{\alpha}{(1 - \alpha^2)^{3/2}} \left[-\alpha\sqrt{\alpha^2 - 1} + \cos^{-1}\alpha \right] & \alpha \leq 1 \end{cases} \quad (3.17)$$

ϕ is the volume fraction of the filler and α is the aspect ratio, defined as the ratio of the filler's longitudinal length to its transverse length.

The previous Eq. (3.17) can be simplified for composite containing aligned platelet inclusions:

$$g = \frac{\pi}{2} \alpha \quad (3.18)$$

Where the aspect ratio $\alpha = h/d$ is the ratio of thickness h over width d of the inclusion (**Fig. 3.10**). In the literature are reported the elastic properties of many different kind of platelets used to design nanocomposite materials but the ones with the highest modulus are pure Graphene nano-sheets (**Table 3.9**)⁽⁶⁵⁾:

SHEETS	E (TPa)	SINGLE layer thickness (Å)
SL-Graphene	1,059	3,31
BL-Graphene	1,059	3,32
TL-Graphene	1,058	3,32
4L-Graphene	1,055	3,32
Graphite (bulk)	1,055	3,32
SL-BN	0,898	3,19
BL-BN	0,891	3,19
TL-BN	0,886	3,19
h-BN (bulk)	0,880	3,19
SL-WS ₂	0,251	6,14
WS ₂ (bulk)	0,242	6,17
SL-MoS ₂	0,222	6,12
MoS ₂ (bulk)	0,219	6,14
SL-MoSe ₂	0,188	6,35
MoSe ₂ (bulk)	0,188	6,36
SL-MoTe ₂	0,132	6,87
MoTe ₂ (bulk)	0,132	6,91

Table. 3.9: Young's Moduli for different nano-sheets.

Applying the Hui-Shia model for a flake of with these characteristics:

- ❖ $E_f = 1059GPa$; (as the graphene sheets);
- ❖ $\phi = 12\%$;
- ❖ $\alpha = \frac{h}{d} = 8 \cdot 10^{-5}$; (for a flake 25 μ m large and 2nm thick);

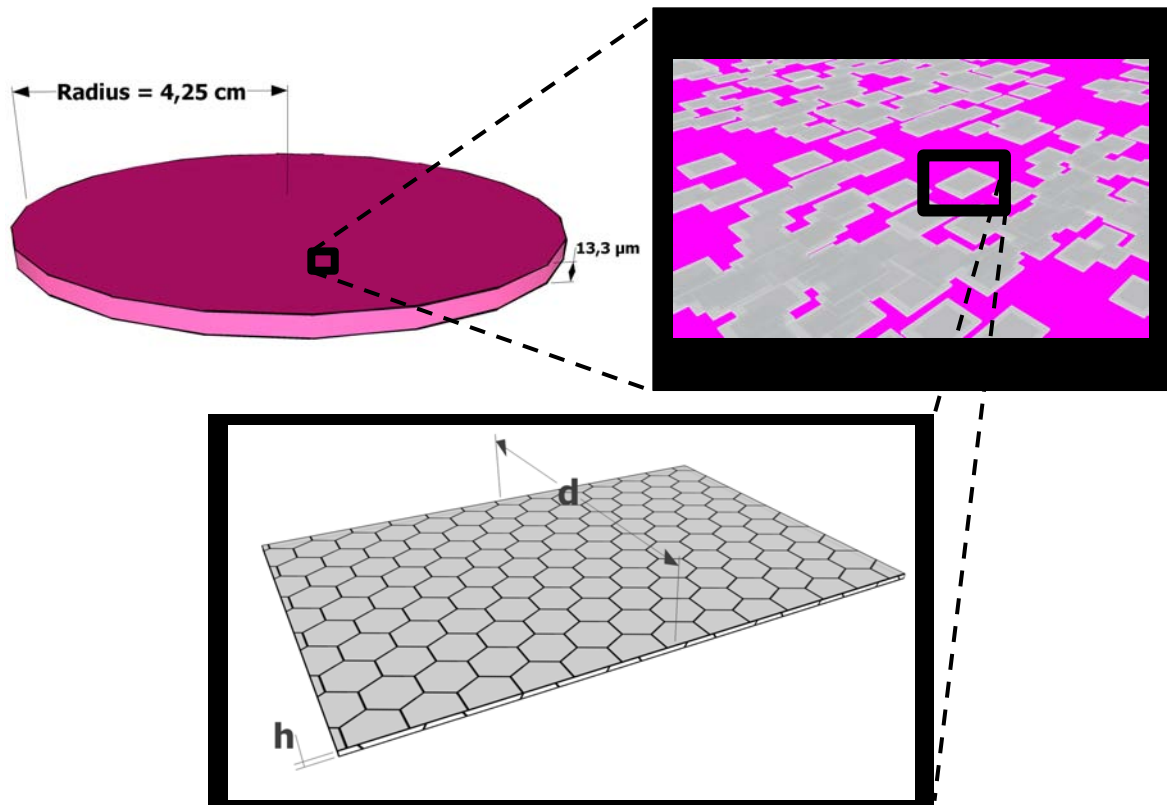


Fig. 3.10: CNF membrane with nanosheets.

the final CNF composite membrane should theoretically increase its Young Modulus one order magnitude from 13GPa to 137GPa. Although the model says that a relevant improvement of the membrane elastic properties can be obtained adding a small amount of graphene, just $\sim 10\%$ in volume, there are some practical problems:

- ❖ It is difficult to well disperse the graphene nanosheets because they tend to agglomerate and then the nanoscale benefit is lost;
- ❖ the interface between matrix and nanofiller is a relevant parameter since it can increase or decrease considerably the final mechanical properties of the composite; however the H-S model doesn't consider this phase, which effect is difficult to predict;
- ❖ in the previous model all the nanosheets must be aligned to the membrane plane in order to explicate the best properties.

3.4.2 Young's modulus prediction for CNF-GO membranes

The choosing of GO as nanofiller for CNF composite membranes has been done since graphene oxide can be well dispersed in aqueous medium, while graphene needs surfactants to stabilize its suspension.

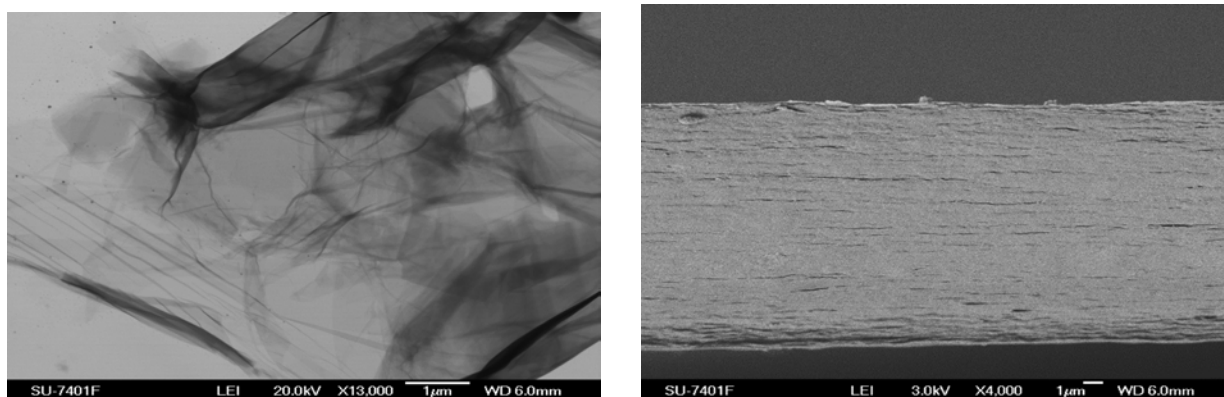


Fig. 3.11: SEM image of one GO sheet (left) and of CNF-GO membrane cross section (right)

Fig. 3.11 shows, on the right, the cross-section of the CNF membrane with 10%GO: the layered structure of **Fig. 3.7** seems to be lost and entangled “yarn” structures are not seen anymore. Some more information about CNF-GO membranes can be obtained through polarized Raman scattering. All carbons show common features in their Raman spectra: the so-called G and D peaks, around 1580 and 1350 cm^{-1} respectively (⁶⁶) (**Fig. 3.12**). The D peak intensity is related to the amount of disorder of graphene layers and not to the number of flakes (^{67,68}): for a low number of structural defects, which is indicative of high crystallinity, the D peak could not be seen and it is present just at the flakes edges since they act as defects (⁶⁹). From **Fig. 3.12** a high intensity for the D-band can be seen, and this means a high number of structural defects for the GO sheets and it is well know that higher is the number of defects higher will be the drop in mechanical properties (⁷⁰).

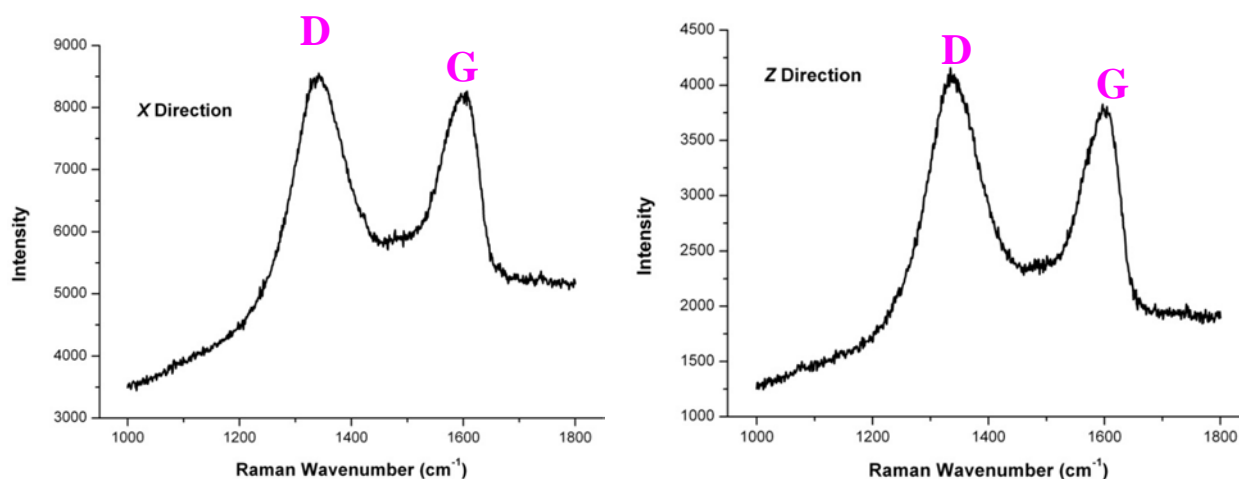


Fig. 3.12: Polarized Raman scattering spectra for CNF+2,5%GO.

Furthermore, polarized Raman shows that the GO nano-sheets are parallel to the membrane plane (**Fig. 3.13**).

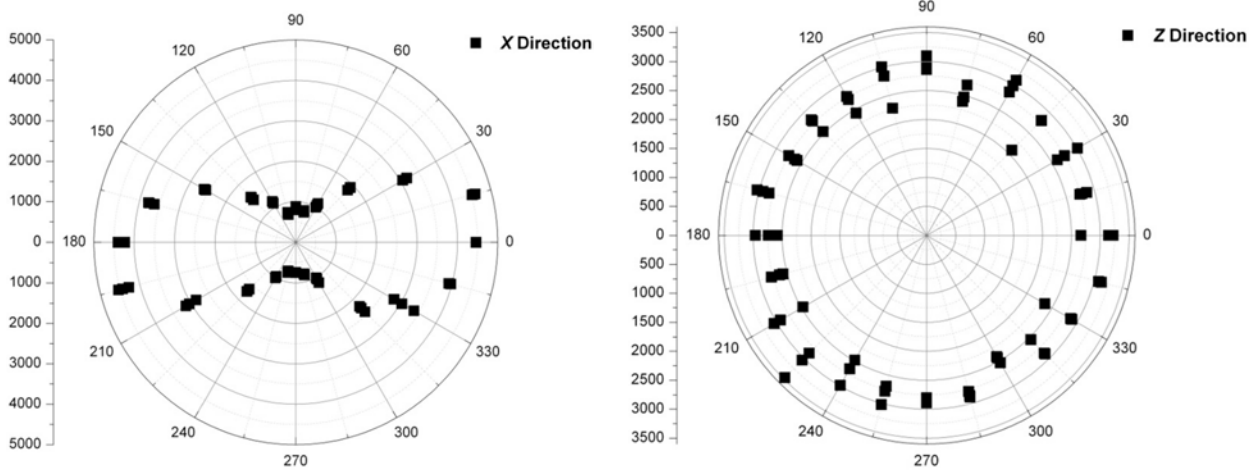


Fig. 3.13: $I(D)/I(G)$ at different angles.

Therefore when the membrane is load along one direction parallel to its plane, all the flakes respond with their maximum resistance and Young’s modulus since they are aligned in the same direction.

However enormous number of structural defects in graphene oxide leads to low mechanical properties:

- ❖ $E_{GO} = 22 - 42GPa$ (^{71,72,73});
- ❖ UTS (max. tensile strength) = $15 - 193MPa$ (^{71,72,73}).

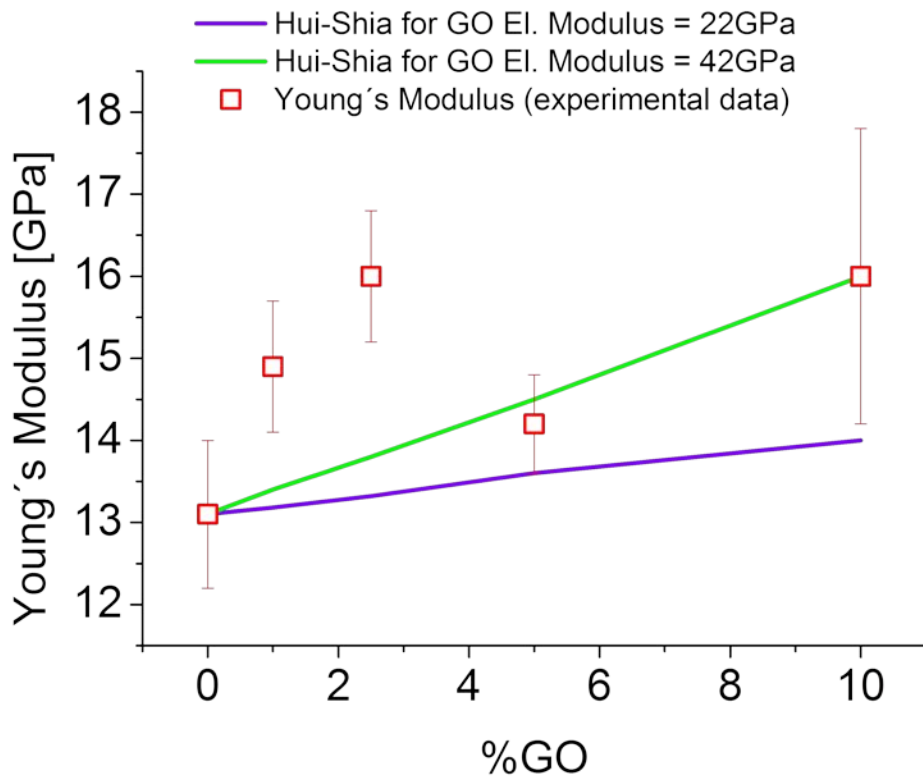


Fig. 3.14: Young’s Modulus experimental data compared with Hui-Shia model.

Some articles report the possibility to improve these mechanical properties via modification of the functional groups on graphene oxide sheets, in particular using divalent cations (Mg^{2+} or Ca^{2+}) to crosslinks edge-bound carboxylic acid groups of adjacent flakes (¹¹). In this case the improvement can be around 10-40% for the elastic modulus and 10-80% for the tensile strength. Applying the Hui-Shia for $E_{GO} = 22$ and for $E_{GO} = 42$ it is possible to obtain the upper and the lower limits for the composite Young's Modulus (**Fig. 3.14**).

Different hypothesis can be done in order to explain why the Hui-Shia model predicts a lower modulus than the one determined experimentally:

1. the model cannot be suitable for this kind of composite membranes;
2. the model doesn't care about the interface contribution on the overall elastic modulus. How the interphase affects the nanocomposites properties is still unknown, however some suppositions are:
 - ❖ the interphase refined the grain size of matrix leads to smaller critical flaw size and higher strength;
 - ❖ the nanofillers impart additional strength of their own matrix through the interphase.

To estimate the elastic modulus of the interphase in polymer nanocomposites, Saber Samandari and Khatibi (⁷⁴) developed a 3D unit cell model to represent the three constituent phases.

The elastic modulus of the interphase at any point, r , is described by a power law as:

$$E_i(r) = \frac{E_m r_i}{r} + (E_f - E_m r_i / r_f) \left(\frac{r_i - r}{r_i - r_f} \right)^{n/2} \quad (3.19)$$

Where E_m and E_f are matrix and nanoparticle elastic moduli respectively, r_f and r_i are the filler and the interphase radii, and n is the intragallery enhancement factor which depends on the chemistry and surface treatment of the particles considered;

3. the GO could change the orientation of the CNF fiber inside the membrane (**Fig. 3.11**) in such a way to increase the Young's modulus.

3.5 Discussions

Despite many argumentations in the literature about the exceptional mechanical properties of CNF fibers, it is quite hard to see these extraordinary features for a neat CNF membrane. This

is due by many factors and the presence of porosity is one of the most cited causes to explain the low mechanical properties of such films. Importantly, from different kind of models it seems reasonable that the CNF Young's modulus is influenced negatively by the presence of amorphous phase, which can be considered approximately as a polymeric glass. However, the studies of these amorphous regions that connect different nanocellulose crystals inside the fibrils seem to not attract the researching interest: to better comprehend the mechanic behavior of CNF is indispensable to evaluate the properties of such amorphous regions and how they are connected with the crystalline domains. Examining in detail the cross-section of a CNF membrane it seems that the fibers dispose their selves not in a totally random orientation, but they make a structure really similar to a cross-ply composite, loosing in this way the benefit of the high mechanical properties of the axial crystalline phase. In fact, it is well known that a preferential orientation of the CNF fibers along a particular direction improve the mechanical properties of the film: in this way the fibers "answer" (resist) better to an external load applied in that direction. In this Chapter a new approach to estimate the elastic behavior of a neat CNF membrane considering it as a cross-ply fabric of fibrils has been considered. This effort in the modelling proposed to give some qualitative interpretations and hypothesis about the mechanic of such films. This model could be further improved, considering other equations coming from textile and composite materials theory, or considering other factor of influence that has been neglected or approximated; a further evolution of the modelling can consider the membrane not as a cross-ply but as real fabric made by warp and weft.

A common practice to increase the mechanical behavior of CNF membrane is to add inorganic fillers in order to make a composite material. One way to make these composites is to start from the initial suspension and therefore the filler should be well dispersible in the same medium that contains the fibers. The kind of mixing and the functionalization of the inorganic particles are essential parameters to consider for make an homogeneous suspension and a good composite, in which the reinforcement is well distributed in all the volume. The GO flakes have similar functionalization to the carboxymethylated fibers, and this turns out in benefit for the homogeneity. However, this functionalization is responsible to the high numbers of structural defects inside the nano-flakes (how it is possible to see from the Raman-spectroscopy), and this leads to lower mechanical properties. In literature are reported values for the GO elastic modulus lower than those registered for the neat CNF membrane. One way to improve these nanocomposites is to try to "repair" these defects or modifying the

functionalization in order to crosslink the CNF fibers with the flakes. A solution can be to test the mechanical properties of nano-composite materials made by carboxymethylated CNF fibers, GO flakes and divalent cations (as Ca^{2+}). Other ways, can be to change filler and try to make a Graphene-CNF nanocomposite, since Graphene has enormous mechanical properties or make a anisotropic CNF-inorganic composite with the fibers oriented prevalently in one direction.

CHAPTER 4

BARRIER PROPERTIES

Transparent CNF films can be used for different applications: food packaging, electronic devices or as reinforcement in nanocomposites (¹).

These bio-based materials together with inorganic nanomaterials can combine impressive properties with a total environmental friendly impact (²). One of the studied characteristics is the (low) permeability to substances as water, oxygen or organic solvents, which is a crucial parameter for barrier applications. In this regard, the physical structure (as the degree of crystallinity) (⁸⁰) and the chemical composition (as the surface functionalization) (⁸¹) of CNF plays a key role on its permeability. Moreover the presence of impermeable flakes or lamellae in the membrane permits to achieve a much lower permeability (⁸²).

This Chapter is initially focused on the analysis of the water vapor transfer rate of such materials, comparing then these results with those obtained in other studies and with the requirements necessities for food packaging.

In the end, also an initial study about the ethanol vapor transmission rate is presented.

4.1 Experimental conditions

The water vapor transmission rate (WVTR) has been measured by the device in **Fig. 1.15** (§1.2.10), at 23°C and 50%RH, using the equation (1.26). It is fundamental to specify thickness of the film, temperature and the partial pressure difference of water vapor during the WVTR measurement.

The same principle has been applied to calculate the ethanol vapor transmission rate: in this case the RH of the chamber was equal to 20%, combined with high ventilation in order to promote the ethanol evaporation. Rather than using silica, the cup has been filled with 10ml of ethanol, measuring the rate of solvent vapor passing from the cup, through the film, to the external environment.

4.2 WVTR of CNF nano-composite membranes

4.2.1 Parameters of influence on the WVTR of CNF membranes

The pure CNF film permeability depends on many parameters and the most important ones are:

1. The source of CNF and production treatment; different sources have different chemical characteristics and different polymorphisms. For example, CNF from bleached hardwood seems to show the highest water vapor barrier property. From the choice of the source, depends all the other parameters (⁸³).
2. Degree of crystallinity; more ordered is the structure, more difficult is for water molecules to pass through. CNC films would seem to provide more of a barrier to water (⁸⁰).
3. Entanglement and nanoporosity; these two parameters seems to exert a very high influence on barrier properties (⁸⁴).
4. Pre-treatments: carboxymethylated CNF films possess a lower water vapor permeability than enzymatic pretreated CNF films, since they are characterized by a lower water diffusivity (⁸¹). Therefore also the fiber's surface functionalization can influence the barrier properties.
5. Post-treatments: another way to reduce the WVTR is to treat the dried film, through, for instance, a hydrophobic surface coating (⁸⁵). This parameter can influence significantly the barrier properties because the CNF membrane is highly hydrophilic due to the presence of carboxylic groups on the fiber's surface.

The neat CNF is also defined as “native network”, due to the fact that the fibers are strongly entangled. Moreover, these membranes are soluble in water: this means that water molecules can easily diffuse between different fibers (since the fibers are carboxymethylated, the $-\text{COO}^-$ groups can be surrounded by water without difficulty).

To increase the effective path length of water molecules along the membrane cross section, it is possible to design a “fiber-brick composite” material through the adding of inorganic nanoplates (²). Therefore it is necessary to have these flakes aligned with the membrane plane (this has been already verified by polarized Raman scattering, §3.4.2) in order to make more tortuous and long the diffusivity path orthogonally to the film.

The theory also affirms that the two flakes parameters that influence more the membrane's permeability are the content of filler and its aspect ratio (⁸²).

In this study the effect of graphene oxide (GO) and reduced-GO flakes for a CNF fiber-brick composite material is considered. Furthermore, also the role of calcium ions is analyzed, since they can modify the interaction between fibers and reduce their hydrophilicity ($-\text{COO}^-$ are coordinated by Ca^{2+} cations).

4.2.2 WVTR Results

The WVTR is a factor highly influenced by the experimental conditions and by the membrane thickness. It has been found that:

$$WVTR = \frac{P \cdot (p_2 - p_1)}{l} \quad (4.1)$$

Where P is the coefficient of permeation, $(p_2 - p_1)$ is the partial pressure difference between the film's surface and l is the thickness of the film. So, thicker is the film lower is the water vapor transmission rate ($WVTR \propto 1/l$).

The dependence of the WVTR from the thickness (and therefore from the film weight, since all the films have the same area) can follow a power law (⁸⁶).

Sometimes, to evaluate the water barrier property, for food packaging applications instead of WVTR is considered another parameter: the “thickness normalized flux”, N (⁸⁷). N is the WVTR multiplied by the thickness, l , of the film:

$$N = WVTR \cdot l \quad (4.2)$$

The thickness normalized flux is expressed in $g \text{ mm}/m^2 d$.

However, it is quite difficult (and takes a lot of time) to measure the thickness of each film. In this sense it is more convenient to calculate it from the grammage, g :

$$l = \frac{g}{\rho} \quad (4.3)$$

Where ρ is the film density. It is necessary to be careful with ρ , because it can change considerably with small amount of GO or r-GO flakes. GO and r-GO nanosheets have approximately the same density of the bulk graphite density, so $\rho_{\text{graphite}} \cong \rho_{\text{GO}} = \rho_{\text{r-GO}}$: then, two films with the same grammage and percentage of nano-flakes have the same ρ , also if one contains GO and the other r-GO.

The problem is to estimate the fluorinated CNF membrane. After the fluorination the membrane results to be thicker, and for many polymers (PS, PC, PMMA) the thickness of the fluorinated layer is proportional to the square root of the fluorination duration (⁸⁸). However it should be possible to calculate the thickness of the fluorinated CNF film considering its final weight and the density of the fluorinated layer, ρ_f .

The total mass of a membrane fluorinated in both surfaces can be calculated as (⁸⁹):

$$m_{tot} = \rho_v \cdot S \cdot t_v + \rho_f \cdot S \cdot 2t_f \quad (4.4)$$

Where ρ_v and t_v are respectively the density and the thickness of the virgin film (neat $12g/m^2$ CNF, so $\rho_v = 1445Kg/m^3$ and $t_v = 8.3\mu m$), S is the surface area, ρ_f and t_f are the density and the thickness of the fluorinated layer. The density of the fluorinated layer depends slightly by its thickness: between $1-6\mu m$ the density is $1600 - 1900Kg/m^3$. Using Eq. (4.4), $t_f \sim 15\mu m$ and since there are two fluorinated surface the total thickness is $\sim 38\mu m$ for a CNF membrane with a grammage of $12g/m^2$ and fluorinated for 25 minutes.

The measured values of the WVTR and N for different CNF composite membranes are reported in the following **Table 4.1**.

Material	Grammage (g/m^2)	Density (Kg/m^3)	Thickness (mm)	WVTR (g/m^2d)	N ($mm \cdot g/m^2d$)
CNF	12	1445	$8.3 \cdot 10^{-3}$	275	2,28
CNF + 2,5%GO vortex	8	1642	$4.8 \cdot 10^{-3}$	297	1,42
CNF + 2,5%GO vortex+shaking	8	1642	$4.8 \cdot 10^{-3}$	254	1,22
CNF + 2,5%GO vort+rolling	8	1642	$4.8 \cdot 10^{-3}$	249	1,20
CNF + 2,5%GO vort+turax 13500rpm 5min	8	1642	$4.8 \cdot 10^{-3}$	225	1,08
CNF + 0,2%Ca	12	1445	$8.3 \cdot 10^{-3}$	228	1,89
CNF + 0,75%Ca	12	1445	$8.3 \cdot 10^{-3}$	258	2,14
CNF + 1,5%Ca	12	1445	$8.3 \cdot 10^{-3}$	256	2,12
CNF + 3%Ca	11	1445	$7.6 \cdot 10^{-3}$	222	1,69
CNF + 5% Ca	12	1445	$8.3 \cdot 10^{-3}$	272	2,26
CNF + 1%-GO _{1min}	12	1481	$8.1 \cdot 10^{-3}$	213	1,73
CNF + 1%-GO _{10min}	12	1481	$8.1 \cdot 10^{-3}$	251	2,03
Fluorinated CNF for 15 minutes	12	/	$\sim 31 \cdot 10^{-3}$	169	5,24
Fluorinated CNF for 25 minutes	12	/	$\sim 38 \cdot 10^{-3}$	154	5,8

Table 4.1: WVTR for different CNF composite membranes ($T=23^\circ C$ and $50\%RH$).

The density of the films with calcium has been taken equal to that one for a pure CNF membrane. Any kind of under-estimation of the density led to an over-estimation of N, so it is better to take a low value of ρ , if necessary, in order to have a more “conservative” value of N.

The thickness normalized flux permit to evaluate qualitatively how much the thickness influences the water vapor permeability of the membrane (**Fig. 4.1**).

The best result is obtain for 2.5% GO, mixed with Turrax at 13500rpm. In this case the water barrier property is increased by about $\sim 53\%$. Small improvements are seen also with calcium

or reduced GO flakes. The percentage of GO has been chosen equal to 2.5% because it is the concentration that gave the maximum mechanical properties.

Moreover, different kinds of mixing seem to modify slightly the WVTR and a tendency has been seen also during the rheological measurements of the initial suspensions.

The fluorinated membranes show a low WVTR because first of all the membrane results much more thick after the treatment.

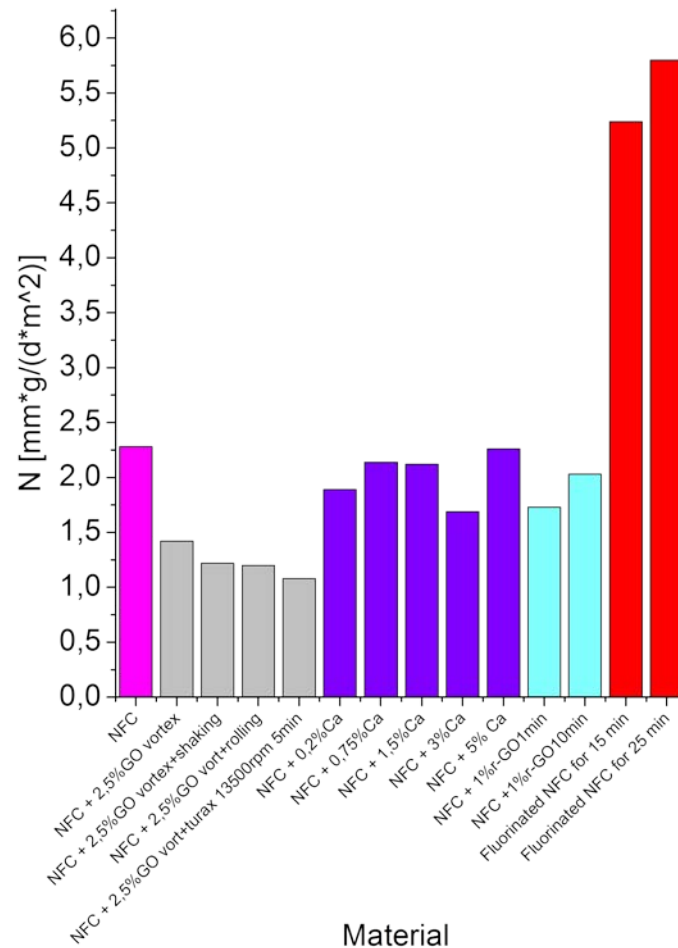


Fig 4.1: Thickness normalized flux for different composite membranes ($T=23^{\circ}\text{C}$ and $50\%RH$).

4.2.3 Membrane hydrophobicity

Another important parameter that characterizes the membrane is its superficial hydrophobicity. The hydrophobicity can be measured evaluating the contact angle of a water drop over the surface. The contact angle, θ , is the angle where a liquid-vapor interface meets a solid surface (**Fig. 4.2**).

The contact angles have most often been used to estimate “surface energy” or “surface wettability”, lead to classification of surfaces as “hydrophilic” or “hydrophobic” or “polar” or “non-polar” or “wetting” or “non-wetting”. These types of classifications may be misleading

or wrong in some cases, so it is necessary to be careful and use this evaluation for qualitative interpretations.

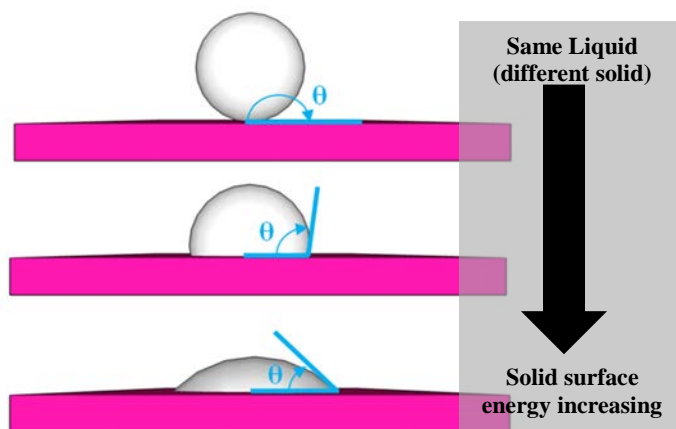


Fig 4.2: Contact angles for solid with different surface energy.

In this study the estimation of the contact angles has been done with a normal camera putting a 50 μ l water drop over different CNF composite membranes:

Substrate	Procedure	Picture
PETRI-DISH (example)	/	
PRISTINE CNF film	/	
CNF film + GO layer	<i>CNF film immersed for 2 seconds in a GO solution 0.2mg/ml</i>	



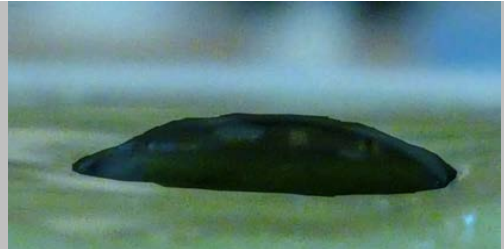
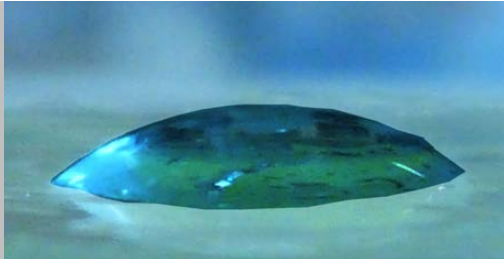
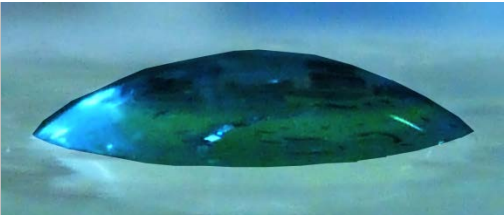
CNF film + fluorinated layer	<i>CNF film fluorinated with fluorosilanes through PVD for 15 minutes</i>	
CNF + 2.5% GO	/	
CNF + 1% r-GO 1minute	/	
CNF + 0.75% Calcium	/	
CNF + 5% Calcium	/	

Table 4.2: Qualitative estimation of contact angles of water drops over different CNF composites.

The contact angle of pristine CNF seems to be quite low: this could be consequence of the CNF hydrophilicity (good wettability), together with the capillary forces exerted by the nanopores present on the surface. The addition of calcium, graphene oxide or reduced-GO to the film does not change considerably the hydrophobicity (wettability) of the membrane.

However, the fluorinated or a GO layer on the surface, give a more spherical water drop. The graphene oxide flakes present the carboxylic groups just in their edge and therefore the center of the flake is more hydrophobic: for this reason, the membrane surface is more hydrophobic if the GO sheets are aligned on its surface.

4.2.4 Comparison between results and literature

The membranes described until now could find application in the food packaging in the near future. The common materials used for food packaging are polymers and they show incredible water vapor permeability (⁹⁰):

Material	N ($mm \cdot g/m^2 d$)
PVdC copolymer	0,041-0,197
Polypropylene	0,078-0,157
HDPE	0,001-0,002
Polyvinyl Chloride	0,197-0,315
LDPE	0,315-0,590
PET	0,01-0,1
EVOH copolymer	5,46
Nylon 6	6,34-8,63

Table 4.3: WVTR for different polymeric membranes ($T=38^\circ C$ and $95\%RH$) (table taken from (⁹⁰)).

In this study the best result has been obtained for CNF with 2.5% of GO: $N=1.08 mm g/d \cdot m^2$ for $T=23^\circ C$ and $RH=50\%$. Polymeric membranes show results much better than the ones for cellulosic film in more aggressive conditions ($T=38^\circ C$ and $RH=95\%$).

The problem to compare data of different sources in the literature arises when WVTR data are achieved for different experimental conditions (different temperature and relative humidity).

However, in general many materials show a linear relation of WVTR with the relative humidity, while the trend is exponential with the temperature (⁸⁶). For example, for a film of $20g/m^2$ LDPE and considering $\rho_{LDPE} = 930 Kg/m^3$ (so $l = 21.51 \cdot 10^{-3} mm$) the dependence of N from RH and T is shown in the next **Fig. 4.3**.

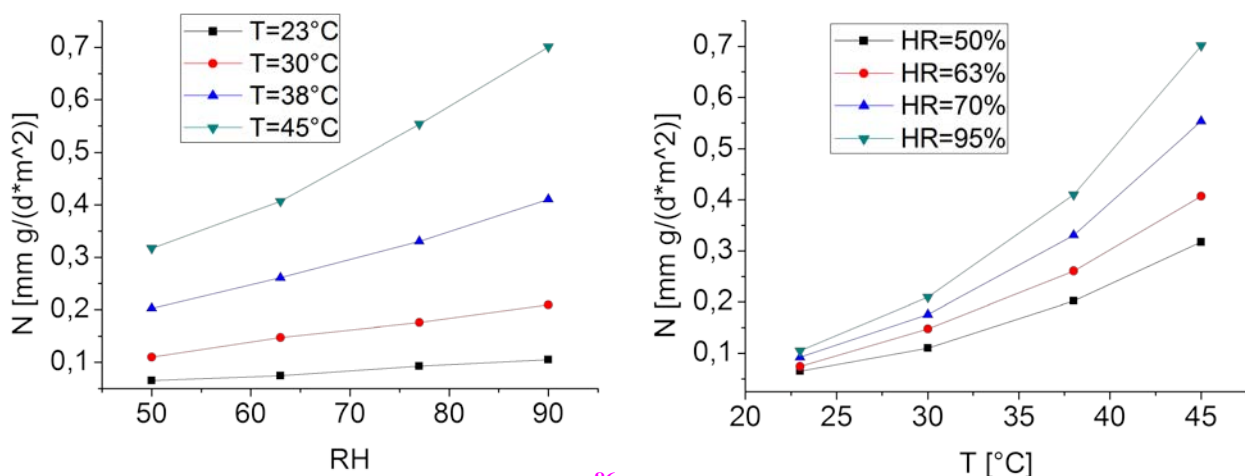


Fig 4.3: Dependence of N of LDPE from T and RH (⁸⁶).

The discussion that follows now try to estimate the thickness normalized flux of CNF composite membranes for $T=38^{\circ}\text{C}$ and $\text{RH}=95\%$, considering them as LDPE films.

This estimation has been necessary for the impossibility to test many samples in a short time. For $T=30^{\circ}$ and $\text{RH}=50\%$, the measured N for a pure CNF membrane is $3.02 \text{ mm g/d} \cdot \text{m}^2$. Therefore for a $\Delta T = 30 - 23 = 7^{\circ}\text{C}$ there is a $\Delta N = 3.02 - 2.28 = 0.74 \text{ mm g/d} \cdot \text{m}^2$, that correspond to an increase of $\sim 32\%$ of the thickness normalized flux (maintaining $\text{RH}=50\%$).

For $\Delta T = 30 - 23 = 7^{\circ}\text{C}$ and $\text{RH}=50\%$ the N of LDPE increases of $\sim 68\%$, so it means that the N of CNF is less subjected to the Temperature than the one of LDPE.

Therefore, using the dependence N_{LDPE} vs T for CNF vs T , there should be an overestimation of the N of CNF for different Temperatures.

From the previous LDPE graph, N at 38°C is the double to that one attested for 30°C (considering the same $\text{RH}=50\%$). If it is considered the same trend also for CNF film, $N \sim 6 \text{ mm g/d} \cdot \text{m}^2$ for $T=38^{\circ}\text{C}$ and $\text{RH}=50\%$.

Using also the dependence N_{LDPE} vs RH for the CNF, it is possible to obtain $N_{\text{NFC}} \sim 12 \text{ mm g/d} \cdot \text{m}^2$ for $T=38^{\circ}\text{C}$ and $\text{RH}=95\%$.

Considering then, that an adding of 2.5% of GO improve $\sim 53\%$ the N of neat CNF film, it is reasonable that: $N_{\text{NFC}+2.5\% \text{GO}} \sim 6 \text{ mm g/d} \cdot \text{m}^2$ for $T=38^{\circ}\text{C}$ and $\text{RH}=95\%$.

Of course these CNF composite membranes must be improved and better designed in order to meet the requirements for food packaging applications, because for now polymeric films offer higher performances. However biomaterials have the extraordinary quality of total environmental friendliness (⁹³), which is the main reason for which it should be necessary to invest more time and efforts to develop them. In order to define the quality of the obtained WVTR data it should be useful to compare them with those achieved for other biomaterials. TMA-CNF membranes with different types of layered silicates (50 wt%) shows the WVTR and thickness normalized flux reported in the following **Table 4.4** (⁴⁵).

Material	Thickness (mm)	WVTR ($\text{g/m}^2\text{d}$)	N ($\text{mm} \cdot \text{g/m}^2\text{d}$)
Commercially used base paper	0,130	1087	141,31
Non-modified CNF	0,047	321	15,09
Non-modified CNF/Mica R120	0,052	260	13,52
TMA-CNF	0,063	284	17,89

TMA-CNF/montmorillonite EXM1246	0,053	451	23,90
TMA-CNF/Kaolin Barrisurf HX	0,068	223	15,16
TMA-CNF/Talc	0,076	204	15,50
TMA-CNF/Vermiculite grade 4	0,067	189	12,66
TMA-CNF/Mica PW30	0,064	197	12,61
TMA-CNF/Mica R180	0,082	167	13,69
TMA-CNF/Micavor 20	0,119	262	31,18
TMA-CNF/Mica MU-M 2/1	0,055	359	19,75
TMA-CNF/Mica SYA 31R	0,046	221	10,17
TMA-CNF/Mica Sublime 325	0,051	184	9,38
TMA-CNF/Rona Flair Silk Mica	0,050	232	11,6
TMA-CNF/Mica SX400	0,078	323	25,19
TMA-CNF/Mica R120	0,051	104	5,30

Table 4.4: *N* and *WVTR* for commercially used base paper, non-modified CNF film and TMA-CNF composites (Table taken from (⁴⁵)).

The composite CNF-2.5%GO has water vapor barrier properties, in the major cases, better than the CNF composites of the previous table. Moreover, the quantity of nano-filler used is really low, 2.5% in weight, while for the CNF-silicate membranes has been used the 50% in weight. However, other works report better results, as the case for nanocellulose composite membranes with vermiculite (⁴⁹):

Material	Thickness (μm)	WVTR ($\text{g}/\text{m}^2\text{d}$)	N ($\text{mm} \cdot \text{g}/\text{m}^2\text{d}$)
CNF	$5,7 \pm 0,1$	70,3	0,40
CNF+5%ver	$4,9 \pm 0,2$	25,2	0,12
CNF+10%ver	$5,6 \pm 0,1$	20,2	0,11
CNF+20%ver	$5,8 \pm 0,2$	15,4	0,09

Table 4.5: *N* and *WVTR* for CNF-vermiculite composites ($T=23^\circ\text{C}$ and $\text{RH}=50\%$) (⁴⁵).

4.3 Ethanol-VTR of CNF nanocomposite membranes

In order to test the organic gas permeability of CNF composite membranes, experiments have been conducted measuring the ethanol vapor transmission rate.

Using the device in **Fig. 1.15** and filling it with 7 grams of ethanol, the evaporation rate has been determined first without any kind of membrane, at 23°C and RH=20%.

In such conditions, three hours are sufficient to loose (evaporate) almost 50% of the ethanol contained in the cup. Furthermore, the evaporation seems to have a linear trend with the time:

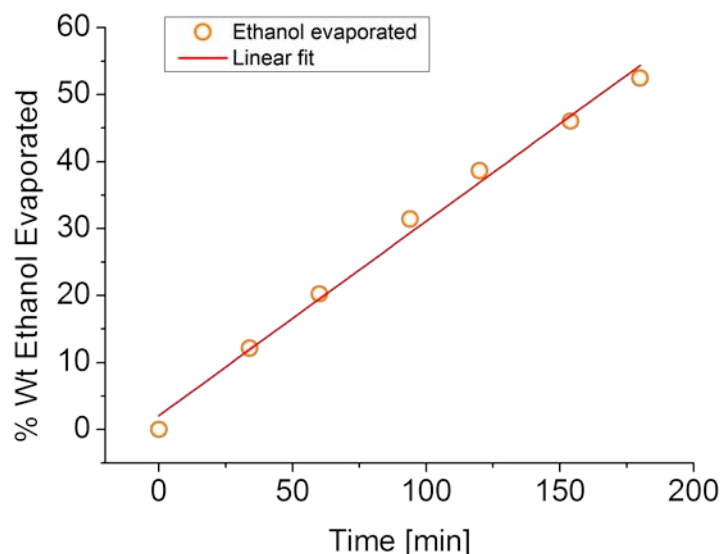


Fig 4.4: Ethanol evaporation at $T=23^{\circ}\text{C}$ and $20\%RH$.

In order to be able to compare different data a parameter similar to the WVTR (or N) , has been used: instead of measuring the weight of the adsorbed water per day and per unit area, it has been evaluated the weight of ethanol lost through evaporation per day and per unit area.

Material	Thickness (μm)	Ethanol-VTR ($\text{g}/\text{m}^2\text{d}$)	N ($\text{mm} \cdot \text{g}/\text{m}^2\text{d}$)
CNF	8.3	113	0,93
CNF + 2,5% r-GO 5min	7.3	80	0,58
CNF + 6.3% r-GO 5min	7.4	79	0,59
CNF + 2,5% r-GO 1min	7.3	69	0,50
CNF + 13.5% r-GO 1min	7.2	81	0,58
CNF + 5% GO	7.5	96	0,72

Table 4.6: N and ethanol-VTR for CNF composite membranes ($T=23^{\circ}\text{C}$ and $RH=20\%$).

The presence of reduced-GO influence the ethanol vapor transmission rate more than GO and it possible to have low ethanol vapor permeability with low content in nanoflakes (**Fig. 4.5**).

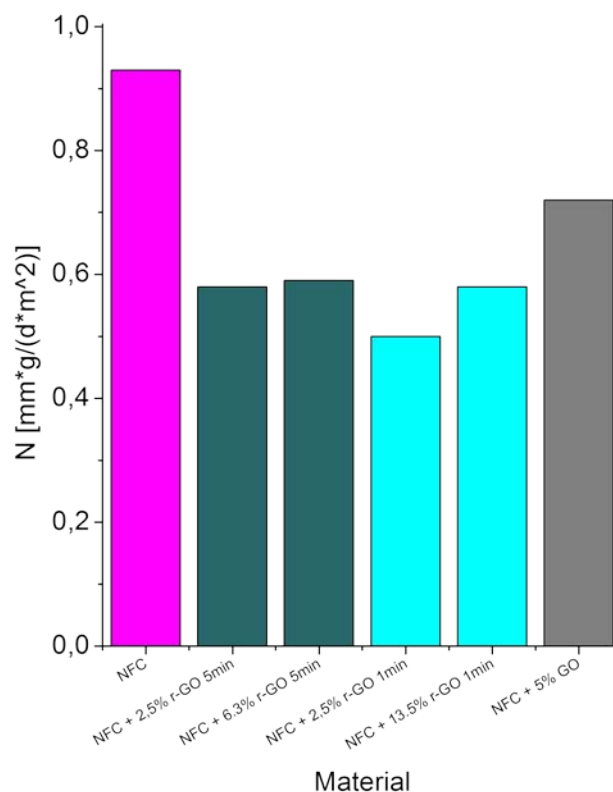


Fig 4.5: Ethanol thickness flux index for different CNF composites at $T=23^{\circ}\text{C}$ and 20%RH.

4.4 Discussions

The water vapor permeability of CNF membranes can be further decrease building a composite film with an inorganic layered structure. GO seems to partially achieve this goal, but the results are in average with other fillers used in previous works. The great potential of nano-flakes is that just a small amount is needed to cover a high surface and then making a more tortuous path for the water molecules along the film thickness. However it has been already discussed in Chapter 3 that GO has many structural defects: this means also that such nano-sheets can probably present holes in their structure and some of them can be big enough to leave the water passing through (so, also for the barrier properties could be taken in account the possibility to repair such defects for example by a methane plasma restoration). Thus, the problem is that perhaps also GO flakes are a bit permeable to water, but more impermeable than CNF since the hydrophilic carboxylic groups are mainly situated in their edges. This fact is well presented by higher contact angle of water drops over a GO layer, demonstrating that their surface is quite hydrophobic. So, future works for increasing the CNF barrier properties can consider also the possibility to make surface coatings of GO. Importantly, **Fig. 4.1** shows that for more vigorous mixing of CNF-GO suspensions the water vapor permeability of the corresponding dried films seems to decrease. During the rheological and UV-VIS

measurements it has been also seen a tendency for different mixing, and one hypothesis considered the breaking of the flakes as possible explication. The GO flakes are quite large ($\sim 25\mu m$) and mechanically weak, so it is reasonable that high number and intensity of impacts with the mixer or with the container walls can break them in smaller pieces. Many small GO nano-sheets can better diffuse between the fibers into the suspension and their statistical distribution in the membrane thickness makes more difficult the passage of the water. Therefore, many small GO flakes can increase more the effective water path inside the film than few big flakes.

CONCLUSIONS

Rheology interpretations of the achieved results suggest that CNF fibers are not completely rigid, but they can be considered as semiflexible polymeric chains and also the gel that their suspension form with the adding of calcium chloride can be considered as a polymeric gel. This semiflexibility is due by the contemporary presence of amorphous and crystalline regions into the fiber and they are also responsible of the global elastic behavior. Many interpretations and models of Chapter 3 were dedicated to the Young's modulus, that is an important property, but also the elongation and stress at break are equally fundamental. For a possible packaging application the material should have a discrete deformability, in order to dissipate energy through plastic mechanisms. Sometimes for polymeric materials some plasticizers are added in order to reach an higher deformability. In general CNF-inorganic hybrids are really stiff, so it can be considered also the role of a possible third component in such composites, as can be the chitosan, a bio-polymer with high elongation at break. In conclusion, it is crucial to find the right compromise between stiffness and deformability: CNF and inorganic fillers many times increase just the first one, with a loss in the second. Nanofibrillated cellulose hide in their selves the potential of good mechanical properties that can be exploited together with other inorganic/organic components in order to substitute petrochemical materials with same features and applications, but is vital to better understand the elastic and plastic mechanism of deformation and the phenomena the lead to the rupture (sliding of fibers, in which phase, amorphous or crystalline, there is more frequently the breaking).

There are many parameter that influence the WVTR of CNF-inorganic layered films, but focusing the attention just on the nanometric flakes is important to consider: the level of hydrophobicity, the presence of structural defect, the dimensions of the sheets and their statistical orientation and distribution in the space (that depends by the degree of well dispersion in the suspension, which is related with the reciprocal interactions with fibers and medium). The Calcium ions seem only slightly affect the water vapor barrier properties: the reasons of a slightly decreasing in the water permeability can be due by a low reduction of the membrane porosity or by a less hydrophilic fiber surface.

A marginal part of the present thesis has been dedicated to the evaluation of the ethanol vapor barrier properties of CNF-GO composite membranes. If GO flakes are a bit permeable to

water they should be more impermeable for larger molecule such methanol or ethanol. This investigation has been conducted just for few samples, in order to have a qualitative idea about the effect of GO and reduced-GO on the organic barrier property. It seems that r-GO block better the ethanol molecules than GO, maybe because r-GO is more hydrophobic or there is some pore healing.

The application of CNF membrane as organic or selective barrier is a hot-topic in the current researching effort, since such films could be a cheap, environmental friendly alternative for the membranes used today in PEM fuel cells. Such membranes have to limit the passage of reagents as methanol and water, and they have to show proton conductivity. In this regard the functionalization of carboxymethylated CNF can play a key role, showing possible applications also in other important fields and not only in the food packaging.

The potential shown by these materials is not negligible, but their properties must be further improved and calibrated, in order to reach the standard for a massive diffusion in the common life. However, to center this task is necessary a collaboration between different “minds” and competencies, analyzing the material from different outlooks (chemical, physical, engineering points of view are different but they must be equally used in order to maximize all the different material performances). The CNF fiber must have the right functionalization in order to improve, for instance, the “relation” with other components or some particular features, but not less important is the comprehension of their “solid mechanics”, since a weak membrane is not useful. The present work has been collocated more under an engineering point of view, considering more the mechanic, rheological and barrier properties, typical and basic engineering instruments.

One of the greatest challenges for the society of the next future is to collocate itself in a more sustainable culture, trying to minimize the consequences of the human habitudes and necessities on the natural mechanisms and equilibriums that govern the world. Petrochemical materials are everywhere, are cheap and reliable but they are not renewable. The effort of governments, companies and universities of the last years is projected towards a more sustainable tomorrow, investing a considerable amount of intellectual and economic resources on developing more green solutions. In this regard bio-materials could dominate the panorama, since they show enough potential to substitute in a near future some of the most common polymers.

Importantly, the properties of nanofibrillated cellulose composite membranes tested in this work show the prospective to reach many different applications, from the food packaging to the selective membranes used in fuel cells.

APPENDIX A

A-1) Effects of mixing on CNF-GO UV-Vis spectra

In order to examine the effect of mixing with another technique, “Turrax” mixing has been applied at maximum power (13500rpm) for different times (0, 15, 30, 45 and 60 minutes) to a CNF-2,5%GO suspension, evaluating the different absorbance curves through the UV-VIS spectrometer (**Fig. 2.4**).

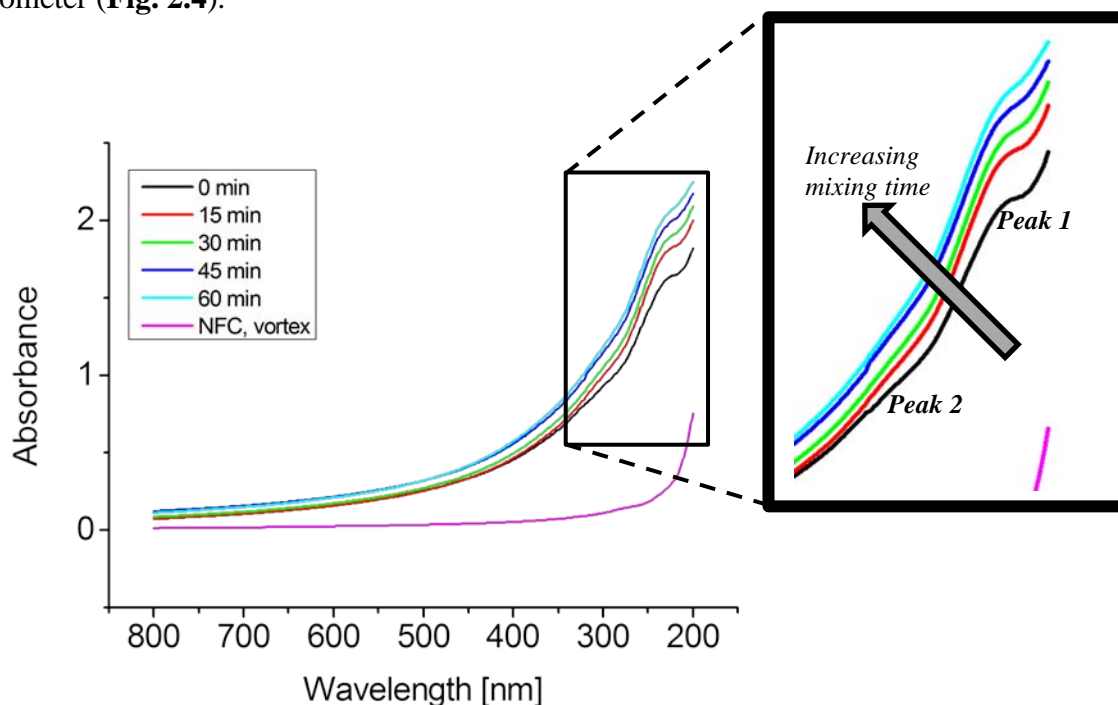


Fig. 2.4: UV-VIS absorbance for 2.3mg/ml NFC (pink curve) mixed with vortex and for NFC-2,5%GO mixed with Turrax (13500rpm) at different times.

In the same graph is also reported the absorbance for a 2,3mg/ml CNF suspension mixed with vortex. Pure GO shows two absorption peaks: one at $\sim 230\text{nm}$ (peak 1) and another shoulder at $\sim 300\text{nm}$ (peak 2) ⁽²⁷⁾. These peaks are registered also for CNF-GO suspensions. Moreover, as the mixing time increases, the absorbance curve shifts to higher values

The **Fig. 2.4** could mean that a vigorous mixing produces GO flakes with smaller dimensions, breaking them in several pieces. Many small GO flakes give an higher contribution to the scattered light than little big flakes: if the amount of scattered light increases, then the amount of total light received by the detector in the spectrometer decreases, and this can be observed as an inferior transmittance or an higher absorbance. Normally, the agglomeration of nanoparticles is accompanied by the opposite phenomena: a decreasing of the absorbance peak and the rising of a new shoulder ⁽²⁸⁾.

A-2) Dynamic Light Scattering for rod shaped particles

To determine the dimension and diffusivity of particles in suspension a common technique is DLS. When the particles are not spherical, different approaches can be used in order to interpret the data. A first common assumption, used often for proteins, is to consider the particles as sphere getting the so called “hydrodynamic diameter”. “*The hydrodynamic diameter of a non-spherical particle is the diameter of a sphere that has the same translational diffusion speed as the particle...*” (⁹⁴). However, this is a valid approximation for objects which are on average in spherical shape, due to conformation changes and aggregation. CNF fibers can show a more coiled conformation when they are “in motion” (during an oscillating test for example), but in the rest state they should remain in a more rod shape, since there are no fluid fields or hydrodynamic interactions that can flex them. Thus, another approach is to analyze the raw correlation data, but it is more complex to obtain quantitative informations. The digital correlator of the DLS system measures the intensity autocorrelation function:

$$g_I(t) = 1 + \beta |g_E(t)|^2 \quad (\text{A.1})$$

β is a measure for the coherence of the optical setup and $g_E(t)$ is the electric field correlation function. Considering no interactions between particles and the approximation of infinite dilution:

$$g_E(t) = \exp(-Dq^2t) \quad (\text{A.2})$$

Where:

$$q = \frac{4\pi n_M}{\lambda} \sin \frac{\theta}{2} \quad (\text{A.3})$$

λ is the vacuum wavelength of the used radiation, θ is the scattering angle and n_M is the refracting index of the medium. Experimentally, it is possible to fit the measured intensity correlation function to a cumulant expansion:

$$\ln[1/\beta \times (g_I(t) - 1)] = 2 \ln[g_E(t)] = -K_1t + (1/2)K_1t^2 - \dots \quad (\text{A.4})$$

For a single diffusing sphere:

$$\frac{K_1}{2q^2} = D \quad \text{and} \quad K_2 = 0 \quad (\text{A.5})$$

Moreover, through the Stoke-Einstein equation it is possible to calculate the diameter d of a sphere inside a medium with viscosity η (Eq. 1.21).

In all the previous analysis the electroviscous effects, that characterize charged particles, are neglected.

If the particle is not spherical but it has a rod shape just a numerical expression for the autocorrelation function is possible, from which the first cumulant can be easily derived (⁹⁵):

$$\frac{K_1}{2q^2} = \bar{D} - \Delta D \left[\frac{1}{3} - f_2 \left(\frac{qL}{2} \right) \right] + \frac{L^2}{12} D_r f_1 \left(\frac{qL}{2} \right) \quad \text{and} \quad K_2 \neq 0 \quad (\text{A.7})$$

Where:

- ❖ $f_1 \left(\frac{qL}{2} \right)$ and $f_2 \left(\frac{qL}{2} \right)$ are functions obtained numerically (⁹⁶),
- ❖ L is the particle length,
- ❖ $\bar{D} = (1/3)D_{\parallel} + (2/3)D_{\perp}$,
- ❖ $\Delta D = D_{\parallel} - D_{\perp}$,
- ❖ D_{\parallel} and D_{\perp} are respectively the translational diffusion coefficients parallel and perpendicular to the rod's long axis, while D_r is the rotational diffusivity.

Considering:

$$\begin{aligned} D_{\parallel} &= \frac{k_B T}{2\pi\eta L} \left(\ln \frac{L}{d} + \gamma_{\parallel} \right) \\ D_{\perp} &= \frac{k_B T}{4\pi\eta L} \left(\ln \frac{L}{d} + \gamma_{\perp} \right) \\ \frac{L^2}{12} D_r &= \frac{k_B T}{4\pi\eta L} \left(\ln \frac{L}{d} + \gamma_r \right) \end{aligned} \quad (\text{A.8})$$

It will be possible to get the length L and the diameter d of the rod (where γ_{\parallel} , γ_{\perp} and γ_r are correcting factors). Analyzing DLS data of CNF suspension with different content in calcium it is possible to have just a qualitative picture of how look like the function for high calcium concentration: the degree of jelling is proportional to the decreasing of the autocorrelation function intercept (**Fig. A.1**). The determination of the fiber floc size due by low calcium concentration (**Fig. 2.18**, section §2.4.2) is not an easy task, since it is necessary to fit the correlation data with Eq. (A.7).

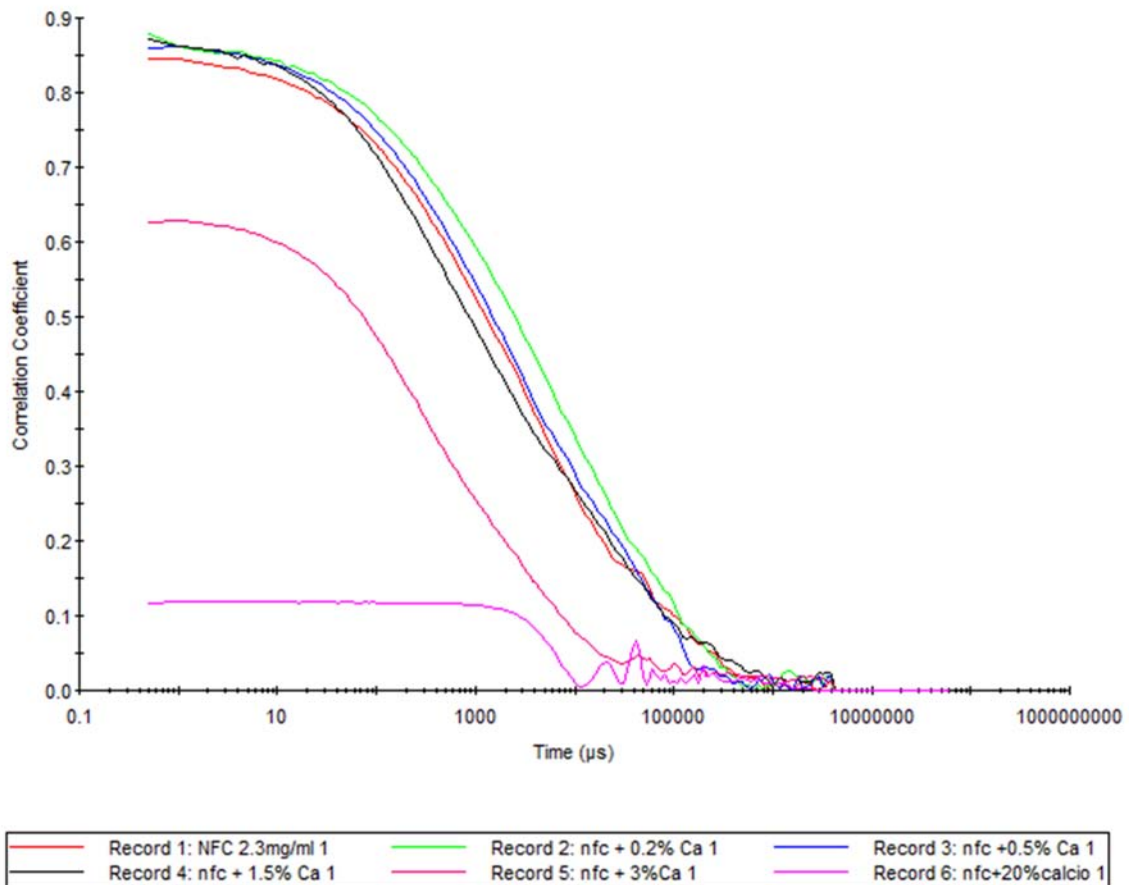


Fig. A.1: Autocorrelation function for CNF (NFC) suspensions with different calcium content.

If the DLS technique is used for investigations of CNF suspensions, first of all it is necessary to work with high diluted systems trying to minimize the fibers interactions. However the CNF fibers still feel their mutual presence also at really low concentrations.

In conclusion, the DLS scattering can be used for general qualitative investigations about systems containing fibers and crosslinkers, but for more precise evaluations (as the average dimensions and diffusivities of fiber flocs), it requires an effort that maybe can be avoided using other techniques.

APPENDIX B

B-1) Engineering Curve

This curve is obtained plotting the “engineering stress” against the “engineering strain”.

The engineering stress is defined as:

$$\sigma = \frac{F}{A_0} \quad (\text{B.1})$$

Where F is the applied load and A_0 is the initial section area of the sample. The engineering strain is:

$$\varepsilon = \frac{\Delta L}{L_0} = \frac{L_f - L_0}{L_0} \quad (\text{B.2})$$

From these two engineering variables is possible to plot a curve that shows a maximum (Ultimate Tensile Strength) before the rupture (**Fig. B.1**).

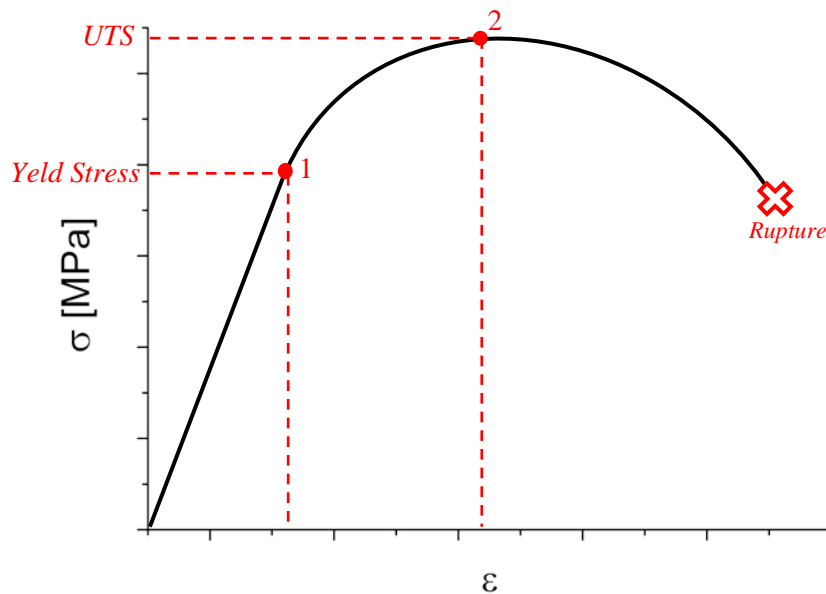


Fig. B.1: Typical Engineering Curve for a general material.

B-2) Continuum Mechanics in composite materials

In the following we are going to consider the linear elastic behavior of a general material, going then in detail for the elastic analysis of an orthotropic material. The generalized Hooke’s law relating stresses to strains can be written as:

$$\sigma_i = C_{ij}\varepsilon_j \quad i, j = 1, \dots, 6 \quad (\text{B.3})$$

Where σ_i are the stress components shown on a three-dimensional cube in x, y, and z coordinates in the stiffness matrix, and ε_j are the strain components.

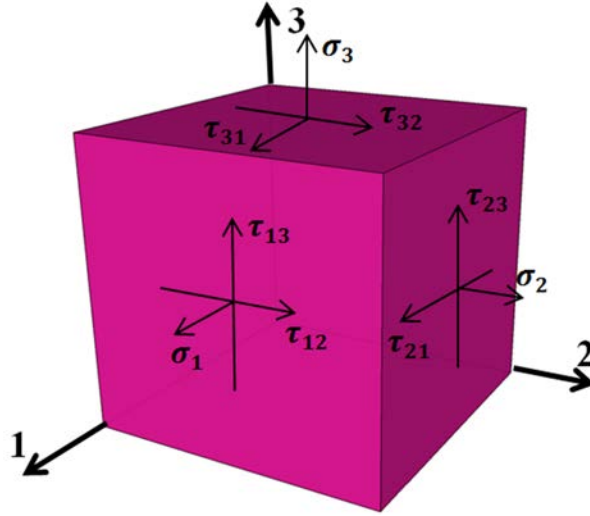


Fig. B.2: General stress state.

The extensional (2.6) and shear (2.7) strains are defined as:

$$\varepsilon_1 = \frac{\partial u}{\partial x}; \quad \varepsilon_2 = \frac{\partial v}{\partial y}; \quad \varepsilon_3 = \frac{\partial w}{\partial z}; \quad (B.4)$$

$$\gamma_{23} = \frac{\partial v}{\partial z} + \frac{\partial w}{\partial y}; \quad \gamma_{31} = \frac{\partial w}{\partial x} + \frac{\partial u}{\partial z}; \quad \gamma_{12} = \frac{\partial u}{\partial y} + \frac{\partial v}{\partial x}; \quad (B.5)$$

Where u, v and w are displacements in the x, y, z directions or the 1, 2, 3 directions (**Fig. 2.4**).

The general condition of stress state is described by the vector:

$$\begin{bmatrix} \sigma_1 \\ \sigma_2 \\ \sigma_3 \\ \tau_{23} \\ \tau_{31} \\ \tau_{12} \end{bmatrix} \quad (B.6)$$

While for a deformation state the vector is:

$$\begin{bmatrix} \varepsilon_1 \\ \varepsilon_2 \\ \varepsilon_3 \\ \gamma_{23} \\ \gamma_{31} \\ \gamma_{12} \end{bmatrix} \quad (B.7)$$

The stress σ_i is the perpendicular force F_i divided by the area A_i on which this force is applied. A stress state leads to a deformation state and viceversa. It is valid:

$$\frac{\partial^2 W}{\partial \varepsilon_j \partial \varepsilon_i} = C_{ji} \quad (\text{B.8})$$

But the order of differentiation of W is immaterial, so:

$$C_{ji} = C_{ij} \quad (\text{B.9})$$

Thus, the stiffness matrix is symmetric, so only 21 of the constants are independent. In a similar manner, it's possible to show that:

$$W = \frac{1}{2} S_{ij} \sigma_i \sigma_j \quad (\text{B.10})$$

Where S_{ij} is the compliance matrix defined by the inverse of the stress-strains relations, namely the strain-stress relations:

$$\varepsilon_j = S_{ij} \sigma_j \quad i, j = 1, \dots, 6 \quad (\text{B.11})$$

Therefore:

$$S_{ji} = S_{ij} \quad (\text{B.12})$$

This means that the compliance matrix is symmetric and hence has only 21 independent constants. So, with the reduction from 36 to 21 independent constants, the stress-strain relations are:

$$\begin{bmatrix} \sigma_1 \\ \sigma_2 \\ \sigma_3 \\ \tau_{23} \\ \tau_{31} \\ \tau_{12} \end{bmatrix} = \begin{bmatrix} C_{11} & C_{12} & C_{13} & C_{14} & C_{15} & C_{16} \\ C_{12} & C_{22} & C_{23} & C_{24} & C_{25} & C_{26} \\ C_{13} & C_{23} & C_{33} & C_{34} & C_{35} & C_{36} \\ C_{14} & C_{24} & C_{34} & C_{44} & C_{45} & C_{46} \\ C_{15} & C_{25} & C_{35} & C_{45} & C_{55} & C_{56} \\ C_{16} & C_{26} & C_{36} & C_{46} & C_{56} & C_{66} \end{bmatrix} \begin{bmatrix} \varepsilon_1 \\ \varepsilon_2 \\ \varepsilon_3 \\ \gamma_{23} \\ \gamma_{31} \\ \gamma_{12} \end{bmatrix} \quad (\text{B.13})$$

Actually this relation is referred to as characterizing “anisotropic” materials because there are no planes of symmetry for the material properties.

If there is an infinite number of planes of material property symmetry, the material is called “isotropic” and the relations are simplified.

Therefore many positions in the stiffness matrix are equal to zero:

$$\begin{bmatrix} \sigma_1 \\ \sigma_2 \\ \sigma_3 \\ \tau_{23} \\ \tau_{31} \\ \tau_{12} \end{bmatrix} = \begin{bmatrix} C_{11}C_{12}C_{12} & 0 & 0 & 0 \\ C_{12}C_{11}C_{12} & 0 & 0 & 0 \\ C_{12}C_{12}C_{11} & 0 & 0 & 0 \\ 0 & 0 & 0 & (C_{11} - C_{12})/2 \\ 0 & 0 & 0 & 0 \\ 0 & 0 & 0 & 0 \end{bmatrix} \begin{bmatrix} \varepsilon_1 \\ \varepsilon_2 \\ \varepsilon_3 \\ \gamma_{23} \\ \gamma_{31} \\ \gamma_{12} \end{bmatrix} \quad (\text{B.14})$$

The same is of course valid also for the compliance matrix:

$$\begin{bmatrix} \varepsilon_1 \\ \varepsilon_2 \\ \varepsilon_3 \\ \gamma_{23} \\ \gamma_{31} \\ \gamma_{12} \end{bmatrix} = \begin{bmatrix} S_{11}S_{12}S_{12} & 0 & 0 & 0 \\ S_{12}S_{11}S_{12} & 0 & 0 & 0 \\ S_{12}S_{12}S_{11} & 0 & 0 & 0 \\ 0 & 0 & 0 & 2(S_{11} - S_{12}) \\ 0 & 0 & 0 & 0 \\ 0 & 0 & 0 & 0 \end{bmatrix} \begin{bmatrix} \sigma_1 \\ \sigma_2 \\ \sigma_3 \\ \tau_{23} \\ \tau_{31} \\ \tau_{12} \end{bmatrix} \quad (\text{B.15})$$

Continuum mechanics is used to describe deformation and stress in an orthotropic material. Normally the majority of composite materials are approximated as orthotropic materials. That is, the material has three mutually perpendicular planes of symmetry. The intersection of these three planes defines three axes that coincide with the fiber direction (1), the thickness direction (2) and an other one (3) perpendicular to the other two.

For an orthotropic material, the compliance matrix components in terms of the engineering constants are:

$$[S_{ij}] = \begin{bmatrix} \frac{1}{E_1} & -\frac{\nu_{21}}{E_2} & -\frac{\nu_{21}}{E_2} & 0 & 0 & 0 \\ -\frac{\nu_{12}}{E_1} & \frac{1}{E_2} & -\frac{\nu_{32}}{E_3} & 0 & 0 & 0 \\ -\frac{\nu_{13}}{E_1} & -\frac{\nu_{23}}{E_2} & \frac{1}{E_2} & 0 & 0 & 0 \\ 0 & 0 & 0 & \frac{1}{G_{23}} & 0 & 0 \\ 0 & 0 & 0 & 0 & \frac{1}{G_{31}} & 0 \\ 0 & 0 & 0 & 0 & 0 & \frac{1}{G_{12}} \end{bmatrix} \quad (\text{B.16})$$

Where:

- ❖ E_1, E_2, E_3 = Young's (extension) moduli in the 1, 2, 3 directions;
- ❖ ν_{ij} = Poisson's ratio (extension-extension coupling coefficient), i.e., the negative of the transverse strain in the j-direction over the strain i-direction when stress is applied in the i-direction:

$$\nu_{ij} = -\frac{\varepsilon_j}{\varepsilon_i} \quad (\text{B.17})$$

for $\sigma_i = \sigma$ and all other stresses are zero;

- ❖ G_{23}, G_{31}, G_{12} = shear moduli in the 2-3, 3-1, and 1-2 planes.

These values can be determined experimentally through tensile tests along the directions 1,2,3 and permit to define the stress/strain state relation of an orthotropic material. The Young's moduli, the Shear moduli and the Poisson's ratio are fundamental properties of a material, and they characterise his mechanical behavior when a stress or deformation state is applied. Therefore, their unique determination permit to define the elastic response of the material. Normally the majority of materials has also a plastic component of deformation, that together with the elastic component define the total deformation that can result for an applied load. The elastic deformation can be always recovered when the material is un-loaded from the applied stress, on the contrary the plastic deformation is permanent. A material always exhibits first the elastic behavior and then the plastic one and in many applications it's preferable to not cross the elastic limit (design the material in such a way that the stress applied during his life will not lead to a plastic deformation), as for example structural applications. If the elastic range is crossed we loose definitely shape and geometry, and the loads are redistributed in other ways. Other times, as in manufacturing processes, crossing the elastic range is necessary to form an artefact with the desired appearance. The matrix above is the "identity document" of a material elastic behavior, and its parameters are his distinctive signs.

B-3) Nano-composite materials: a brief introduction

The general definition of "composite material" is: two or more materials combined on a macroscopic scale to form a useful third material. The advantage of composite materials is that, if well designed, they can exhibit the best properties of their constituents. Some of the qualities that can be improved are:

- | | |
|------------------------|----------------------------------|
| ❖ Strength | ❖ Fatigue life |
| ❖ Stiffness | ❖ Thermal insulation |
| ❖ Weight | ❖ Thermal conductivity |
| ❖ Corrosion resistance | ❖ Temperature-dependent behavior |
| ❖ Attractiveness | ❖ Acoustical insulation |

However it's impossible to improve all these properties in the same time, because some of them are in conflict. Therefore the right components must be selected in order to improve those properties that are more important for the required applications.

Normally, we can define four types of composite materials:

1. "Fibrous materials" that consist of fibers in a matrix;
2. "Laminated composite materials" that consist of layers of various materials;
3. "Particulate composite materials" that are composed of particles in a matrix;
4. Combination of some of the previous types.

In the first and third case there are two major phases: one is called matrix and the second one is the filler, that can be fibers or particles. However, it's always possible to see at least other two phases: porosity (or inclusions) and the interface. The interface is the local volume of the matrix around the filler, that has been modified by the presence of the filler itself (the interface forms from the interaction between matrix and filler).

The performances of the composite material depend by these four phases.

If the filler starts to have a nanometric scale, the percentage of superficial atoms of the filler is considerably higher, so the interfacial region increases quickly. Let's consider a cross section of a simple composite material, made by spherical particles with the same dimensions inside a matrix: for the same amount of filler (in volume fraction over the total volume), in the case of nano-particles the interface volume is higher (**Fig. B.3**).

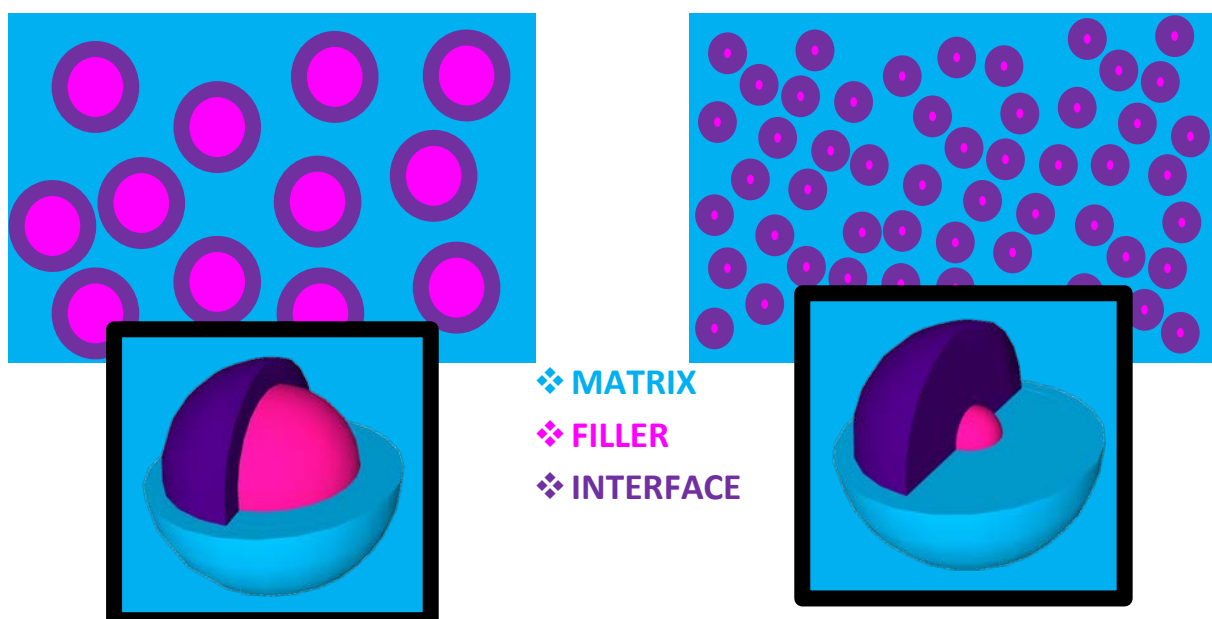


Fig. B.3: Composite materials with micro-particles (left) and nano-particles (right).

This phenomena is called “nanoeffect”, and small amount of nanofiller is enough to increase a lot the properties of the composite material. For example to guarantee comparable performances is enough the 5-6% in weight of nanofiller, instead using a percentage of 20% for normal microscale fillers.

Nanomaterials are generally considered as the materials that have a characteristic dimension (grain size, layer thickness, diameter of cylindrical cross section) smaller than 100nm. The nanomaterials can be classified into three categories, based on different geometries:

1. Nanoparticles: when the three dimensions have nanoscale magnitude (nanoparticles, nanogranules, nanocrystals);
2. Nanotubes: when two dimensions are in the nanoscale, and the third one is larger (nanotubes, nanofibers, whiskers, nanorods);
3. Nanolayers: when just one dimension is in the nanoscale (nanoplatelets, nanoclays, nanosheets, nanolayers).

Compared to the normally used microcomposites, the nanocomposites have extraordinary physical and mechanical properties. We can attest the following advantages, using a nanoscale reinforcement:

1. High density of particles per particle volume (10^6 - 10^8 particles/ μm^3);
2. High interfacial area per volume of particles (10^3 - 10^4 m^2/ml);
3. Short distance between particles (10-50nm at 1-8 vol. %).

In the last years carbon nanotubes and nanoplates are two kinds of nanoparticles that gained particular attention from the scientist’s community.

B-4) Popular Micromechanical models for Young’s Modulus prediction

In the literature are presented many models for the Young’s modulus prediction. Some of them are more elegant than others or more appropriated to model nano-composite than micro-composite, taking in considerations different parameters.

Voigt and Reuss models (V-R model)

To describe the elastic modulus of a composite material made by parallel aligned fibers, it’s necessary to take in account that the the anisotropic fiber’s behavior will be reflected in the final properties of the composite material. To calculate the Elastic modulus of the composite

material along the fiber direction, Voigt proposed the well known “rule of mixture” (the fibers are subjected, together with matrix, to the same uniform strain along the fiber direction):

$$E_A = V_f E_f + (1 - V_f) E_m \quad (\text{B.18})$$

Where E_A is the Young’s modulus of the composite along the direction 1 (direction of the fibers), E_f is the Axial Young’s modulus of the fibers, E_m the Young’s modulus of the matrix and V_f is the volume fraction of the fibers inside the material.

Voigt designed the previous formula making some assumptions; if we consider the load (σ_1) applied along the fiber direction (direction 1) the Voigt model is based on some restrictions:

1. Continuous fibers;
2. The fibers are parallel;
3. Perfect linking between fibers and matrix: $\varepsilon_f = \varepsilon_m = \varepsilon_1$. That means that the strains of matrix and fibers are equal;
4. $\nu_f = \nu_m$;
5. Fibers and matrix have a perfect elastic behaviour (Hooke’s Law).

Therefore the model states that, fixed E_f and E_m (so chosen the two materials), the elastic modulus E_A of the composite, increases linearly with the fiber volume fraction.

Reuss estimate the Transversal Young’s modulus for a the same composite material analyzed by Voigt in the axial direction. In the Reuss model the load is applied in transversal direction (direction 2), and we have $\sigma_f = \sigma_m = \sigma_2$ (the other hypothesis of the Voigt model are still valid). Therefore:

$$E_T = \frac{E_f E_m}{E_m V_f + E_f (1 - V_f)} \quad (\text{B.19})$$

Where E_T is the Young’s modulus of the composite along the direction 2 (the transversal direction of the fibers), and E_m , E_f , V_f are defined as in the Voigt model.

However the Reuss and Voigt equations can be extended to any two-phase composites regardless the shape of the filler, and E_A and E_T represent the upper and lower bounds of the modulus of the composite, respectively. V-R model involves just three parameters.

Halpin-Tsai Model (H-T model)

Considering aligned fiber reinforced composite materials, the H-T model provided a semi-empirical equations for the longitudinal and transverse moduli:

$$E_A = \frac{1 + 2\left(\frac{l}{d}\right)V_f\eta_A}{1 - V_f\eta_A} E_m \quad (\text{B.20})$$

$$E_T = \frac{1 + 2\left(\frac{l}{d}\right)V_f\eta_T}{1 - V_f\eta_T} E_m \quad (\text{B.21})$$

Where l and d are the length and the diameter of the fiber and η_A and η_T are defined as:

$$\eta_A = \frac{E_f - E_m}{E_f + 2\left(\frac{l}{d}\right)E_m} \quad (\text{B.22})$$

$$\eta_T = \frac{E_f - E_m}{E_f + 2E_m} \quad (\text{B.23})$$

For aligned nanoplates we must replace in the previous equations the value (l/d) with (D/t) , where D and t are respectively the diameter and the thickness of the platelet.

H-T model takes the consideration of the fiber geometry and has five independent parameter.

Other models

Other models often used are the Wang-Pyrz model (W-P model) and the Cox model (Shear lag model), but for our study the model previously mentioned are enough.

Anyway in modeling mechanical properties of nanocomposites there are two main approaches: the molecular dynamics simulation using direct methods and the other is finite element simulation using “continuum” methods.

ACKNOWLEDGMENTS

I would like to thank first of all Christian Aulin from Innventia for providing the CNF and discussion of the CNF properties, and WWSC for financial support. It has been a great opportunity to increase my knowledge and experience in the scientific researching world, with the possibility to test my attitudes and my capabilities in a scenario that for me was completely unknown before my arrival here at MMK.

“Ovviamente speciali ringraziamenti vanno a German e Bernd, per avermi supportato, aiutato e stimolato all’eccellenza in ogni dettaglio della mia esperienza. Mi mancherà tremendamente sentire Bernd imprecare in tedesco nei momenti bui o fare i goal di testa su assist di German nelle giornate di calcetto del mercoledì. Avete sempre cercato di rendermi partecipe in ogni decisione, spronandomi ad avere più fiducia nelle mie capacità, a trovare il mio “unicorno” nascosto. Spero manteniate il ricordo del Fede di inizio tirocinio, quello sereno e felice e non quello delle ultime settimane, rabbuiato nelle frustrazioni dei mulinelli intellettuali provocati da tesi ed esperimenti!

Vi auguro il meglio dalla vita, che ognuno di noi possa trovare la sua piena realizzazione nel caos e nella ripetitività che governano i destini di tutti.

Grandi ringraziamenti vanno a Prof. Lennart, che mi ha sempre manifestato grande umanità in tutti i nostri incontri, dandomi la possibilità di viaggiare e scoprire la varietà del mondo che circonda la nostra consuetudine. Un grazie di cuore!”

“Dedico questa tesi e tutti gli sforzi necessari al raggiungimento di tale traguardo ai miei genitori. Parte della determinazione che mi caratterizza, la devo a voi, costante inflessibile esempi di sacrificio, umiltà, dedizione e benevolenza. Non ci sono eroi più grandi degli umili, che ogni mattina si alzano alle quattro per andare a lavoro in fabbrica, senza rimpianti o pieghe nella anima, ma con la naturale semplicità di chi contraddistingue i buoni. In questo mondo carnefice di spiriti, di etica ed esempi, siete voi le figure a cui guardo nei momenti più bassi. Dedico questa tesi anche a tutti i miei nonni, che hanno sofferto vite di calli e carnose fatiche, per dare un futuro migliore ai propri figli e di conseguenza anche ai nipoti.

Ciò che fa un uomo grande è la statura del suo cuore e la forza che ha nel braccio della determinazione. Questo l’ho imparato nei miei viaggi e nelle mie esperienze da solitario...non

c'è nulla che curvi l'anima nell'occhio lucido di speranza di colui che crede in sé stesso, non esiste passo che possa oscurare tale sguardo. Sebbene a volte la vita sferzi di venti immondi le nostre esistenze, ciò che conta veramente è avere quel braccio saldo nel giusto e nel bene che si celano dentro di noi. Il bene non è relativo ma è assoluto e totale, è la linfa che lega i sorrisi degli amici e le lacrime nella tragedia, è il buon umore nel cielo riflesso in pozze dopo i tuoni e i rami spezzati. Ci sarà sempre una primavera, un celeste sereno in un grigia pozza, un pallone colorato che rotola in un verde prato.

Con questa tesi concludo la mia carriera universitaria, fatta di tante regine di fiori e re di picche. Spero che il domani mi riservi opportunità non superiori alle mie qualità, perché non c'è gusto nella corsa senza l'adrenalina della ferocia e perché l'ingiustizia fa schifo e nessuno la merita.”

REFERENCES

- 1** H.P.S. Abdul Khalil, A.H. Bhat, A.F. Ireana Yusra (2012). “Green composites from sustainable cellulose nanofibrils: A review”, **Carbohydrate Polymers**, **87**, 963-979
- 2** Wicklein and Salazar-Alvarez (2013). “Functional hybrids based on biogenic nanofibrils and inorganic nanomaterials”, **J. Mater. Chem. A**, **2013**, **1**, 5469
- 3** Nathalie Lavoine, Isabelle Desloges, Alain Dufresne, Julien Bras (2012). “Microfibrillated Cellulose – Its barrier properties and applications in cellulosic materials: A review”, **Carbohydrate Polymers**, **90**, 735-764
- 4** Dieter Klemm, Friederike Kramer, Sebastian Moritz, Tom Lindström, Mikael Ankefors, Derek Gray, Annie Dorris (2011). “Nanocelluloses: A new Family of Nature-Based Materials”, **Angew. Chem. Int.**, **50**, 5438-5466
- 5** Robert J. Moon, Ashlie Martini, John Nairn, John Simonsen, Jeff Youngblood (2011). “Cellulose nanomaterials review: structure, properties and nanocomposites”, **Chem. Soc. Rev.**, **40**, 3941–3994
- 6** Marie-Cécile Klak, Elodie Lefebvre, Laure Rémy, Rémy Agniel, Julien Picard, Sébastien Giraudier, Véronique Larreta-Garde (2013). “Gelatin-Alginate Gels and Their Enzymatic Modifications: Controlling the Delivery of Small Molecules”, **Macromol. Biosci.**, **13**, 687-695
- 7** Bishop M, Shahid N, Yang J, Barron AR (2004). “Determination of the mode and efficacy of the cross-linking of guar by borate using MAS 11B NMR of borate cross-linked guar in combination with solution 11B NMR of model systems”, **Dalton Trans.**, **17**, 2621-2634
- 8** Byung Min Yoo, Hye Jin Shin, Hee Wook Yoon, Ho Bum Park (2013). “Graphene and Graphene Oxide and Their Uses in Barrier Polymers”, **Applied Polymer Science**, **131**, 39628
- 9** Hyunwoo Kim, Ahmed A. Abdala, and Christopher W. Macosko (2010). “Graphene/Polymer Nanocomposites”, **Macromolecules**, **43**, 6515-6530
- 10** Dmitriy A. Dikin, Sasha Stankovich, Eric J. Zimney, Richard D. Piner, Geoffrey H. B. Domett, Guennadi Evmnenko, SonBinh T. Nguyen, Rodney S. Ruoff (2007). “Preparation and characterization of graphene oxide paper”, **Nature**, **448**, 457-460

- 11 Owen C. Compton and SonBinh T. Nguyen (2010).** “*Graphene Oxide, Highly Reduced Graphene Oxide, and Graphene: Versatile Building Blocks for Carbon-Based Materials*”, **Small**, **6**, 711-723
- 12 Meng Cheng, Rong Yang, Lianchang Zhang, Zhiwen Shi, Wei Yang, Duoming Wang, Guibai Xie, Dogxia Shi, Guangyu Zhang (2012).** “*Restoration of graphene from graphene oxide by defect repair*”, **Carbon**, **50**, 2581-2587
- 13 Howard A. Barnes (2000).** “*A handbook of elementary rheology*”, **Aberystwyth (United Kingdom), The University of Wales Institute of Non-Newtonian Fluid Mechanics**
- 14 Alexander Ya. Malkin (1994).** “*Rheology Fundamentals*”, **Toronto-Scarborough (Canada), ChemTec Publishing**
- 15 Tatsumi, Ishioka, Matsumoto (2002).** “*Effect of Fiber Concentration and Axial Ratio on the Rheological Properties of Cellulose Fiber Suspension*”, **Journal of Society of Rheology**, **30**, 27-32
- 16 Ishii, D., Saito, T., & Isogai, A. (2011).** “*Viscoelastic evaluation of average length of cellulose nanofibers prepared by TEMPO-mediated oxidation*”, **Biomacromolecules**, **12**, 548–550
- 17 Marjo Kettunen née Pääkkö (2013).** “*Cellulose Nanofibrils as a Functional Material*” **Doctoral dissertation, Aalto University (Finland)**
- 18 Andreas B. Fall, Stefan B. Lindstrom, Joris Sprakel and Lars Wagberg (2013).** “*A physical cross-linking process of cellulose nanofibril gels with shear-controlled fibril orientation*”, **Soft Matter**, **9**, 1852
- 19 Cristopher W. Macosko (1994).** “*Rheology Principles, Measurements and Applications*”, **USA, WILEY-VCH**
- 20 M. Paakko, M. Ankerfors, H. Kosonen, A. Nykanen, S. Ahola, M. Osterberg, J. Ruokolainen, J. Laine, P. T. Larsson, O. Ikkala, and T. Lindstrom (2007).** “*Enzymatic Hydrolysis Combined with Mechanical Shearing and High-Pressure Homogenization for Nanoscale Cellulose Fibrils and Strong Gels*”, **Biomacromolecules**, **8**, 1934-1941
- 21 Iotti, M., Gregersen, Ø. W., Moe, S., and Lenes, M. (2011).** “*Rheological studies of microfibrillar cellulose water dispersions*”, **J. Polym. Env.**, **19**, 137
- 22 H.A. Barnes, J.F. Hutton and K. Walters (1989).** “*An Introduction to Rheology*”, **Amsterdam (Netherlands), Elsevier Science Publisher**
- 23 Howard A. Barnes (1996).** “*Thixotropy a review*”, **J. Non-Newtonian Fluid Mech.**, **70**, 1-33

- ²⁴ **Nick Triantafillopoulos (1988).** “*Measurement of Fluid Rheology and Interpretation of Rheograms*”, **Michigan (USA), Kaltec scientific Inc.**
- ²⁵ **Malvern Instrument Ltd (2005).** “*Determining And Measuring Thixotropy and Rheology For Coatings Applications Using Equipment From Malvern Instruments*, **Worcestershire (United Kingdom)**
- ²⁶ **Shubin Yang, Xinliang Feng, Sorin Ivanovici, Klaus Müllen (2010).** ”*Fabrication of Graphene-Encapsulated Oxide Nanoparticles: Towards High-Performance Anode Materials for Lithium Storage*”, **Angewandte Chemie International Edition, 49, 8408-8411**
- ²⁷ **Gurunathan S, Han JW, Dayem AA, Eppakayala V, Kim JH, (2012).** “*Oxidative stress-mediated antibacterial activity of graphene oxide and reduced graphene oxide in Pseudomonas aeruginosa*”, **Int J. Nanomedicine, 7, 5901-5914**
- ²⁸ **nanoComposix (2012).**”*UV/VIS/IR spectroscopy analysis of nanoparticles*”,**San Diego (USA)**
- ²⁹ **C. Goussé, H. Chanzy, M.L. Cerrada, E. Fleury (2004).** “*Surface silylation of cellulose microfibrils: preparation and rheological properties*”, **Polymer, 45, 1569-1575**
- ³⁰ **Andreas B. Fall (2013).** “*Colloidal interactions and orientation of nanocellulose particles*”, **Doctoral Thesis, Royal Institute of Technology (Sweden)**
- ³¹ **Mason S.G. (1950).** “*The flocculation of pulp suspensions and the formation of paper*”,**Tappi, 33, 440-444**
- ³² **Andreas Fall (2011).** “*Cellulose nanofibril materials with controlled structure: the influence of colloidal interactions*”, **Licentiate Thesis, Royal Institute of Technology (Sweden)**
- ³³ **Evans F. D. and H. Wennerstrom (1999).** “*The Colloidal Domain*”, **VCH, New York (USA)**
- ³⁴ **Ronald G. Larson (1999).** “*The structure and rheology of complex fluids*”, **Oxford University Press, New York (USA)**
- ³⁵ **Ralph H. Colby (2010).** “*Structure and Linear Viscoelasticity of Flexible Polymer Solutions: Comparison of Polyelectrolyte and Neutral Polymer Solutions*”, **Rheologica Acta, 49, 425-442**
- ³⁶ **C. M. Roland, L. A. Archer, P. H. Mott, J. Sanchez-Reyes (2004).** “*Determining Rouse relaxation times from the dynamic modulus of entangled polymers*”, **Journal of Rheology, 48, 395**

- ³⁷ **Francois Chambon and H. Henning Winter (1987).** "Linear Viscoelasticity at the Gel Point of a Crosslinking PDMS with Imbalanced Stoichiometry" **Journal of rheology**, **31**, 683-97
- ³⁸ **N. Ashwin Bharadwaj, James T. Allison, Randy H. Ewoldt (2013).** *Early-stage design of rheologically complex materials via material function design targets*, **ASME 2013, University of Illinois, Urbana (USA)**
- ³⁹ **Bala T., Prasad BL, Sastry M, Kahaly MU, Waghmare UV (2007).** "Interaction of different metal ions with carboxylic acid group: a quantitative study", **J Phys Chem A**, **111**, 6183-90
- ⁴⁰ **Leonard H. Switzer III and Daniel J. Klingenberg (2003).** "Rheology of sheared flexible fiber suspensions via fiber-level simulations", **Journal of Rheology**, **47**, 759
- ⁴¹ **Nawab, M. A. and S. G. Mason (1958).** "The viscosity of dilute suspensions of thread-like particles," **J. Phys. Chem.**, **62**, 1248–1253
- ⁴² **Goto, S., H. Nagazono, and H. Kato (1986).** "The flow behavior of fiber suspensions in Newtonian fluids and polymer solutions. I. Mechanical properties", **Rheol. Acta**, **25**, 119–129
- ⁴³ **Wahren, D. (1964),** "On the visco-elastic properties of fiber networks", **Sven. Papperstidn.**, **67**, 378–381
- ⁴⁴ **Mani Rahnema, Donald L. Koch (1994).** "The effect of hydrodynamic interactions on the orientation distribution in a fiber suspension subject to simple shear flow", **Physics of Fluids**, **7**, 487
- ⁴⁵ **Thao T. T. Ho, Tanja Zimmermann, Steffen Ohr, and Walter R. Caseri (2012).** "Composites of Cationic Nanofibrillated Cellulose and Layered Silicates: Water Vapor Barrier and Mechanical Properties", **CS Appl. Mater. Interfaces**, **4**, 4832–4840
- ⁴⁶ **Muzzarelli, R., (2009).** "Chitins and chitosans for the repair of wounded skin, nerve, cartilage and bone", **Carbohydr. Polym.** **76**, 167–182
- ⁴⁷ **Rinaudo, M., (2006).** "Chitin and chitosan: properties and applications", **Prog. Polym. Sci.** **31**, 603–632
- ⁴⁸ **Tongfei Wu, Ramin Farnood, Kevin O’Kelly, Biqiong Chen (2014).** "Mechanical behavior of transparent nanofibrillar cellulose–chitosan nanocomposite films in dry and wet conditions", **Journal of the mechanical behavior of biomedical materials**, **32**, 279 – 286

- ⁴⁹ **Christian Aulin, German Salazar-Alvarez and Tom Lindstrom (2012).** *High strength, flexible and transparent nanofibrillated cellulose–nanoclay biohybrid films with tunable oxygen and water vapor permeability*, **Nanoscale**, **4**, 6622
- ⁵⁰ **Yottha Srithep, Lih-Sheng Turng, Ronald Sabo, Craig Clemons (2012).** “*Nanofibrillated cellulose (NFC) reinforced polyvinyl alcohol (PVOH) nanocomposites: properties, solubility of carbon dioxide, and foaming*”, **Cellulose**, **19**, 1209-1223
- ⁵¹ **Zainoha Zakaria, Md. Saiful Islam, Azman Hassan, M. K. Mohamad Haafiz, Reza Arjmandi, I. M. Inuwa, and M. Hasan (2013).** “*Mechanical Properties and Morphological Characterization of PLA/Chitosan/Epoxidized Natural Rubber Composites*”, **Advances in Materials Science and Engineering**, Article ID 629092
- ⁵² **Xiawa Wu, Robert J. Moon, Ashlie Martini (2013).** “*Crystalline cellulose elastic modulus predicted by atomistic models of uniform deformation and nanoscale indentation*”, **Cellulose**, **20**, 43-55
- ⁵³ **S.J. Eichhorn & R.J. Young (2001).** “*The Young’s modulus of a microcrystalline cellulose*”, **Cellulose**, **8**, 197-207
- ⁵⁴ **Harris B. (1999).** “*Engineering Composite Materials*”, **London (United Kingdom), The Institute of Materials**
- ⁵⁵ **Young R.J., Lovell P.A. (1991).** “*Introduction to Polymers*”, **Polymer International**, **27**, 207-208
- ⁵⁶ **Fernando L. Dri, Louis G. Hector Jr., Robert J. Moon, Pablo D. Zavattieri (2013).** “*Anisotropy of the elastic properties of crystalline cellulose density functional theory with Van der Waals interactions*”, **Cellulose**, **20**, 2703-2718 □□ from
- ⁵⁷ **Pakzad A., Simonsen J., Heiden P.A., Yassar R.S. (2012).** “*Size effects on the nanomechanical properties of cellulose I nanocrystals*”, **Journal of Material Research**, **27**, 528–536
- ⁵⁸ **Houssine Sehaqui, Ngesa Ezekiel Mushi, Seira Morimune, Michaela Salajkova, Takashi Nishino, and Lars A. Berglund (2012).** “*Cellulose Nanofiber Orientation in Nanopaper and Nanocomposites by Cold Drawing*”, **ACS Applied materials & interfaces**, **4**, 1043-1049
- ⁵⁹ **Jeng-Jong Lin (2010).** “*Prediction of Elastic Properties of Plain Weave Fabric Using Geometrical Modeling*”, **Woven Fabric Engineering**, **Polona Dobnik Dubrovski**
- ⁶⁰ **Hearle, J.W.S., Grosberg, P., & S. Baker (1969).** “*Structural Mechanics of Fibers, Yarns, & Fabrics*”, **John Wiley & Sons, New York (USA)**

- ⁶¹ **Y. Qiu, Y. Wang, J.Z. Mi (2001).** “*A Novel Approach for Measurement of Fiber-on-fiber Friction*”, **National Textile Center Annual Report, F98-S09**
- ⁶² **Roberts Joffe and David Mattsson (2006).** “*NCF cross-ply laminates: damage accumulation and degradation of elastic properties*”, **Gdoutos E. E., Alexandroupolis (Greece)**
- ⁶³ **Sonali Gholap, Dr. Dhananjay R. Panchagade, Vinay Patil (2014).** “*Continuum Modeling Techniques to Determine Mechanical Properties of Nanocomposites*”, **International journal of Modern Engineering Research, 4, 9-15**
- ⁶⁴ **D.Shia, C.Y.Hui, S. D. Burnside, E. P. Giannelis (2004).** “*An Interface Model for the Prediction of Young’s Modulus of Layered Silicate-Elastomer Nanocomposites*”, **Polymer Composites, 19, 608-617**
- ⁶⁵ **Philipp Wagner, Viktoria V. Ivanovskaya, Mark J. Rayson, Patrick R. Briddon, Christopher P.Ewels (2013).** “*Mechanical properties of nanosheets and nanotubes using a new geometry independent volume definition*”, **J. Phys. Condens. Matter, 25, 155302**
- ⁶⁶ **Ferrari, A. C., Robertson J., (2004).** “*Raman spectroscopy in carbons: from nanotubs to diamond*”, **Phil. Tans. R. Soc. Lond, 362, 2267–2565**
- ⁶⁷ **Tuinstra, F. And Koenig J. L. (1970).** “*Raman spectrum of graphite*”, **J. Chem. Phys., 53, 1126**
- ⁶⁸ **Ferrari A. C., Robertson J., (2000).** “*Interpretation of Raman spectra of disordered and amorphous carbon*”, **Condensed Matter and Materials Physics, 61, 14095-14107**
- ⁶⁹ **Ferrari A. C., Meyer J. C., Scardaci V., Casiraghi C., Lazzeri M., Mauri F., Piscanec S., Jiang Da., Novoselov K. S., Roth S., Geim A. K. (2006).** “*Raman spectrum of graphene and graphene layers*”, **Phys. Review Letters, 97, 187401**
- ⁷⁰ **Ardavan Zandiatashbar, Gwan-Hyoung Lee, Sung Joo An, Sunwoo Lee, Nithin Mathew, Mauricio Terrones, Takuya Hayashi, Catalin R. Picu, James Hone, Nikhil Koratkar (2014).** “*Effect of defects on the intrinsic strength and stiffness of graphene*” **Nature Communications, 5, 3186**
- ⁷¹ **D. A. Dikin, S. Stankovich, E. J. Zimney, R. D. Piner, G.H.B. Dommet, G. Evmenenko, S.T. Nguyen, R. S. Rouff (2007).** “*Preparation and characterization of graphene oxide-based paper*”, **Nature, 448, 457-460**
- ⁷² **O. C. Compton, D. A. Dikin, K. W. Putz, L. C. Brinson, S. T. Nguyen, (2010).** “*Electrically conductive alkylated graphene paper via chemical reduction of amine-functionalized graphene oxide paper*”, **Adv. Mater., 22, 892-896**

- ⁷³ S. Park, K. Lee, G. Bozoklu, W. Cai, S. T. Nguyen, R.S Ruoff (2008). "Graphene oxide papers modified by divalent ions-enhancing mechanical properties via chemical cross-linking", *ACS Nano*, **2**, 572-578
- ⁷⁴ Saber-Samandari S, Afaghi-Khatibi A. (2006). "The effect of interphase on the elastic modulus of polymer based nanocomposites", *Key Engineering Materials*, **312**, 199-204
- ⁷⁵ Joby J. Kochumalayil and Lars A. Berglund (2013). "Water-soluble hemicelluloses for high humidity applications – enzymatic modification of xyloglucan for mechanical and oxygen barrier properties", *Green Chemistry*, DOI: 10.1039/c3gc41823e
- ⁷⁶ Christina Schutz, Jordi Sort, Zoltan Bacsik, Vitaliy Oliynyk, Eva Pellicer, Andreas Fall, Lars Wagberg, Lars Berglund, Lennart Bergstrom, German Salazar-Alvarez (2012). "Hard and Transparent Films Formed by Nanocellulose– TiO₂ Nanoparticle Hybrids", *PLOS ONE*, **7**, 45828
- ⁷⁷ Joby J. Kochumalayil, Seira Morimune, Takashi Nishino, Olli Ikkala, Andreas Walther, and Lars A. Berglund (2013). "Nacre-Mimetic Clay/Xyloglucan Bionanocomposites: A Chemical Modification Route for Hygromechanical Performance at High Humidity", *Biomacromolecules*, **14**, 3842-3849
- ⁷⁸ Chun-Nan Wu, Quanling Yang, Miyuki Takeuchi, Tsuguyuki Saito and Akira Isogai (2014). "Highly tough and transparent layered composites of nanocellulose and synthetic silicate", *Nanoscale*, **6**, 392
- ⁷⁹ Parvez Alam (2011). "Porous Particle-Polymer Composites, *Advances in Composite Materials - Analysis of Natural and Man-Made Materials*", Dr. Pavla Tesinova (Ed.), ISBN: 978-953-307-449-8
- ⁸⁰ Belbekhouche S., Bras J., Siqueira G., Chappey C., Lebrun L., Khelifi B., et al. (2011). "Water sorption behavior and gas barrier properties of cellulose whiskers and microfibrils films", *Carbohydrate Polymers*, **83**, 1740–1748
- ⁸¹ Minelli M., Baschetti M. G., Doghieri F., Ankerfors M., Lindström T., Siró I., et al. (2010). "Investigation of mass transport properties of microfibrillated cellulose (MFC) films", *Journal of Membrane Science*, **358**, 67–75
- ⁸² E.L. Cussler, Stephanie E. Hughes, William J. Ward, and Rutherford Aris (1988). "Barrier membranes", *Journal of Membrane Science*, **38**, 161-174
- ⁸³ Spence, K. L., Venditti, R. A., Habibi, Y., Rojas, O. J., & Pawlak, J. J. (2010). "The effect of chemical composition on microfibrillar cellulose films from wood pulps: Mechanical processing and physical properties", *Bioresource Technology*, **101**, 5961–5968

- 84** Hubbe Martin A., Rojas Orlando J., Lucia Lucian A., Jung Tae Min. (2007). “Consequences of the nanoporosity of cellulosic fibers on their streaming potential and their interactions with cationic polyelectrolytes”, **Cellulose**, **14**, 655-671
- 85** Michaela Salajkova (2013). “Wood Nanocellulose Materials and Effects from Surface Modification of Nanoparticles”, **Doctoral Thesis, Royal Institute of Technology (Sweden)**
- 86** Kimmo Lahtinen and Jurkka Kuusipalo (2007). “Prediction of WVTR with General Regression Models”, **11th Tappi European PLACE Conf., TAPPI, Athens (Greece)**
- 87** Gordon L. Robertson (2012). “Food Packaging: Principles and Practice”, **CRC Press, Brisbane (Australia)**
- 88** Ira V. Gardiner Editor (2007). “Fluorine Chemistry Research Advances”, **Nova Science Pub Inc, New York (USA)**
- 89** A. P. Kharitonov (2008). “Direct fluorination of polymers”, **Nova Science Pub Inc, New York (USA)**
- 90** Geoffrey Campbell-Platt (2009). “Food Science and Technology”, **Blackwell Publishing Ltd, Oxford (United Kingdom)**
- 91** S. Kalia, B. S. Kaith, I.Kaur (2011). “Cellulose Fibers: Bio- and Nano- Polymer Composites”, **Springer, London (United Kingdom), New York (USA)**
- 92** Henrikki Liimatainen, Ngesa Ezekiel, Rafal Sliz, Katja Ohenoja, Juho Antti Sirvio, Lars Berglund, Osmo Hormi and Jouko Niinimäki (2013). “High-Strength Nanocellulose–Talc Hybrid Barrier Films”, **ACS Appl. Mater. Interfaces**, **5**, 13412-13418
- 93** Daniela Gabor, Ovidu Tita (2012). “Biopolymer used in food packaging: a review”, **Acta Universitatis Cibiniensis Series E: FOOD TECHNOLOGY**, Vol. XVI, no.2
- 94** Dejan Arzensek (2010). “Dynamic light scattering and application to proteins in solution”, **Seminar-4th year, Department of Physics, Ljubljana (Slovenia)**
- 95** C. Sinn (1998). “Dynamic light scattering by rodlike particles: examination of the vanadium(V)-oxide system”, **The European Physical Journal B**, **7**, 599-605
- 96** T. Maeda, S. Fujime (1984). “Spectrum of light quasielastically scattered from solutions of very long rods at dilute and semidilute regimes”, **Macromolecules**, **17**, 1157